Investigations of Two-Photon Absorption and Dissociation of Nitrodibenzofuran Based Photocages

A dissertation submitted to the faculty of the University of Minnesota

by

Michael H. Hodny

in partial fulfillment of the requirements for the degree of

Doctor of Philosophy

Professor David A. Blank
Department of Chemistry

August 2022

"Mathematics began to seem too much like puzzle solving. Physics is puzzle solving too, but of puzzles created by nature, not by the mind of man."

Maria Goeppert-Mayer

Acknowledgements

Many people have contributed to the successes that I have achieved, not only through graduate school, but throughout my life up to this point. Their contributions to my journey need to be acknowledged.

Foremost, I want to convey my deepest gratitude to Professor David Blank for putting his trust in me and having the patience to enthusiastically guide me through this journey. Throughout my tenure in the Blank Research Lab, your mentorship and encouragement for me to push my boundaries outside of what I thought possible has led me to not only be a better scientist, but a better mentor, leader, and person. Thank you deeply.

Thank you to the members of the Blank Research Lab: To Dr. Andy Healy for always lending a hand to solve problems big and small and to be a role model that everyone looks up to. To Meghan Knudtzon and Rachel Swedin for training me and providing support to me on all our instruments. You ensured that I got off to a great start. To Jacob Schaffner, Hridya Premnathan, Mik Patel, Katie Huber, and the undergrads for putting up with me and always sharing a good conversation and a good laugh. Special thanks to Reid Anderson for his early work in getting the calculations to work.

I would like to thank my friends, too numerous to name, for supporting me. Your friendship, food, and company were a comfort during stressful times.

To my other mentors, Scott Hetherington, Dr. Krystel Kizer, and Dr. John Hershberger for fostering my love of chemistry and setting me down the path that I'm still on.

Lastly, thank you to my loved ones: Celina Harris, my kind and caring partner. To my parents, brother, and sister, for making all of this possible. I hope I have made you proud. I cannot thank you all enough.

Abstract

The ability to selectively deliver bioactive molecules with high spatial and temporal resolution has applications in many areas of chemical biology and drug delivery. Using photocages, drugs can be selectively released within specific areas of tissue. When chemically bound, these groups deactivate the drug's biological activity. Light of a sufficient energy can then be used to break the bond linking the drug to the cage. Photocages typically require the energy of one UV photon to dissociate, but UV photons have low penetration depth and can damage tissue. Two-photon absorption (2PA) can be used to break the bond using the energy of two NIR photons. There is, however, a lack of understanding of the design principles for producing photocages that have both high 2PA cross sections and high uncaging efficiencies. The purpose of this research was to study the structure of a photocage affects the dynamics of two-photon absorption and two-photon induced dissociation in a series of dibenzofuran based photocages.

The first two sections of this dissertation investigate the effect that structural modification of the photocage and choice of leaving group have on the photophysical properties of the NDBF system. Extending the conjugation or adding electron-donating groups to NDBF can increase the 2PA cross section and dissociation rate. The leaving group choice strongly influences the dissociation rate, but affects the 2PA cross section much less.

The third section investigates the dynamics of dissociation and to what extent they influence the overall dissociation rate. It was found that the amount of photocages that initially dissociate does not correlate with overall dissociation rate.

Lastly, computational methods were used to investigate potential molecular structures that can be used as more efficient photocages. It was determined that NDBF dimers exhibit greatly enhanced 2PA cross sections and should be pursued synthetically.

Table of Contents

List of Figures

List of Tables

Abbreviations

1PA – **1-P**hoton **A**bsorption

2PA – **2-P**hoton **A**bsorption

2PEF – **T**wo-**P**hoton **E**xcited **F**luorescence

2PFM – **2-P**hoton **F**luorescence **M**icroscopy

A – Electron **A**cceptor

BODIPY – **Bo**ron **Dipy**romethene

Cys-FMOC – **cys**tine-**f**luorenyl**m**eth**o**xy**c**arbonyl

D – Electron **D**onor

DFT - Density **F**unctional **T**heory

DMSO **-** Dimethyl Sulfoxide

FWHM – **F**ull **W**idth at **H**alf of **M**aximum

GM – **G**oeppert-**M**ayer, 10^{-50} cm^4 s $molecule^{-1}$ $photon^{-1}$

HOMO – **H**ighest **O**ccupied **M**olecular **O**rbital

IR – **I**nfra**r**ed

LUMO – **L**owest **U**noccupied **M**olecular **O**rbital

NDBF – **N**itro**di**ben**zof**uran

NTO – **N**atural **T**ransition **O**rbital

o-NB – **o**rtho-**n**itro**b**enzyl

PPG – **P**hotoremoveable **P**rotecting **G**roup

UV - Ultra**v**iolet

Chapter 1

Introduction

The ability to deliver bioactive molecules to specific areas of a cell or other biological sample with high spatial and temporal resolution is important to many areas of science and medicine. For example, the timed delivery of fluorescent probes and tags within a cell allows for the visualization of various cellular structures and processes.[1] Of equal importance is the ability to selectively deliver a drug molecule to specific areas of a tissue sample, leaving other areas of the tissue unaffected by the drug. Photoremoveable protecting groups (PPGs), or photocages, can be used for these applications, using light as a trigger (Figure 1.1).

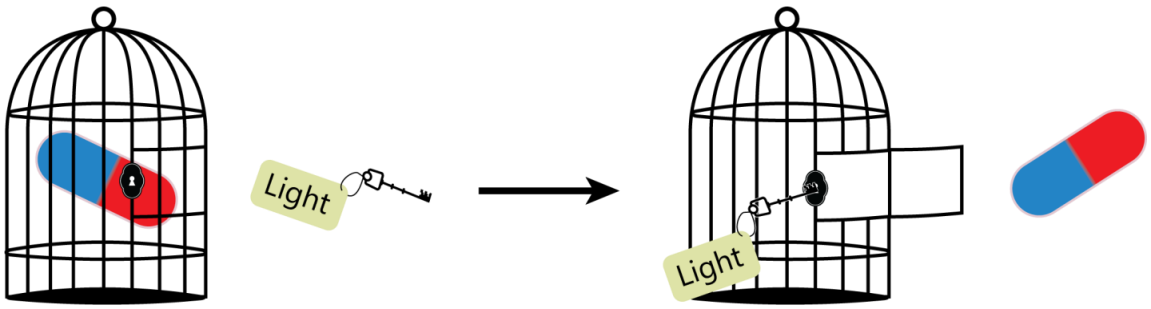

Figure 1.1: General reaction diagram of a photocage-drug conjugate with light.

This work seeks to understand the underlying principles that govern the relationship between a photocage's structure and its ability to be effectively used in the aforementioned applications with the goal of designing photocages that are more efficient

at delivering bioactive molecules where they are needed. Currently, there is limited knowledge of the relationship between the structure of a photocage and its two-photon absorption (2PA) and dissociation properties. This thesis focuses on studying the structure/property relationship of a model set of photocages based on nitrodibenzofuran (NDBF) in order to better understand how to design more efficient photocages for biological use. Changes in the structure of the cage and identity of the leaving group are correlated with changes in absorption and dissociation. Currently, it is also unknown if the dissociation rates and recombination rates of these photocages differ. It is equally important to be able to predict the absorption properties of photocages before they are synthesized. Trial and error via synthetic chemistry is both time and resource intensive. The potential to bias that work towards more promising targets could significantly speed up development of photocages that exhibit more advantageous absorption properties. The question of whether standard computational methods can be used to accurately predict the absorption properties of photocages is investigated.

1.1 – TARGETED DRUG DELIVERY

Targeted drug delivery is a method for delivering bioactive molecules to specific areas within a sample. The goal is to increase the concentration of an active drug in an area of the sample while having a low concentration of the active drug everywhere else. Isolating the dose to a localized area minimizes adverse effects everywhere else.[2,3] Using targeted drug delivery, diseases such as cancer and heart disease can be more effectively treated with reduced side effects.[4,5]

The targeted delivery of drugs can be accomplished in several ways, one of them being through the use of drug delivery vehicles. Three of the main classifications of delivery vehicles currently discussed in the literature are liposomes, polymer-drug conjugates, and photocages, each of which has different properties, uses, advantages, and disadvantages. With each class, the bioactive molecules are attached to the vehicle by a chemical bond or are physically encapsulated. The vehicles then release their payload in response to different chemical or physical stimuli.

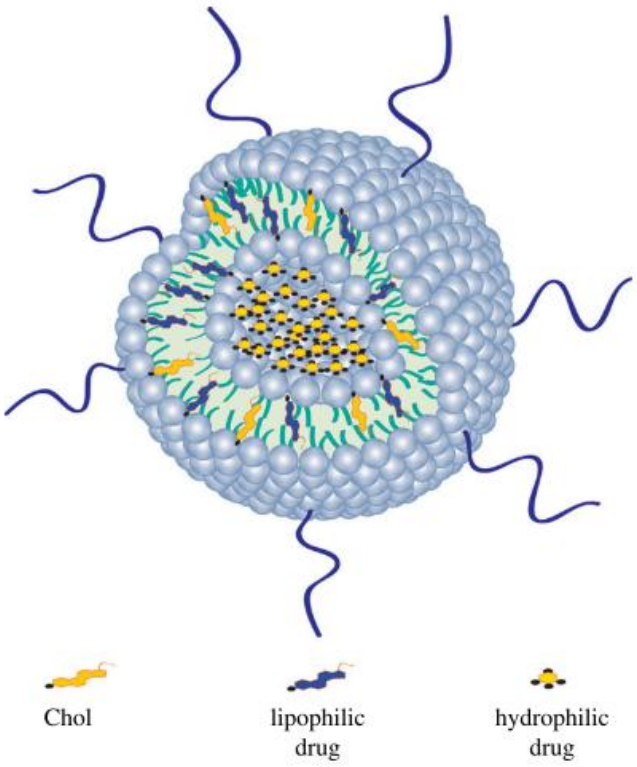

Figure 1.2: A hydrophilic drug encapsulated in the inner core of a liposome. A lipophilic drug is encapsulated in the lipid bilayer. (Reproduced from Monteiro et al.)[6]

Liposome delivery vehicles work by encapsulating a drug payload within the cavity of a liposome. Lipophilic payloads are incorporated into the phospholipid shell and hydrophyllic payloads are encapsulated within the liposome's aqueous center as shown in Figure 1.2.[7] Liposomes are known to be biocompatible and nontoxic.[8–10] Different

ligands and polymers, such as polyethylene glycol, can be attached to the surface of the liposome to increase its circulation time within a body, protect it against immune destruction, and help the liposome to interact with targeted cells by attaching to cell specific receptors.[6,7,9] The liposome then either fuses with a cell's lipid membrane or an instability is introduced in its structure causing it to liberate its payload, which is then absorbed by the cell. This instability can be caused by changes in pH, temperature, magnetic fields, or even light in some circumstances.[9,11] Some downsides of using liposomes for drug delivery are their high manufacturing cost, low shelf stability, and the need to be produced in a specialized environment.[12]

Polymers have also been studied for use in targeted drug delivery. Unlike liposomes which physically encapsulate the drug, water soluble polymer chains can be chemically attached to many drug molecules at once through biodegradable linkers.[2] Once in the body, targeting ligands on the polymer facilitate localization of the polymer-drug conjugate in the targeted site. The drug is then liberated through degradation of the linker. Linkers can be designed to be degraded in a variety of ways including, but not limited to, pH and temperature changes, interaction with enzymes, and through reduction pathways.[13] Many polymer-drug conjugates are already on the market in the form of chemotherapy drugs.[14] Polymer delivery vehicles deliver drugs in a well controlled and efficient manner, can deliver highly lipophilic drugs, and their physical and chemical properties are highly tunable. One potential disadvantage however, is that there have been reports that the polymers have been observed to be potentially toxic to cells.[15]

Photocages are another promising delivery vehicle for targeted drug delivery as they offer a way to control the release of drugs in a very small area. Like polymer-drug conjugates,

drug molecules are chemically bound to the photocage.[16] Unlike polymers however, which are larger and can bond to more than one drug molecule, photocages are typically smaller and bind to only one drug molecule. After introduction into the tissue and allowing the photocage to accumulate, the target area for delivery is then irradiated with light and the drug is released from the photocage in its active form.[17] Due to the drug being inert when attached to the PPG, only the area irradiated with light will initially contain the active drug. This allows for efficient buildup of the drug at high concentration in the target location and low concentration of the active drug in non-irradiated areas, reducing side effects. Many different photocage motifs have been published; each exhibiting different absorption and dissociation properties.

Similar to the other delivery vehicles, photocages require a trigger to release their payload. Unlike liposomes and polymers, which can liberate their payloads via temperature and pH changes, magnetic fields, etc., photocages are designed to liberate their payload only in response to light, which reduces the chances of the payload being released in unintended locations. One advantage of using photocages for drug delivery is that they offer very high spatial and temporal resolution of delivery because the light can be focused to a very small volume. Photocages are also typically less chemically complex than liposomes or polymers, a benefit when investigating structure/property relationships.

1.2 – PHOTOCAGES

The first photoremoveable protecting groups were reported in the 1960s and 1970s. Their first uses were for protecting and deprotecting products during chemical synthesis.[18–22]

Photocages being applied to biology came soon after with Engels and Schlaeger releasing cyclic adenosine monophosphate to activate enzymes.[23] This was closely followed by Kaplan with the timed release of adenosine triphosphate to activate sodium/potassium pumps in cells.[24] Today, photocages are heavily studied in medical and biology labs where they are used as a delivery vehicle for various biosensors,[25,26] fluorescent dyes,[27,28] and bioactive molecules.[29,30] Attaching a fluorescent dye, which only fluoresces when unbound, to a photocage allows for the imaging of cells and cellular structures with high spatial and temporal resolution. This ensures only areas of interest within a cell and not the cell as a whole are imaged.[31,32] Several biomolecular sensors have also been bonded to photocages and they have aided in the imaging of cells and DNA.[1,26] In medicine and medical research, photocages are used in the delivery of drugs and other bioactive molecules. Various drugs and prodrugs,[29,33–36] proteins[37,38] and peptides,[39–43] calcium and iron chelators,[44–50] RNA and DNA,[51–59] nitric oxide,[60–62] and neurotransmitters[63–68] have all been caged with PPGs and uncaged using light, often within biological samples. Because of the ability of photocages to deliver this vast array of payloads, they are a valuable tool in biochemical and medicinal research.

Figure 1.3 shows several of the more commonly used photocage structural frameworks. Many early photocages were based on an o-nitrobenzyl (o-NB) and o-nitroanilide framework.[69–74] These photocage motifs have historically been the ones most commonly used as their structure can be readily modified synthetically and they are known to be strong absorbers in the ultraviolet (UV) region.[71] Over time, photocages with higher absorption cross sections and red-shifted absorption maxima have been sought. One such group of photocages is based on a coumarin backbone and was discovered by Givens and

Matuszewski.[33,66,75–77] More recently, green and red light absorbing photocages with large one photon absorption cross sections have been synthesized such as BODIPY photocages which have even been reported to absorb light in the infrared (IR) region.[78–80]

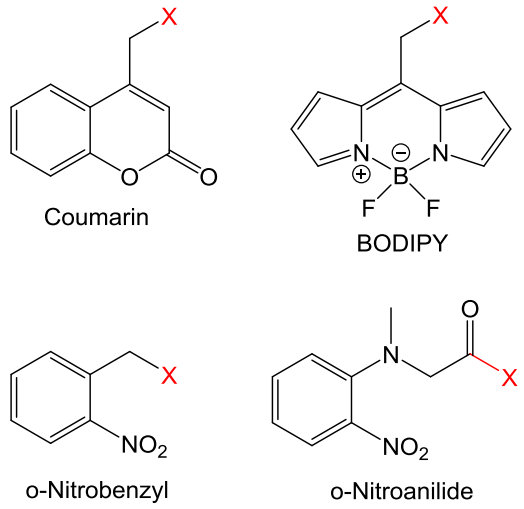

Figure 1.3: Structures for a few widely used PPGs. X indicates the position of the leaving group.

The structure of the photocage and how the leaving group is bonded to the photocage both play a large role in determining the photocage's spectral and dissociative properties. A wide variety of leaving groups have been reported to be successfully bound and released by cages of these types. Coumarin cages are typically bound through carbon-oxygen bonds.[81–83] Boron dipyromethene (BODIPY) typically bonds to leaving groups through a carbon-oxygen bond, but has been reported to bond using carbon-nitrogen and carbon-sulfur bonds as well.[84] The o-nitrobenzyl and o-nitroanilide cages have been extensively studied and they are known to bind through carbon-oxygen, carbon-nitrogen, and carbon-sulfur bonds to their leaving groups.

In 1982, a set of guiding design principles for photocages was developed by Lester et al. and are now commonly referred to as "Lester's Rules".[85] Summarizing this work:

1. For use in a biological system, a photocage must be soluble in aqueous solutions of moderately high ionic strength.
2. The photo-induced reaction must succeed within the biological system and not just in solution.
3. The photo-induced reaction should take place instantaneously with respect to the time scale of the physiological phenomenon being studied and should not create active reactive byproducts or intermediates.
4. The products of the reaction should be thermally stable in the biological system on the same time scale of the irradiation so as to produce a 'jump' in concentration of the active molecules.
5. Irradiation wavelengths longer than those which would damage tissues should be used to initiate the reaction. Reactions which use lower energy light than UV are favored.
6. The efficiency of the reaction should be high enough so as to not require very powerful sources of light. Collimated pulsed lasers and non-coherent light sources are preferable.
7. Both the precursor and photoproduct(s) should have simple, well characterized equilibrium effects on the biological system and there should be no interactions with proteins or membranes.

In summary, high concentrations of a photocage-payload conjugate in an aqueous solution should be used in conjunction with 400 nm light or longer. This conjugate should have a high dissociation quantum yield, the photo-induced

reaction should happen fast within the biological system, and the conjugate should dissociate into products which are not phototoxic to cells.

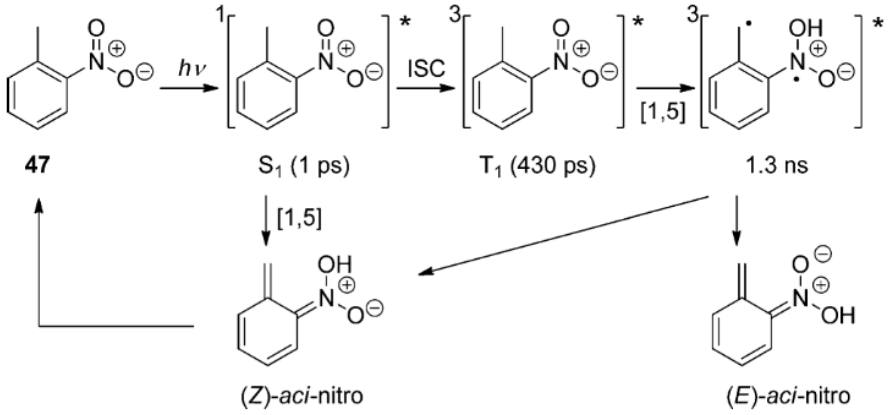

Figure 1.4: Rearrangement of an o-NB photocage after absorption of light. Reproduced from Klan et. al.[16]

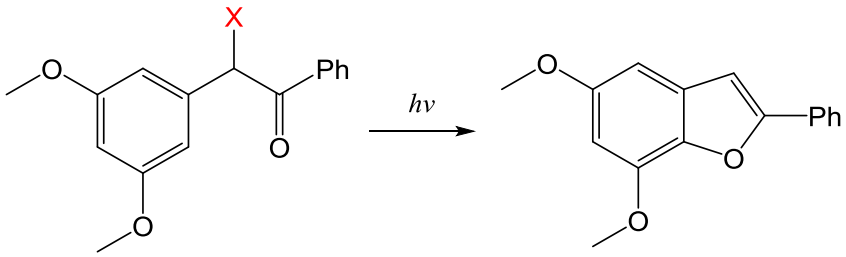

Figure 1.5: Photocyclization of a benzoin based photocage. X indicates the position of the leaving group.

Care must be taken during the design of photocages so that any products made after photolysis do not damage biological systems nor compete with the photocage-payload conjugate by absorbing the same wavelength of light. Release of the leaving group is not the only thing that can happen after a photocage absorbs light. Following release, some PPGs will undergo structural rearrangement. The o-NB groups for example have been shown to follow the rearrangement as shown in Figure 1.4 where the oxygen of the nitro group is moved to the site of the leaving group and forms a ketone or aldehyde.[86] Benzoin photocages can undergo photocyclization as shown in Figure 1.5.[87] BODIPY

compounds, which are typically designed to be used in alcohol solvents, replace the leaving group with the alcohol, bonded through the oxygen.[78] Coumarin photocages also exhibit nucleophilic substitution when a nucleophile is present in solution, much like BODIPY cages.[16] With the proper design of photocagse and the proper leaving group motif, successful release of the leaving group can be readily achieved with minimal negative effect to the system.

1.3 – TWO-PHOTON ABSORPTION AND TWO-PHOTON INDUCED DISSOCIATION

Most of the commonly used and studied photocages typically bond to leaving groups through carbon to carbon single bonds, carbon to oxygen single bonds, carbon to nitrogen single bonds, and less commonly, through carbon to sulfur single bonds. These systems typically require the energy of one blue or UV photon in order to dissociate. Recently there have been photocages reported which undergo dissociation at longer wavelengths approaching the red and near-IR regions.[79,88,89] These systems include similar bonding motifs with their leaving groups, but also exhibit a high degree of conjugation in the cage. While these can be dissociated at longer wavelengths, they typically have challenges with aqueous solubility and uncaging efficiency, especially when bonded through carbon-sulfur bonds.[84] The requirement of the high energy photons needed for the dissociation of many photocages presents significant drawbacks when PPGs are used to deliver drugs within a biological setting. Blue and UV light are limited by small tissue penetration depths (Figure 1.6).[90–92] UV light also has the potential to initiate photochemistry within the tissue itself and has been known to damage compounds found

in tissue, such as DNA.[93,94] One of the ways around these problems, is to excite the high energy transition using two lower energy photons (red or IR) instead of one higher energy photon, a process known as two-photon absorption.

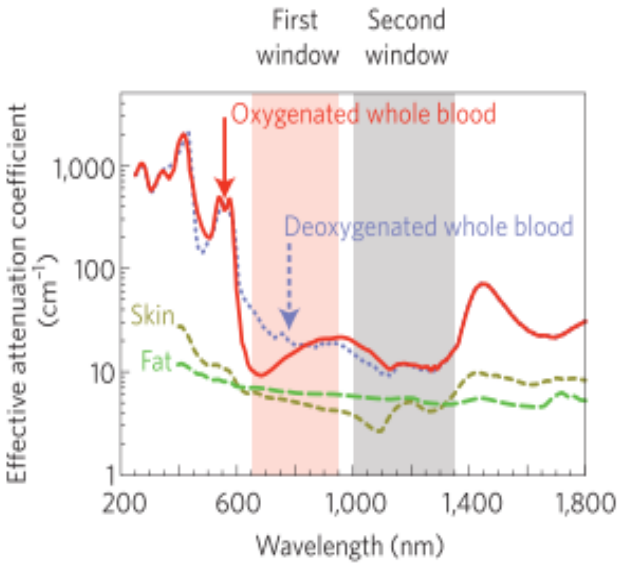

Figure 1.6: Attenuation spectra of blood and biological tissue components. (Reproduced from Smith et al.)[92]

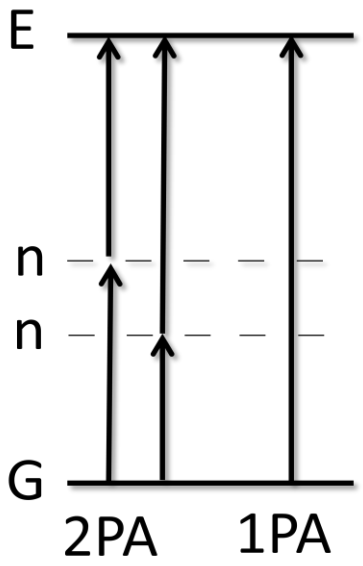

Figure 1.7: Diagram of 1PA and degenerate 2PA occurring between a ground (G) and an excited state (E) passing through a virtual state (n).

The theoretical basis of the two-photon absorption was first introduced by Maria Goeppert-Mayer in 1931[95], but the first experimental observations of 2PA didn't occur until three decades later when high intensity light sources became available.[96] In 2PA, both photons are simultaneously absorbed and the system is brought from the ground state to an excited state via a short lived intermediary state. A schematic of the difference between one-photon absorption (1PA) and 2PA is presented in Figure 1.7. In 2PA the energies of each photon can be the same (degenerate 2PA) or they can be different (nondegenerate 2PA).

The selection rules for 1PA and 2PA are different. For example, in centrosymmetric molecules, 1PA transitions are only allowed between states of the opposite inversion symmetry (gerade → ungerade or vice versa). 2PA transitions are only allowed between states of the same inversion symmetry (gerade → gerade or ungerade → ungerade).[97] For noncentrosymmetric molecules, there is no such exclusivity between 1PA and 2PA allowed transitions. A one-photon transition may occur between two states and a two-photon transition can happen between those two states as well. The relative absorption intensity, or cross section, for each state may be different, however. It is for this reason that 1PA and 2PA spectra may look different, as the probability to excite to higher lying states is governed by different selection rules.

The two-photon absorption cross sections for most molecules are about 30 orders of magnitude lower than their one-photon absorption cross sections.[98–100] This is reflected by the common unit for 2PA cross section, 10^{-50} cm^4 s $molecule^{-1}$ $photon^{-1}$, or the Goeppert-Mayer (GM). The rate at which two-photon absorption occurs, R_{2PA}, is proportional to the square of the total incident light intensity, I: $R_{2PA} \propto I^2$. So, as the

intensity increases, the rate of two-photon absorption increases quadratically. With high powered, ultrafast lasers, high enough intensities can be reached to allow for the measurement of 2PA.

Another benefit gained by using two-photon absorption is that it is possible to get three-dimensional control over the interaction volume. The interaction volume is the volume in which 2PA occurs within a sample due to a single tightly focused laser beam or two spatially overlapped laser beams. At the focal point of a laser beam or at the crossing of two laser beams, intensity is much higher than at other areas along the beam(s). Due to the quadratic dependence of 2PA on the intensity of incident light, 2PA is amplified at this crossing or focal point compared with along the rest of the laser beams. Thus, 2PA is tightly confined to near the laser focus in all three dimensions. This interaction volume can be very small, even femtoliter in size.[46] Because 2PA primarily happens within the interaction volume, absorption and dissociation can be spatially controlled in three dimensions by translating the focal point or crossing of the light in the sample.[101] This is advantageous in many situations, especially when using two-photon absorption to probe biological systems. An application utilizing this three dimensional control with 2PA is two-photon fluorescence microscopy (2PFM).[102–105] 2PFM is an imaging technique which uses 2PA to excite a fluorophore in a very small interaction volume. Since the two lower energy photons are nonresonant with the sample they are not individually absorbed, but they can be simultaneously absorbed within the interaction volume. The interaction volume can then be moved throughout a sample, the resulting fluorescence detected, and the three dimensional location of the fluorescent tag/probe can be mapped throughout the sample.

1.4 – MEASURING TWO-PHOTON ABSORPTION

The low probability of 2PA occurring makes measuring it very difficult compared to the routine measurement of a 1PA spectrum. If the light intensity used is too low, then 2PA will not be observed, but if it is too high, higher order multi-photon absorption, scattering, and sample damage can occur, all of which will interfere with the measurement of 2PA spectra. Here we consider the most commonly used methods to measure 2PA and compare them to the approach used in this thesis. Three different methods have been reported for measuring two-photon absorption cross sections: z-scan[106–109], two-photon fluorescence[48,100,103,110–113], and broadband two-photon absorption.[114–120]

The Z-scan technique uses one laser beam and a lens that focuses the light.[107,109,121] The sample is placed on a translation stage which is set to move the sample along the z-axis, along the path of the beam. The fraction of light transmitted through the sample is determined by measuring the integrated light intensity before and after the sample. Due to the beam being focused, the intensity of the light at different z-axis positions is different. By measuring the attenuation of light as a function of the sample position along the z-axis, the two-photon cross section can be determined. Z-scan measures degenerate 2PA and the cross section at only one wavelength is measured at a time. A full spectrum can be measured by iteratively stepping the wavelength of the incident light and repeating the measurement.

Two-photon excited fluorescence (2PEF) is another common method for measuring the 2PA spectrum of a compound.[100,112,122] In this method, two photons are absorbed by a

fluorescent molecule. The resulting fluorescence, rather than attenuation of the incident beam, is detected. Like z-scan, 2PEF is typically implemented in a degenerate configuration and only one wavelength is measured at a time. In order to collect the 2PA spectrum over a range of wavelengths, 2PA measurements are individually collected and assembled into a spectrum. The requirement that the system is fluorescent excludes compounds that relax rapidly via non-radiative pathways. Particularly relevant to this thesis, this includes compounds that primarily relax via bond cleavage.

A more recently developed method is based on measuring a nondegenerate 2PA cross section over a broad range of wavelengths simultaneously.[99,116] With this method, the output of a pulsed laser is split into two separate beams, crossed, and focused into the sample. The two pulses are configured so that one has a smaller bandwidth (around 20 nm), but is more intense and the other has a larger bandwidth (hundreds of nanometers) and is less intense by around three orders of magnitude. When the two beams are spatially and temporally overlapped within the sample, one photon from the small bandwidth beam and one from the larger bandwidth beam are simultaneously absorbed. The light in the larger bandwidth pulse is dispersed into its component wavelengths and each wavelength is simultaneously detected. When the beams are overlapped, attenuation of the light from the large bandwidth pulse indicates 2PA if the attenuation is linearly dependent on the power of the short bandwidth pulse and linearly dependent on the power of the large bandwidth pulse, leaving it quadratically dependent overall. Using this method, a broadband spectrum covering ~1 eV can be measured. This was the chosen method used to measure 2PA cross sections throughout this thesis because a broadband spectrum can be collected over a short period of time and the simultaneous

measurement of all wavelengths increases confidence in the relative 2PA cross section at different wavelengths.

1.5 – DISSERTATION OVERVIEW

The relationship between the structure of two-photon chromophores and their spectroscopic properties has been studied since the first experimental example of 2PA was reported.[96] One structural motif that has been discovered to enhance a molecule's ability to absorb two photons is a combination of electron donor (D) and acceptor groups (A) with a conjugated π system linking them; D – π – D, D – π – A, or A – π – A.[123] It has been found that the electron donating and accepting strength of these groups influences the two-photon cross sections.[124,125] The spatial extent of conjugation within the chromophore has an impact on the cross section, with longer conjugation in a molecule leading to the stronger two-photon absorption.[126]

Few studies have been published on correlating the structure of the photocage with its dissociation properties. The dynamics of dissociation, the fraction of leaving groups that initially dissociate after light is absorbed and the fraction of leaving groups that geminately recombine with the photocage after dissociation both influence the overall dissociation rate of photocages. The extent to which both of these quantities independently affect the total dissociation rate is not well known. By understanding how changes in structure affect the dissociation dynamics as well as the absorption cross section, photocages can be designed that exhibit both larger cross sections and faster, more efficient dissociation leading to greater overall efficiency.

The chromophore used in this research was nitrodibenzofuran, NDBF (Figure 1.8), a promising new class in the o-NB family of photocages.[127] This photocage exhibits one and two-photon absorption around 300-400 nm and is known to efficiently release leaving groups through cleavage of C-S bonds. NDBF provides synthetic access to caged thiols and cystine containing proteins, something that many other photocages cannot do.[128] NDBF is well suited to structural modification and exhibits different properties with different substituents and leaving groups attached to it.[129,130] The effect that structural changes have on the 2PA cross section and dissociation properties of NDBF has not been thoroughly studied. It is also not known to what extent the 2PA cross section and dissociation quantum yield have in determining the dissociation rate of NDBF. NDBF has been the subject of a few computational studies and it has been reported to have strong redshifts in its 1PA and 2PA spectra with the addition of various substituents to the conjugated core.[129,131] Few computational studies however, compare computational results to experimental data. Many which test the accuracy of various computational methods do so using more complex and rigorous theoretical methods as a benchmark. This thesis compares the 2PA cross sections obtained from computational methods to experimentally measured cross sections to better gauge the accuracy of the methods.

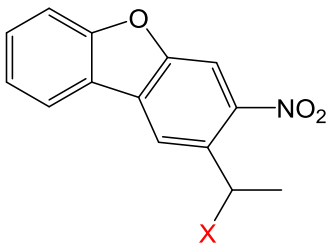

Figure 1.8: General structure for the NDBF photocage. X denotes the site of the leaving group.

In Chapter 2 of this thesis, I describe the methods used for calculating 1PA and 2PA spectra and why these methods were chosen. In Chapter 3, using a series of NDBF derivatives, I investigate the effect that structural modifications have on the spectroscopic and dissociation properties of the photocage and whether computationally efficient calculations can be used to predict 2PA properties. In chapter 4, I investigate whether or not the choice of leaving group affects these properties and whether the leaving group itself can act as a chromophore. Chapter 5 investigates the dissociation dynamics of a series of NDBF photocages. Finally, chapter 6 describes using the computational methods tested in this thesis to explore the effects that various modifications have on the NDBF photocage and if increased 2PA cross sections and lower energy absorption maxima can be predicted to identify potential synthetic targets for future studies. Strong electron donating and accpeting groups added to the backbone of the photocage, as well as substituting the oxygen in the central furan ring with a sulfur, nitrogen, and carbon are explored.

Chapter 2

Calculation of 2PA Cross Sections

2.1 – INTRODUCTION

In this research, calculations were performed on many NDBF derivatives to investigate how accurately computationally efficient methods predict absolute 2PA cross sections. These calculations were also used as a guide to interpret experimental observations. Calculations of excitation energies and transition probabilities have long been used to supplement experimental results, yielding information about the nature of the transitions between states and helping to interpret spectroscopic observables. This chapter describes how one and two-photon transitions were calculated for a variety of molecules. A better understanding of the methods informs the value, limitations, and accuracy of 2PA computational predictions. Methods known to accurately predict 1PA and 2PA spectra can be a powerful tool to inform the design of future molecules, saving time and resources by only pursuing molecules that are likely to be effective in photocaging applications.

To date, several different methods have been reported to calculate two-photon absorption cross sections. Quadratic response theory in conjunction with wavefunction based methods, such as coupled cluster-equation of motion, have been previously reported to accurately calculate transition energies and 2PA cross sections to within 10% of those

calculated using higher levels of theory.[132–135] This accuracy, however, comes with the drawback of higher computational cost.[136] Density functional theory (DFT) combined with nonlinear response theory is also used for calculating 2PA cross sections with a lower computational cost and greater accessibility.[137] The accuracy of many different functionals and basis set combinations have been benchmarked against higher levels of theory and experiment.[138] The B3LYP and CAM-B3LYP functionals have been reported to produce results for low lying excited states with accuracy (when compared to experiment) similar to that for more complex functional like M05-2X, but with less accuracy for higher lying excited states.[139,140] Due to the reduction in accuracy associated with calculating 2PA cross sections for higher lying excited states, Salem and Brown have suggested using DFT only as method for determining the energies and absolute 2PA cross sections of the lower lying excited states.[141] When compared to the B3LYP functional, CAM-B3LYP has been reported to produce more accurate results for calculations involving charge transfer states.[142]

Nayyar *et. al.* compared calculated 2PA cross sections using the B3LYP functional, CAM-B3LYP functional, and several more complex functional to experimental values for a variety of oligophenylvinylenes.[139] They found that the M05 functional and B3LYP functional outperformed the other functionals when compared to experiment. The other functionals, including CAM-B3LYP, predicted energies higher than what was experimentally measured by almost 1 eV in some cases. These predictions also had greater error in absolute 2PA cross sections than B3LYP. Due to the B3LYP functional predicting more accurate excitation energies and cross sections when compared to other functional, and its low computational cost, it was chosen as the functional for this work.

The choice of the B3LYP functional for 2PA calculations was further supported by the fact that the molecules studied by Nayyar[139] and shown in Figure 1 are of a similar size and exhibit roughly the same degree of conjugation as the molecules studied in this work. The more complex functional, M05, was not chosen as it is less computationally efficient than B3LYP for calculating 2PA cross sections of larger molecules while offering a similar degree of accuracy.

The calculations completed during this research followed previously established methods.[118,129,143–145] Briefly, the ground state geometries of all molecules were optimized with DFT in Guassian 16[146] using the B3LYP[147–149] functional and the 6-31G(d)[150,151] basis set. The influence of the solvent (DMSO or water in most cases) was modeled using an IEFPCM solvent model.[152] The Dalton[153] quantum chemistry program was used to calculate the one and two-photon transitions using the same functional and basis set. To simulate spectral broadening, a 0.4 eV wide (FWHM) Gaussian function was convoluted over each transition.

It should be noted that Dalton uses two different implementations of the B3LYP functional. The functional, B3LYP, implemented in Dalton differs from the B3LYP functional as implemented in Gaussian 16. The difference arises because the two programs treat electron correlation using different equations.[147,153,154] Dalton however has implemented the B3LYPg functional which implements electron correlation the way Gaussian implements it. This functional, however, has not been tested by the developers of Dalton. Thus, a comparison of calculations using the two functional, B3LYP and B3LYPg is made later in this chapter.

2.2 – CALCULATING 1PA SPECTRA

One-photon absorption (1PA) spectra were calculated using DFT in conjunction with linear response theory as implemented in Dalton to calculate the oscillator strength (dimensionless), *f*, for electronic excitations between a ground state, |g>, and an excited state, |*f*> (Equation 2.1).[155,156]

$$f = \frac{2*\omega_{f}*\left|D_{gf}\right|^{2}}{3} \tag{2.1}$$

In Equation 1, ω_f is the excitation energy of the g → *f* transition in atomic units (Hartree) and D_{gf} is defined by Equation 2.2.

$$D_{gf} = \sqrt{\sum_{\alpha}|\langle g|\widehat{\mu_{\alpha}}|f\rangle|^{2}} \tag{2.2}$$

In Equation 2.2, μ_α is the α^{th} component of the transition dipole moment operator where α is the x, y, or z direction of the molecular frame of reference. The molar extinction coefficients were calculated using the Harada-Nakanishi equation (Equation 2.3).[157–159]

$$\varepsilon(\nu) = N * \frac{f}{\sigma} * e^{-(\frac{\nu-\nu_i}{\sigma})^{2}} \tag{2.3}$$

In Equation 2.3, *N* is a constant equal to $1.6198*10^4$ cm^2 eV mol^{-1}, σ is the full width at half of maximum, FWHM, of the Gaussian broadening function which is convoluted over the transition, in eV, ν is the transition energy (eV), and ν_i is the photon energy (eV). The final unit for the molar extinction coefficient is L mol^{-1} cm^{-1}.

2.3 – CALCULATING 2PA CROSS SECTIONS

The two-photon cross sections were calculated using TD-DFT in the Dalton computational chemistry package by computing the single residue of the quadratic response function for each excited state.[160,161] Dalton calculates the cross section for transitions to each excited state using Equation 2.4.

$$\sigma_{2PA} = \frac{8*\pi^3*\alpha*a_0^5*\omega^2*\delta_{2PA}}{c} * \mathrm{g}(\Gamma) \qquad (2.4)$$

In Equation 2.4, α is the fine structure constant 0.0072973525693, a_0 is the bohr radius of $5.29177210903\times10^{-9}$ cm, ω is the photon energy in hartree, c is the speed of light in cm/s, δ_{2PA} is the transition strength in atomic units, and $g(\Gamma)$ is a broadening function.[107,134,139,144,162] Two-photon transition strengths for two parallel, linearly polarized photons and rotationally averaged over isotropic molecular orientation are given by Equation 2.5 in atomic units.

$$\langle\delta_{gf}\rangle = \frac{1}{30}\sum_{ij} 2S_{ii}^{gf}(S_{jj}^{gf})^* + 4S_{ij}^{gf}(S_{ij}^{gf})^* \qquad (2.5)$$

In Equation 2.5, the g and f subscripts denote the ground state and final excited state, respectively, i and j represent the Cartesian coordinates,[144,163,164] and S is the matrix element given by Equation 2.6.[134,137,160,165,166]

$$S_{ij}^{gf} = \frac{1}{2\hbar}\sum_k \left[\frac{\langle g|\hat{e}*\hat{\mu}_i|k\rangle\langle k|\hat{e}*\hat{\mu}_j|f\rangle}{\omega_{gk}-\omega} + \frac{\langle g|\hat{e}*\hat{\mu}_j|k\rangle\langle k|\hat{e}*\hat{\mu}_i|f\rangle}{\omega_{gk}-\omega}\right] \qquad (2.6)$$

In Equation 2.6, the variable k denotes the intermediate state of the transition. The photon angular frequency and transition frequency are ω and ω_{gk}, respectively. Equation 2.6 is for the degenerate case. For the nondegenerate case, S is larger by a factor of 2.[134,165] 2PA transition moments can be calculated by directly evaluating Equation 2.6,

but this is computationally inefficient due to its slow convergence.[136,167] Due to this slow convergence Equation 2.6 is rarely evaluated directly and instead S_{ij}^{gf} and the transition dipole moments between *g* and *f* are evaluated from the single and double residues of the quadratic response function.[168]

The lineshape function, $g(\Gamma)$, in Equation 2.4 describes the broadening of the calculated excitations due to lifetime broadening and collisional dynamics in solution. Typically, a Lorentzian function is used when the calculations are done in the gas-phase (Equation 2.7) where ω is the photon energy, ω_{gf} is the excitation energy, and Γ is a broadening term describing the FWHM of the Lorentzian in Hartree.

$$g(\Gamma) = \frac{1}{\pi}\frac{\Gamma}{(2\omega-\omega_{gf})^2+\Gamma^2} \tag{2.7}$$

When double the photon energy equals the transition energy (resonant transition), Equation 2.7 reduces to Equation 2.8.

$$g(\Gamma) = \frac{1}{\pi\Gamma} \tag{2.8}$$

A Lorentzian is used as the broadening function for gas-phase calculations due to the broadening being mostly homogenous. When condensed phase calculations are considered the broadening is more heterogenous and the lineshape takes the form of a Gaussian function, Equation 2.9.

$$g(\Gamma) = \frac{\sqrt{\ln(2)}}{\sqrt{\pi}\Gamma} e^{[-\ln(2)\left(\frac{2\omega-\omega_{gf}}{\Gamma}\right)^2]} \tag{2.9}$$

When the excitation frequency equals the frequency of transition, Equation 2.9 is reduced to Equation 2.10.[134]

$$g(\Gamma) = \frac{\sqrt{\ln(2)}}{\sqrt{\pi}\Gamma} \quad (2.10)$$

The calculations completed in this work used a Gaussian lineshape, Equations 2.9 and 2.10.

2.4 – METHOD EVALUATION

To evaluate the effectiveness of the chosen computational methods at calculating 2PA cross sections, the spectra of a series of molecules were calculated and then compared to previously reported cross sections. Due to the difficulty of accurately measuring 2PA cross sections, few reliable standards have been reported. Of those reported, different techniques are oftentimes used. For this series of compounds, some were measured using the z-scan technique[107,121], some with the fluorescence based technique,[100,111,112,124] and others with the broadband 2PA technique.[115,169] This can present challenges when comparing 2PA spectra collected with different methods and using them as reference standards when more than one measurement technique is involved. Figure 2.1 gives the structure of the compounds that were used in evaluating the methods used in this work. The compounds were chosen because their 2PA cross sections were previously reported.[100,107,111,112,115,124,169] The chosen molecules were measured with a variety of 2PA techniques including z-scan, broadband 2PA, and two-photon excited fluorescence. This was intentionally done to compare the computational results to a range of cross sections collected under different experimental conditions with different experimental techniques.

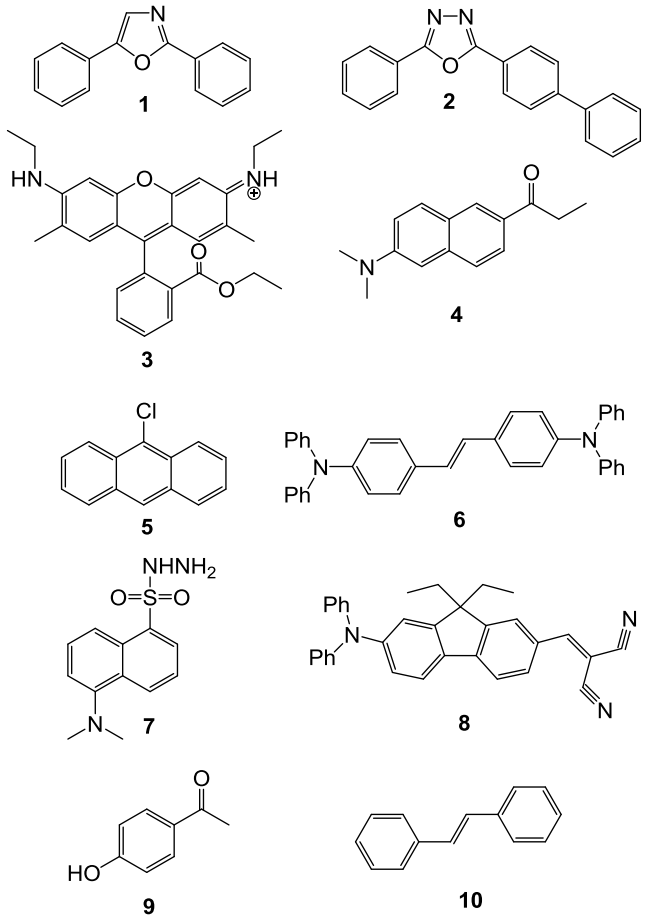

Figure 2.1: Compounds used in evaluating the accuracy and effectiveness of the computational methods.

As mentioned, the B3LYPg functional has not been fully tested in Dalton. The 2PA spectra calculated using the B3LYP functional were compared to spectra calculated using the B3LYPg functional. For both functionals, the calculated transition energies were nearly equal to one another with differences of up to 0.01 eV and the strength of the computed cross sections differed, on average, by less than half a percent. It is concluded that for this series of molecules, the results of calculations done using the B3LYPg and B3LYP functional, as implemented in Dalton, result in very similar predictions.

2.4.1 – Comparing B3LYPg Calculated Cross Sections to Measured Cross Sections

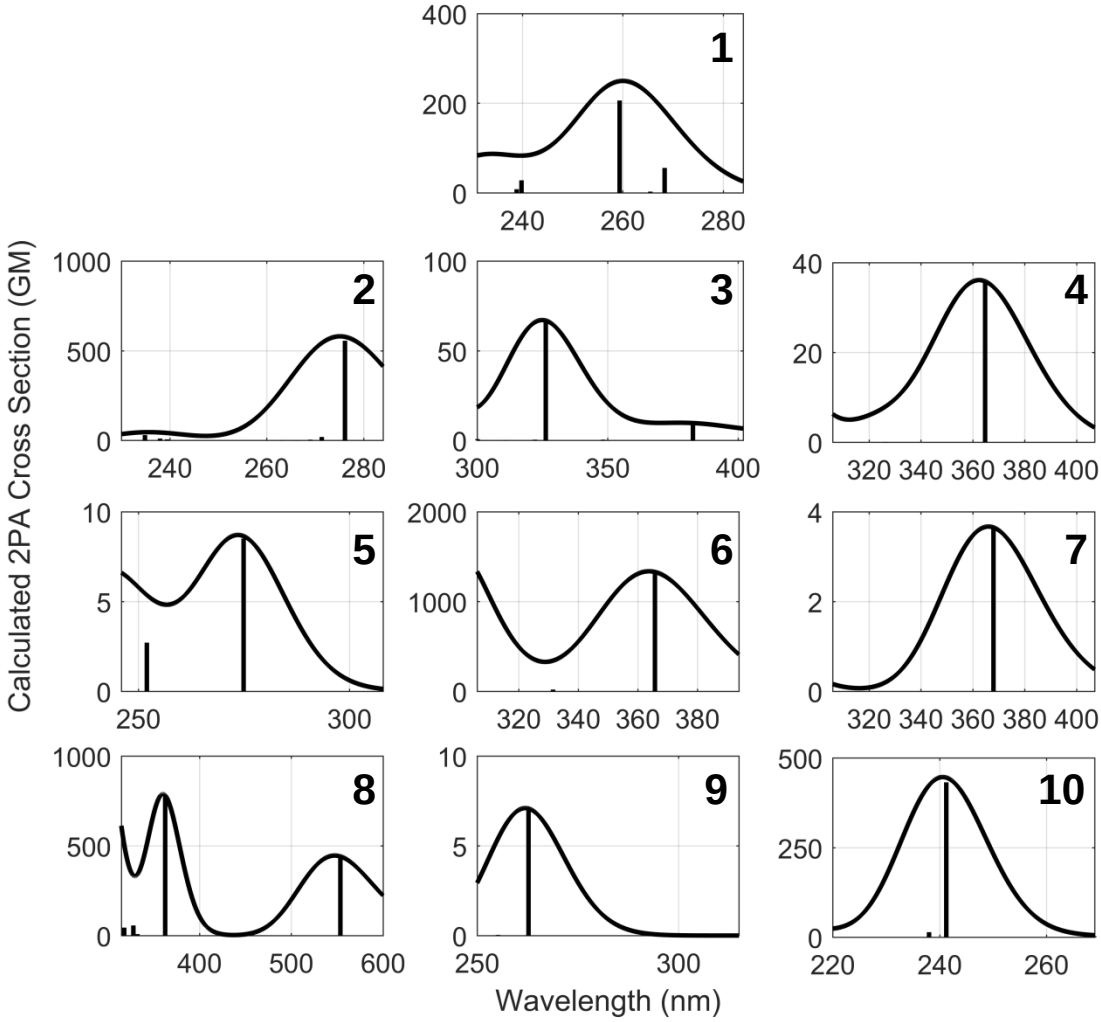

Figure 2.2: Calculated 2PA spectra of **1**-**10** using the B3LYP functional. The vertical bars represent the calculated transitions.

Figure 2.2 presents the calculated 2PA spectra for this series of compounds. The spectra shown in Figure 2.2 only show a 1 eV portion of the calculated 2PA spectra centered on the measured absorption maxima for each compound except for **8**, which shows 2 eV of the calculated spectrum. These regions were chosen to give a broad view of the calculated transitions for each compound, centered on where the compounds were experimentally measured to absorb. Table 2.1 gives the calculated 2PA absorption

maxima and cross sections at the absorption maxima within the calculated window compared to the previously measured 2PA cross sections and absorption maxima.

Compound	Measured λ_{max} (nm)	Measured 2PA Cross Section (GM) at λ_{max}	B3LYP λ_{max} (nm)	B3LYP 2PA Cross Section (GM) at λ_{max}
1	255	27	260	250
2	255	84	275	580
3	346	202	325	67
4	350	20	362	36
5	N/A	4.7	274	9
6	340	350	364	1337
7	N/A	.8	365	2.5
8	440	620	360	790
9	280	23	262	7.1
10	243	40	241	447

Table 2.1: Table of measured and calculated 2PA absorption maxima, λ_{max}, within the calculated window and 2PA cross sections at λ_{max}. Calculated data computed using the B3LYP functional.

With most molecules in this series, the calculated spectra show the presence of more than one absorption peak while in the measured spectra typically only one peak is observed within the measured spectral range. For each molecule, the calculated peak that was assigned to be responsible for the measured 2PA cross section was the absorption maximum within the 1 eV window shown in Figure 2.2. In most cases, these absorption bands were closest in energy to the measured absorption maxima. The measured absorption maximum for **8** lies in between two calculated absorption bands. The absorption band at 360 nm was assigned as being responsible for the measured peak at 440 nm as it was closer than the peak at 550 nm. The measured cross sections for **5** and **7** did not contain a peak and thus the two cross sections are compared at the absorption maximum of the calculated spectra. The average difference in energy between the

measured and calculated absorption maxima for the B3LYPg functional is 0.25 eV and the 2PA cross sections differ by an average factor of 4.5.

2.4.2 – Comparing CAM-B3LYP Calculated Cross Sections to Measured Cross Sections

One potential explanation for the differences in energy between the measured and calculated absorption maxima is that the transition energy of charge transfer/long range excitations are not accurately calculated using the B3LYP functional.[170–172] If the excitations of these molecules have charge transfer character to them, then errors of up to 1 eV are possible in the calculation of excitation energy.[173] One way around this problem is to use a functional which better takes into account long range excitations, such as CAM-B3LYP. Using the same methods as with B3LYP, but using the CAM-B3LYP functional, the calculated and measured 2PA cross sections were compared.

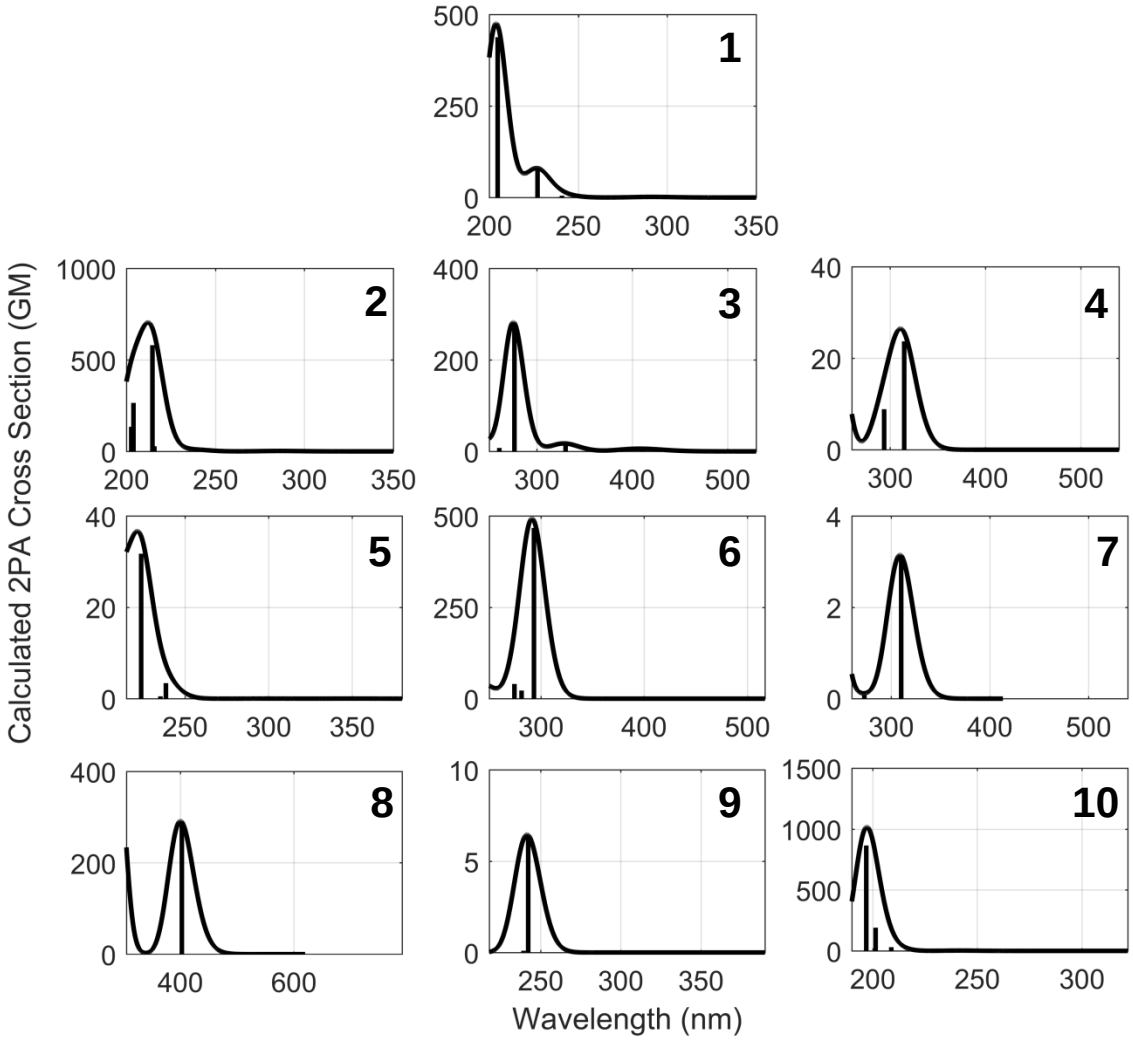

Figure 2.3: 2PA spectra of **1-10** calculated using the CAM-B3LYP functional. The vertical bars represent the calculated transitions.

Figure 2.3 shows the calculated 2PA spectra for this series of compounds calculated with the CAM-B3LYP functional. The spectra show a 2.5 eV portion of the calculated 2PA spectra centered on the measured absorption maxima for each compound. The regions shown in Figure 2.3 are wider than in Figure 2.2 because CAM-B3LYP calculates transitions which are higher in energy than B3LYPg. Table 2.2 gives the calculated 2PA absorption maxima and cross sections at the absorption maxima and the previously measured 2PA cross sections and absorption maxima.

Compound	Measured λ_{max} (nm)	Measured 2PA Cross Section (GM) at λ_{max}	CAM-B3LYP λ_{max} (nm)	CAM-B3LYP 2PA Cross Section (GM) at λ_{max}
1	255	27	204	476
2	255	84	212	705
3	346	202	275	283
4	350	20	311	26
5	N/A	4.7	222	36
6	340	350	291	493
7	N/A	0.8	309	0
8	440	620	400	292
9	280	23	242	6.5
10	243	40	197	1017

Table 2.2: Table of measured and calculated 2PA absorption maxima, λ_{max}, within the calculated window and 2PA cross sections at λ_{max}. Calculated data computed using the CAM-B3LYP functional.

As with the B3LYP functional, for each molecule, the calculated transition that was assigned to be responsible for the measured 2PA cross section was the absorption maximum within the 2.5 eV window shown in Figure 2.3. In most cases, these absorption bands were closest in energy to the measured absorption maxima. In cases of multiple transitions overlapping with each other in the same band, the absorption maximum of the whole band was assigned to the measured transition. The average difference in energy between the measured and calculated absorption maxima was 0.79 eV which is in agreement with previously published results for similarly sized molecules.[139] The magnitude of the 2PA cross sections between the measured and calculated cross sections differed, on average, by a factor of 7.65.

2.5 – CONCLUSION

Comparing the results from calculations using the B3LYPg and CAM-B3LYP functional, calculations using the B3LYPg functional are associated with smaller differences in calculated and measured absorption maxima and 2PA cross sections which are in better agreement with experimental observation than results using CAM-B3LYP. Based on the performance evaluation in this chapter, we conclude that B3LYPg is the better choice of DFT functional for predicting 2PA cross sections. This is the method that will be employed in the rest of the investigations presented in this dissertation.

Chapter 3

The Impact of Structure on the Two-Photon Absorption Cross Section and Overall Dissociation Rate of Nitrodibenzofuran Based Photocages: Calculation and Experiment

3.1 – INTRODUCTION

The ability to selectively deliver bioactive molecules with high spatial and temporal resolution has applications in many areas of chemical biology and drug delivery.[17,91,174] Photoremovable protecting groups (PPGs), or photocages, are chromophores that inhibit the bioactivity of molecules that are chemically bound to them and release an active form of those molecules following the absorption of light.[16,175,176] Most PPGs require energy equivalent to one photon in the UV region of the spectrum in order to dissociate.[17,75] This presents challenges in biological systems since UV light has limited penetration depth and can damage tissue.[92,94,177] For biological samples, there is a spectral window where absorption of light by the constituents of the sample is at a minimum, from 600 nm to 1000 nm.[92] Using light that is within this window to dissociate photocage systems ensures that damage to the system is minimized while also ensuring as much light as possible reaches the photocage. Two-photon absorption can be used to reach the energy

required to dissociate photocages while also staying within this biological window by using the combined energy of two near IR photons instead of one higher energy blue/UV photon.[112,121] In order for the 2PA approach to be effective, optimization of the 2PA cross section of 2PA-PPGs becomes very important due to the inherently small cross sections associated with 2PA.

Many structural motifs have been developed for PPGs. They include modified boron-dipyrromethene,[78,79,84] nitroaryl groups such as o-nitrobenzyl (o-NB),[69–72,178] and groups based on a coumarin core.[75,76] Many of these motifs have only been investigated as single-photon photocages, but all are also two-photon active.[179–181] The o-NB based photocages have been widely studied and are reported to release a large variety of leaving groups including carbonates, carbamates, carboxylates, alkoxides, phosphates, and thiolates.[182] They have also been reported to release two leaving groups with a single photon.[183] One drawback of many PPGs, including those based on the o-NB framework, is that they typically require a photon energy of 3.1 - 4.1 eV in order to initiate dissociation.[71,178] They have also been reported to have small two-photon dissociation cross sections, δ_p (the product of the 2PA cross section, $\sigma_{2PA,}$ and the dissociation quantum yield, $\phi_{p)}$.[46,184] Modifications made to the o-NB framework such as the addition of a second nitro group, extending the conjugated framework, and modifications made at the benzylic position and on the aromatic ring have been shown to improve absorption and increase dissicoation.[16,129] One of the more effective derivatives of o-NB, nitrodibenzofuran, has been reported to be an effective two-photon photocage, especially in the caging and delivery of thiols.[128,130,185] NDBF has been reported to exhibit stronger one and two-photon absorption cross sections and higher one-photon dissociation

quantum yields when compared to o-NB.[127] To date, there have been only a few studies investigating modified o-NB PPGs, and specifically modified NDBF, designed to increase their 2PA cross sections, dissociation rates, and redshift their absorption.[129–131] In one experiment, Becker *et. al.* investigated the effect of modifying the NDBF core by substituting dimethylamine, a strong electron donor, opposite the nitro group. They found that the 1PA and 2PA absorption maxima of the modified compound was redshifted nearly 100 nm, allowing for longer wavelength dissociation.[130] In that study, however, only the 1PA cross section of NDBF was measured. Due to the difficulty of measuring two-photon absorption compared to one-photon absorption, 1PA spectra are often used as a surrogate for what wavelengths 2PA will occur in a given molecule. However, due to the different selection rules between 1PA and 2PA, the greater the symmetry a molecule has, the larger contrast between 1PA and 2PA intensity for a given transition. As symmetry is relaxed, the contrast between 1PA and 2PA transition probabilities is relaxed.

This study involved a series of four molecules, each based on the NDBF chromophore containing the cysteamine leaving group (Figure 3.1). This series allowed us to investigate the impact that the addition of one or more electron donating methoxy groups to the chromophoric unit and extending the conjugation of the chromophoric unit had on the measured and computationally predicted 2PA spectrum of the NDBF system. There are few, if any, direct comparisons between the measured and computationally predicted 2PA cross section and two-photon induced dissociation rates of photocages. In this study, the measured 2PA cross sections are compared to two-photon induced dissociation

rates with the goal of better understanding the factors that control the overall dissociation rate of these photocages.

Computational predictions can offer insight into the nature of one and two-photon transitions as well as provide an initial understanding of the energies where these molecules are likely to absorb. The NDBF system has previously been the subject of computational study.[129] Dreuw et. al. used TDDFT/BHLYP to calculate the 2PA spectra of two NDBF photocages, without leaving groups or solvent effects included in the calculation, and found that the primary transitions of the two molecules were due to $\pi \rightarrow \pi^*$ transitions located on the conjugated core and $n \rightarrow \pi^*$ transitions localized on the nitro groups. That study also predicted a redshift in the 2PA spectrum due to the addition of an electron donating methoxy group to the core of the system.[129] Few studies have been published directly comparing 2PA calculations to measured 2PA, with fewer still using computationally efficient methods.[139,186] Canola *et. al.* used the CAM-B3LYP functional to calculate the 2PA cross sections for a variety of dyes and measured the low energy portion of the 2PA spectrum, but could not directly compare the two.[186] Nayyar, *et. al.* compared the results from DFT calculations to previously published measured Two-photon absoprtion cross sections of different oligophenylvinylenes and found that cross sections and transition energies using the B3LYP functional was in good agreement with experiment. In this study, a series of four NDBF based photocages were investigated. Two-photon absorption spectra of each compound were measured using a technique that directly measured cross sections over a broad range of wavelengths. Two-photon absorption cross sections were computed with DFT using the B3LYP functional. The measured and calculated cross sections were compared to two-photon induced

dissociation rates to better understand the factors that are involved in absorption and dissociation of the NDBF system and how the structure of the photocage changes these factors. 2PA cross sections were also compared to results from DFT calculations to assess the value that computationally efficient calculations have in predicting 2PA spectra of PPGs and to better understand the nature of 2PA transitions in the NDBF photocage.

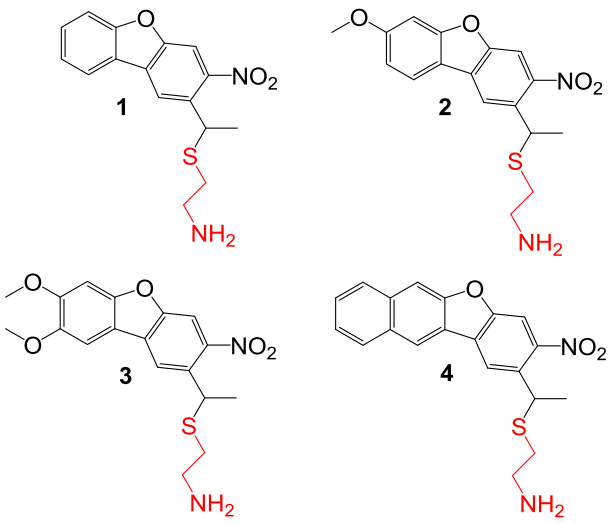

Figure 3.1: The structures of the four NDBF derivatives with the leaving group in red. The compounds in this chapter were synthesized by Dr. Feng Xu in collaboration with the Distefano Research Group at the University of Minnesota.

3.2 – EXPERIMENTAL

3.2.1 – Spectral Measurements

One-photon absorption spectra were measured for each molecule in a 1 cm quartz cuvette using a Cary 4000 UV-Vis spectrometer. All compounds were dissolved in either DMSO (for the 1PA measurements) or d6-DMSO (for the 2PA measurements). D6-DMSO was used for the 2PA measurements to reduce interference from the Raman scattering from

DMSO. The solvent Raman scattering peaks from d6-DMSO are redshifted compared to the scattering from DMSO. The broadband 2PA spectra were measured using a previously reported technique based on a broadband ultrafast pump/probe experimental setup.[118,169,187] A homebuilt, amplified, Ti:Sapph based laser system generated pulses centered at 810 nm with a FWHM of 25 nm and a repetition rate of 1 kHz.[188] After exiting the laser, the beam was split in two. The time delay between the two pulses was controlled by a mechanical delay. Waveplate/polarizer pairs were used to select polarization and attenuate the power of each pulse. A continuum from 450 nm to 750 nm was generated by focusing one beam into a 2 mm thick sapphire crystal. Both beams were independently focused and crossed within the sample. The samples were contained in a 3 mm path length quartz cuvette (Starna 23-3.45-Q-3). The temporal profile of the 25 nm bandwidth pulse was Gaussian and measured to be 70 fs (FWHM) at the sample. The diameter of this beam was imaged at the sample using a Logitech c170 webcam and the diameter was measured to have a $1/e^2$ halfwidth of 152 μm. Pulse energy of this beam ranged from 10 uJ to 30 uJ. The continuum beam was measured to have a diameter of 119 μm ($1/e^2$ halfwidth) with a pulse energy of 53 nJ at the sample. The relative polarization of the two pulses was set parallel. After passing through the sample, the white light was spectrally dispersed and detected on a linear 256 pixel photodiode array. Each group of six adjacent pixels was averaged to create an array of 42 effective pixels and a resolution of 6 nm per effective pixel.

Both of the crossing pulses were at wavelengths longer than the onset of the 1PA spectrum of all measured compounds. There was no evidence of absorption of either beam alone. Two-photon absorption only occurred when the pump and probe pulses

were spatially and temporally overlapped in the sample. The relative time delay between the two pulses was scanned ±1 ps. Outside of the temporal pulse overlap, no signal was observed. Integrating the signal over time accounted for the temporal chirp in the broadband probe and suppressed signals from cross-phase modulation.[189,190] All measurements were repeated with the neat solvent and the resulting background was subtracted from each measurement. The spectral width of the continuum, when combined with the 810 nm pump, determined the accessible experimental spectral range. In this case the experimental spectral range was the two-photon equivalent of 300 nm to 370 nm.

Equation 1 was used to convert from integrated two-photon absorption signals to 2PA cross sections using the Raman calibrated cross section for deprotonated p-hydroxyacetophenone (p-HA^-) as an external standard.[169,191]

$$\sigma_{sample} = \frac{\left[\frac{\int A_{sample}(\tau)d\tau}{E_{sample}{}^{*}N_{sample}}\right]}{\left[\frac{\int A_{standard}(\tau)d\tau}{E_{standard}{}^{*}N_{standard}}\right]} * \sigma_{standard} \qquad (3.1)$$

In Equation 3.1, σ_{sample} and $\sigma_{standard}$ are the 2PA cross section (in GM, 10^{-50} $cm^4 \cdot s \cdot molecules^{-1}$) of the sample and the standard, respectively, E_{sample} and $E_{standard}$ are the energy of the pump beam (in J) in the sample and standard experiments, respectively, N_{sample} and $N_{standard}$ are the number densities of the sample/standard (in $molecules \cdot cm^{-3}$), and $\int A_{sample/standard}(\tau)d\tau$ is the time integrated 2PA signal in OD·s for the sample and standard. The 2PA spectrum of p-HA^- was measured in the same configuration as each sample. See SI for more detail.

The 2PA cross section of each compound was also measured at 405 nm. The cross section at this specific wavelength was measured to extend the measurement out past the limit of the broadband measurement and because the dissociation rates of each compound were measured using a single beam of 810 nm laser light (405 nm combined wavelength).

Using the same configuration as the broadband measurements, in a separate experiment the continuum pulse was replaced by a duplicate of the narrow bandwidth pulse to measure the degenerate 2PA at the equivalent of 405 nm ± 12 nm. The two parallel polarized Gaussian pulses were both centered at 810 nm with a FWHM of 25 nm and pulse duration of 87 fs. One beam had a diameter of ~400 μm ($1/e^2$ halfwidth) with a pulse energy that ranged from 2.5 μJ to 30 μJ. The probe beam had a diameter of ~130 μm ($1/e^2$ halfwidth) and average pulse energy of 30 nJ. After the sample, neutral density filters were used to attenuate the intensity of the probe beam. The probe light was detected using the same method and equipment as the broadband measurements. The signal was integrated over time and the cross section was determined using the same procedure as the broadband measurements, but using the average of 6 pixels from 807 nm to 812 nm as the time integrated absorption signal for the calculation. Rhodamine B (Rhodamine 610) in methanol was used as the external 2PA standard for these measurements.[100] The gap in the 2PA cross sections between ~370 nm to 405 nm was unable to be measured due to the white light continuum becoming increasingly noisy and unusable closer to the driving fundamental at 810 nm.

3.2.2 – Determination of Dissociation Rates

For the two-photon induced dissociation rate experiments, a 1 kHz laser pulse with a pulse power between 68−76 mW was used to initiate dissociation. The pulse was centered around 810 nm with a FWHM of 12 nm. Each pulse had a Gaussian profile with a FWHM of 80 fs. This setup is described in detail elsewhere.[185] The beam was focused into the sample using a 35 cm focusing lens. 30 uL samples were irradiated in a quartz microcuvette (Starna 16.10-Q-10/Z15, 1 mm × 1 mm sample window, 10 mm path length) 15 cm after the focal plane of the lens. The irradiated samples were analyzed by HPLC-UV.

The dissociation rate experiments in this chapter were completed via collaboration with Taysir Bader and Dr. Matt Hammers from the Distefano Research Group at the University of Minnesota.

3.2.3 – Computational Methods

All molecular structures were optimized in Gaussian 16[146] using density functional theory (DFT) with the B3LYP functional[147–149] and the 6-31G(d) basis set.[150,151] An IEFPCM solvent model for DMSO was included.[152] Using the optimized structures, one and two-photon transition energies and strengths were calculated using the Dalton quantum chemistry package, which calculates the 1PA spectra using linear response theory and 2PA spectra using the quadratic response (see SI for details).[153] The 2PA calculations assume two parallel, linearly polarized photons and are rotationally averaged over an isotropic distribution of molecular orientations. The 10 lowest energy transitions were calculated and a Gaussian broadening function with a fixed 0.4 eV width (FWHM) was

convoluted over each transition. Natural Transition Orbitals (NTOs) were generated for the strongest transition of each compound using Gaussian 16.[192]

3.3 – RESULTS

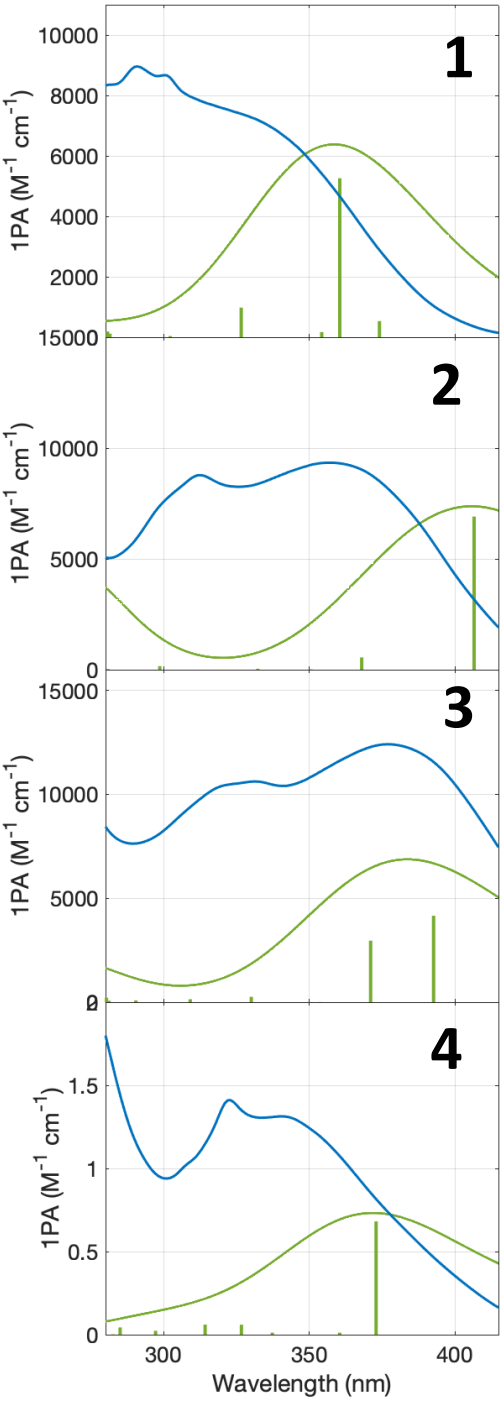

Compound	Measured 1PA λ_{max} (nm)	Measured ε ($M^{-1}cm^{-1}$) at λ_{max}	Calculated 1PA λ_{max} (nm)	Calculated ε ($M^{-1}cm^{-1}$) at λ_{max}
1	291	8960	360	6380
2	357	9340	405	7375
3	377	12410	384	6875
4	323	14100	372	7325

Figure 3.2: One-photon absorption spectra of the four compounds. The blue lines indicate the measured 1PA spectra, the vertical bars indicate calculated 1PA transitions, and the green lines show a convolution over the calculated transitions.

The dissociation rate for **1** has been previously reported and is reproduced here for comparison.[193]

Figure 3.2 presents the calculated and experimental 1PA spectra for **1**-**4**. The measured spectra exhibit broad absorption in the UV region from 300 nm to 450 nm. The addition of one or two electron donating methoxy groups to the core of the NDBF system caused a shift in the maximum absorption to longer wavelength in the 1PA spectrum of 45 nm and 70 nm, respectively, while extending the conjugation through an additional benzyl ring resulted in a 30 nm shift to longer wavelength. Compared to **1**, all of the structurally modified compounds exhibit larger molar extinction coefficients at λ_{max} with **4** exhibiting the largest molar absorptivity.

Comparing the energies of the dominant calculated transition with the measured absorption maxima, the average difference in energy is 0.34 eV. The difference between the calculated and measured molar absorptivities at λ_{max} was, on average, 30% lower than the measured values. The trends in the strength of the calculated molar absorptivities did not match the trends in measured values. In each calculated spectrum, there were one to two transitions to longer wavelength than the spectral window shown in Figure 2. For **1**, **2**, and **3**, one transition to longer wavelength was calculated. Compound **4** has two

transitions to longer wavelength that are not shown. The calculated molar absorptivities of these transitions are 10% or less than the strength of the largest transition shown within the spectral window.

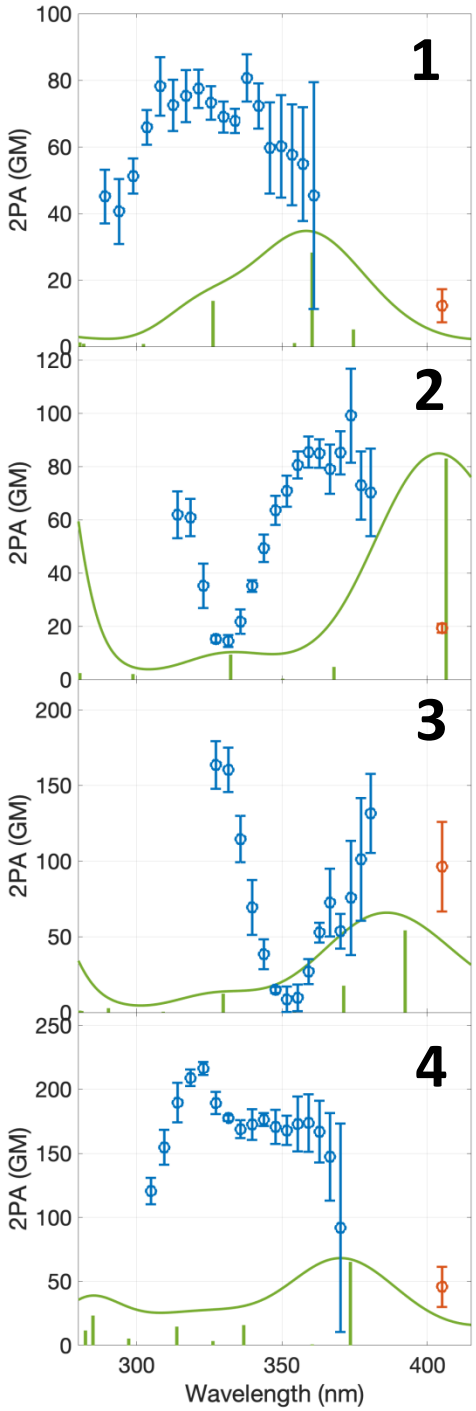

Compound	Measured 2PA λ_{max} (nm)	Measured σ_{2PA} at λ_{max} (GM)	Cross Section at 405 nm (GM)
1	330	75	12.3 ± 5.0
2	365	85	19.3 ± 1.7
3	330*	180	96.4 ± 29.6
4	330	215	45.7 ± 15.7

Figure 3.3: Two-photon absorption spectra and cross sections of the four compounds. The circles represent the measured 2PA spectra, the vertical bars represent calculated 2PA transitions, and the lines represent a Gaussian convolution over the predicted transitions. (*): The cross section did not come to a maximum, but the reported λ_{max} was the wavelength of the largest cross section measured.

The spectral range probed for these experiments was around 3.1 eV to 4.1 eV. Because two-photons were used to probe this range, the individual photon energy ranged from ~1.5 eV to ~2 eV, within the window for minimum absorption from biological samples.[92] Figure 3.3 presents the measured and calculated two-photon absorption spectra for **1**-**4**. Compound **1** exhibited broad 2PA across the experimental range of 300 – 360 nm with a maximum around 330 nm. With the addition of the methoxy group, **2**, the peak shifted 35 nm to longer wavelength. The 2PA for **2** also exhibited an absorption minimum at 330 nm with the cross section increasing to the high and low energy ends of the spectrum. The 2PA cross section for **3** increased to the high and low energy ends of the spectrum and had an absorption minimum around 353 nm. Much like the 1PA spectrum, the 2PA spectrum for **4** showed no major shift in the absorption maximum compared to **1**, but the 2PA cross section at λ_{max} was much larger than the cross section for the unmodified compound. The shifts in the wavelength regions probed between the compounds is due to variable amounts of noise in the white light continuum at wavelengths approaching the laser fundamental, 810 nm, as well as with the tail of the 1PA spectra for some compounds interfering with the low wavelength end of the 2PA measurements. Figures A1-A4 in Appendix A show the power dependence plots for the

2PA cross sections measurements for **1**-**4**. They show that the measurements for each compound depend linearly on the power of the 810 nm pulse. The additional measurements at 405 nm facilitated direct comparisons to the dissociation experiments which were measured using an 810 nm light source.

Within the spectral window shown in Figure 3.3, the calculated 2PA spectra all had absorption maxima lower in energy than the measured absorption maxima with an average energy difference between the measured and calculated 2PA absorption maxima of 0.29 eV. The calculated cross section for each compound at the absorption maximum were lower by an average factor of two. The calculated cross section for **2** was roughly equal to the measured 2PA cross section. In each calculated 2PA spectrum, there were one to two transitions to longer wavelength than the spectral window shown in Figure 3.2.

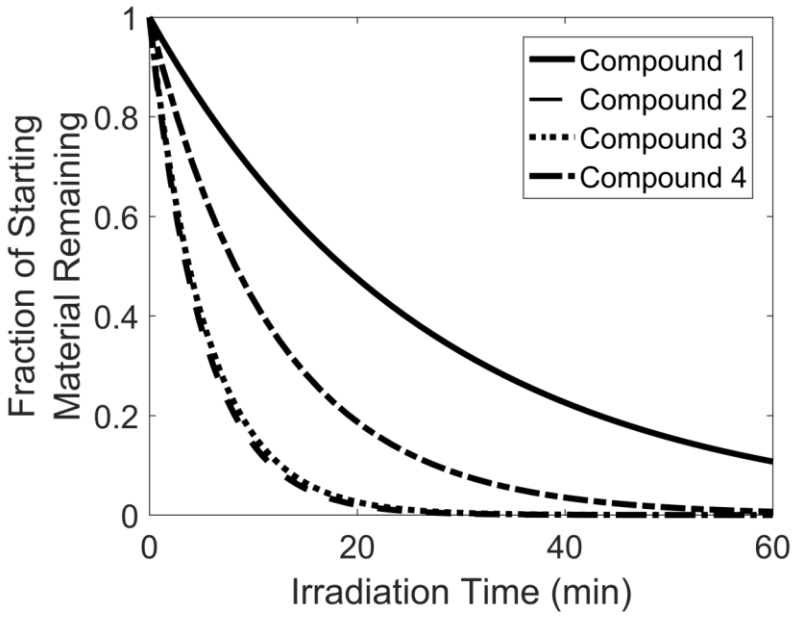

Figure 3.4: Dissociation of each compound after a given irradiation time using an 810 nm light source.

Figure 3.4 shows the fraction of starting material remaining as a function of time as the compounds are dissociated. Each of the three modifications made to the NDBF chromophore increased the dissociation rate compared to the unmodified compound with **2** and **3** being equally fast and **4** having a slower rate than **2** and **3**, but faster than **1**.

3.4 – DISCUSSION

3.4.1 – Nature of the 1PA and 2PA Transitions

For these NDBF based photocages, the second and third transitions dominated the 1PA and 2PA spectra within the measured spectral window with smaller contributions from the fourth, fifth, and sixth transitions. For **1**, transitions to the third and fifth excited state dominate. The third transition is primarily characterized as an excitation from the HOMO-1 orbital to LUMO while the fifth excited state is mostly characterized as being from HOMO-5 to LUMO (Figures A5 and A6). The spectrum for **2** was dominated by the second transition with additional contributions from the third and fourth transitions. These are characterized as primarily being from the HOMO, HOMO-3, and HOMO-2 to LUMO, respectively (Figures A7 and A8). The spectrum for **3** is primarily made up of contributions from the second, third, and fourth transitions. These transitions are from the HOMO-2, HOMO-3, and HOMO-4 orbitals to LUMO, respectively (Figures A9 and A10). The spectrum for **4** is primarily made up of third fourth and sixth transitions which are characterized as being from HOMO-2 to LUMO, HOMO-3 to LUMO, and HOMO-4 to LUMO, respectively (Figures A11 and A12). Within the spectral window, the dominant 1PA transition and dominant 2PA transition is the same for **1**, **2**, and **4**, with compound **3** being the only exception. The 1PA spectrum for this compound has

significant contribution from the second and third transition, with the second transition being slightly stronger. The fact that the dominant transitions between 1PA and 2PA spectra are similar for all compounds is unsurprising given the relaxation of the selection rules that comes with the low degree of symmetry of the NDBF photocage.

We assign the tail end of the dominant transitions for **2-4** as being responsible for the absorption in the experiments at 405 nm. The dominant calculated transition was closer in wavelength to 405 nm than all other transitions and any transition to longer wavelength of 405 nm was calculated to have a cross section lower than 7% of the dominant transition. However, in the case of **1**, the second transition also contributes to the 2PA cross section at 405 nm. This transition is characterized as being from a mixture of HOMO-3, HOMO-2, and HOMO-1 to LUMO.

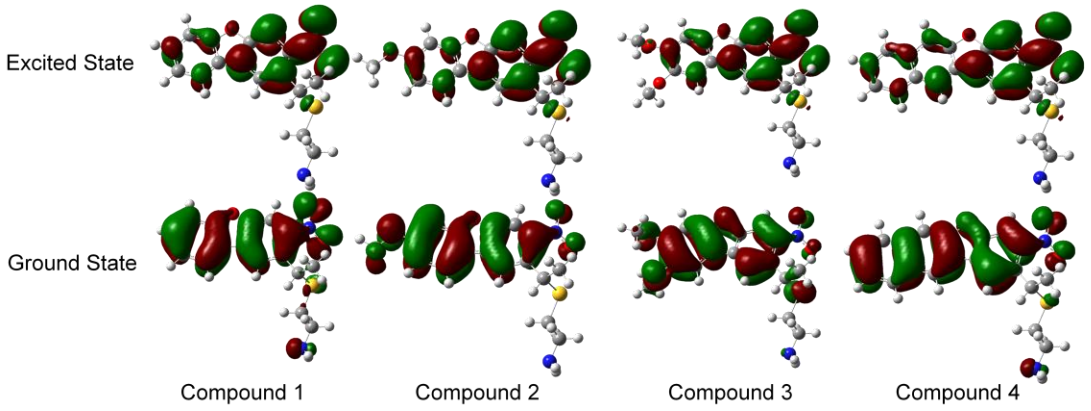

Figure 3.5: NTOs for the strongest calculated transition of each of compound within the spectral window probed.

To better understand the combined orbital character of the dominant transitions, the transitions were visualized using NTOs. Figure 3.5 presents the ground state and excited state NTOs for the dominant transition of each of the compounds. In every case, the dominant transition for each molecule is a π to π^* transition delocalized over the

conjugated backbone of the photocage. In the excited state, there was more electron density near the nitro group than on the other side of the NDBF core while in the ground state, the electron density was distributed evenly across the whole core. There was little electron density on the leaving group in either the ground or excited state NTOs for any compound which indicates that the leaving group has little involvement in the main transitions of the NDBF system. These results were consistent with what has been previously published on compounds similar to **1** and **2** and the NTO analysis indicates that the addition of a second methoxy group or conjugated ring do not significantly change the nature of the dominant transitions.[129]

A tool for characterizing the degree of charge transfer character for an excitation was proposed by Peach *et. al.* and is characterized by the variable, Λ.[173,194] The value of Λ ranges from 0 to 1 with 0 being a charge transfer excitation with no orbital overlap between the ground and excited states and a value of 1 signifies a local excitation with complete orbital overlap between the ground and excited states. Analysis of the Λ values for the dominant transitions of each compound (Table 3.1) shows Λ varying from 0.44 to 0.5 indicating transitions which are halfway between a local excitation and a charge transfer excitation. These values correlate with what is seen in the NTOs for each compound with electron density shifting towards the nitro group.

Compound (Transition)	Λ
1 (3)	0.49
2 (2)	0.48
3 (2)	0.48
4 (3)	0.50

Table 3.1: Orbital overlap values for the dominant transitions of each compound.

By extending the conjugation, **4**, the measured 1PA shifts to longer wavelengths by around 20 nm. Shifts of the absorption maxima for molecules to longer wavelengths due to extending the conjugation is well established for π to π* transitions.[195–197] The addition of an electron donating methoxy group, **2**, also causes a redshift in the one-photon absorption maxima of 40 nm. With the addition of a second methoxy group, **3**, the spectrum redshifts another 20 nm. The additions of electron donating methoxy groups and extended conjugation to the NDBF system increased the 2PA cross section in the spectral region measured. Compared to **1**, **2** exhibits an increase in the 2PA cross section of 30 GM, and a redshift of λ_{max} of 30 nm. The electron donating methoxy group together with the electron withdrawing nitro group on **2** creates a push-pull architecture on the photocage, the strength of which has been reported with other molecules to increase two-photon cross sections.[198] This is also the case with **3** which exhibits an even greater degree of charge separation due to the second methoxy group and thus a further enhancement of the 2PA cross section. The increases in 2PA cross section of **2** and **3** follow previously published trends in NDBF and similar molecules.[125,199] The large increase in the two photon cross section for **4** compared to **1** is due to the increased conjugation length and associated increased polarizability of the photocage. The transitions that dominate the 2PA spectra within the spectral region probed are characterized as π to π* transitions involving the orbitals of the conjugated NDBF core. They are very similar in character across the series with slightly more charge transfer character in **2** and **3** than **1**, and the highest σ_{2PA} in **4**.

3.4.2 – Comparison of Absorption and Dissociation

The rate of dissociation for a photocage depends, in part, on the two-photon absorption cross section and the dissociation quantum yield. We can learn about the role the 2PA cross section plays in overall dissociation by comparing it to the measured dissociation rates. If the two-photon absorption cross section at 405 nm were the only factor in determining the rate of dissociation, **3** would have a faster dissociation rate than **2** due to its 5 times larger 2PA cross section. What was measured instead was **2** and **3** exhibit very similar dissociation rates. When compared to the unmodified compound, **2** had a 5 times greater dissociation rate. This is not the only deviation from the expected trend. The cross section at 405 nm of **4** is nearly 4 times greater than compound **1**, but has a dissociation rate only twice that of the unmodified compound. The lack of direct correlation between the 2PA cross section and the dissociation rate indicates that the cross section is not the only determining factor for dissociation rate. One property that could be different between the compounds is the dissociation quantum yield; the ratio of photocages that dissociate after absorbing two photons to those that do not. One possible origin for the differences in dissociation dynamics that could impact the factors such as the geminate recombination rate would be differences in the nature of the transitions. However, the transitions are all characterized by a similar π to π^* transition. The transitions for each molecule also exhibit a similar degree of charge transfer character (Table 3.1). With no evidence of a transition into a directly dissociative state, the four compounds are likely to undergo internal conversion to the ground state followed by intermolecular vibrational energy relaxation and statistical dissociation. Differences in the dynamics of dissociation, including the fraction of geminate recombination, will

contribute to the overall dissociation rates of these compounds. The dissociation dynamics are investigated in Chapter 5.

3.4.3 – Calculation of 2PA Cross Sections

The average difference between calculated and measured two-photon absorption maxima was similar to that reported in previous studies using similar methods on similarly sized molecules.[200,201] Lower calculated molar absorbtivities using the B3LYP functional has also been reported. B3LYP is known to underestimate the oscillator strength of even small molecules such as ethylene and formaldehyde by 10%.[157,202] Similar to the 1PA calculated molar absorptivities, the calcualted 2PA cross sections are within the same order of magnitude of the measured cross sections, but are smaller by an average of 40%. These results, on average, are closer to experiment than what was reported for similarly sized where the calculated 2PA cross sections of a series of azobenzenes were an average of 50% lower than experiment.[138] The trend in the strength of the calculated 2PA cross sections differs from the trend in the strengths of the measured cross sections. This could be because to the differences in the cross sections of between the compounds are small, only differing by up to a factor of two, and thus, the trends are more challenging to accurately predict. The differences in energy between the measured and calculated absorption spectra is consistent with what is known about the B3LYP functional. B3LYP is known to be less accurate when calculating the energy of charge transfer excitations.[170–173] The primary transitions of the NDBF system have charge transfer character to them, a Λ value of ~0.5, which has been reported to cause errors in predicted energy of up to 1 eV.[173] Even given the error between measured and calculated transition

energies, the computational method used produces results which are able to guide and assist the experimental observation of 2PA.

3.5 – CONCLUSION

Studies of the structure/property relationships of photocages have been reported previously, including on the NDBF photocage.[84,131,182] These studies, however, do not investigate the relationship between the structure of a photocage, its 2PA cross section, and its dissociation dynamics. Understanding the relationship between these quantities is key to designing more photocages for more efficient photorelease. In this work, the two-photon absorption spectra of four NDBF based photocages were measured and computationally predicted and compared to two-photon induced dissociation rates. By extending the conjugation of or adding electron donating groups to the system both redshift 1PA and 2PA maxima, increase 2PA cross sections, and increase the two-photon induced dissociation rate. It was demonstrated that the strength of the 2PA cross section does not correlate with dissociation rate, indicating that the dissociation dynamics, such as the quantum yield and the rates of geminate recombination also play a role in determining the relative overall dissociation rates of the NDBF photocage.

The 1PA and 2PA calculations were a valuable tool in determining the nature of the dominant transitions of these molecules through the analysis of NTOs and charge transfer character. The predicted 1PA and 2PA spectra were all redshifted from the measured spectra. The molar absorptivities and 2PA cross sections for each molecule were

predicted to be within a factor of two which indicates these methods can be used in the future to estimate the strength and energy of two-photon transitions.

This work also emphasizes the importance of choosing the appropriate wavelength for dissociation for these photocages. The choice of wavelength is not as simple as choosing the absorption maxima of these compounds, as differing dissociation dynamics can enhance or lower overall dissociation rates. Because these compounds that have limited symmetry the 1PA and 2PA spectra are similar indicating that the 1PA spectra of NDBF photocages can be used as an initial guide to inform where they will absorb two photons.

Chapter 4

Influence Of The Leaving Group On The Absorption and Dissociation Of Photocages

4.1 – INTRODUCTION

Photocages are typically constructed with a chromophoric unit that dissociates from a biologically active constituent when photoexcited.[16,17] While bound to the chromophore, the constituent, or leaving group, is rendered inactive.[203] Photocages are frequently used in biochemistry, delivering fluorescent dyes and bioactive molecules.[26–28,31] For example, drug molecules can be attached to a photocage and then can be delivered to a biological sample with very high spatial and temporal resolution.[29,204] This allows for an increased concentration of the active molecule in a localized area while the concentration of active molecule outside the area of irradiation is left comparatively low. Photocages typically require energy equivalent to a photon in the UV or blue region of the spectrum in order to release their payload.[16] This poses particular challenges in biological applications because UV and blue photons have shorter penetration depth in tissue and can be phototoxic to DNA and cells.[49,90,92,94,104,205] A spectral window exists for biological samples where the scattering and absorption of photons by the constituents of a sample is at a minimum, from 600 nm to 1000 nm.[92] Using photons of wavelength

within this window to initiate dissociation ensures that damage to the system is minimized while also maximizing penetration depth.[126,206] Using two-photon absorption (2PA), two lower energy near-IR photons, rather than one high energy UV photon, are absorbed simultaneously by the photocage.[95,207] The probability of molecules absorbing two photons is typically low compared to one-photon absorption (1PA) and is dependent on light intensity. In more intense light fields, such as those produced by lasers, the probability of 2PA is greater.[208,209] Due to the probability of 2PA being proportional to light intensity, it will occur more in the higher intensity parts of the laser beam, such as at the focal point of a single beam or the crossing point of two beams. This means that two-photon induced dissociation can be confined to smaller volumes than one-photon dissociation and be moved three-dimensionally within a sample by moving the focal or crossing points.[46,101,210–213] A requirement for the 2PA approach to be effective is that 2PA-PPGs must be designed with high 2PA cross sections and fast dissociation rates.

Common structural motifs for photocages include BODIPY[78,86,88,214,215], those based on a coumarin core[75,81,83,216], and ortho-nitrobenzene (o-NB).[70–72,178,217] These motifs have been reported to cage and release many different leaving groups such as proteins[37,38], peptides[39,41,42], RNA and DNA,[51–53,55,56,58,59] and drugs and prodrugs.[29,33–36] Each of these motifs exhibit different spectral and dissociative properties with different cross sections, dissociation quantum yields, and dissociation rates. The focus of many experimental and computational studies has been on modifying the structure of the chromophoric unit of these motifs to increase their 2PA cross sections and enhance their dissociation rate/quantum yield.[86,129,131,176,215,218] One of the more effective modifications of the o-NB motif is nitrodibenzofuran (NDBF). NDBF exhibits stronger two-photon absorption than

o-NB and has been reported to release leaving groups bonded through a C-S bond with a high yield.[129,131,185,193,219]

Few studies have focused on the leaving group itself and its role in the dissociation process. Specifically how, if at all, they influence the amount of light absorbed or the rate at which the system dissociates. One study looked at how photocage structure and choice of the leaving group affected one-photon absorption and dissociation in BODIPY photocages.[86] The authors found that the pKa correlated with dissociation rate, with an acetate leaving group having a lower pKa and lower dissociation quantum yield compared to a chloride leaving group by a factor of ~3.5.

This work seeks to better understand the role of the leaving group in influencing the absorption and dissociation properties of photocages. A series of three leaving groups attached to two NDBF based photocages (Figure 4.1) was used to investigate how different leaving groups and bonding motifs affect the absorption of light and the dissociation rate of the NDBF system. The compounds with the different leaving groups, acetate (bonded through an oxygen), cysteamine (bonded through a sulfur), and cys-FMOC (bonded through a sulfur) were compared to a control, where the leaving group was replaced with a hydrogen atom. The fraction of photocages and leaving groups that geminately recombine could be influenced by the size and structure of the leaving group. This hypothesis is investigated by comparing the 2PA cross sections and dissociation rates between structurally large and small leaving groups. Computational results were used to assist in the interpretation of spectroscopic observables and investigate whether or not the leaving group plays an active role in the absorption of light. Broadband 2PA spectroscopy and time resolved dissociation measurements were used to measure 2PA

cross sections and dissociation rates, respectively. Comparison of these properties provides insight into the role of the leaving group in the absorption and dissociation process.

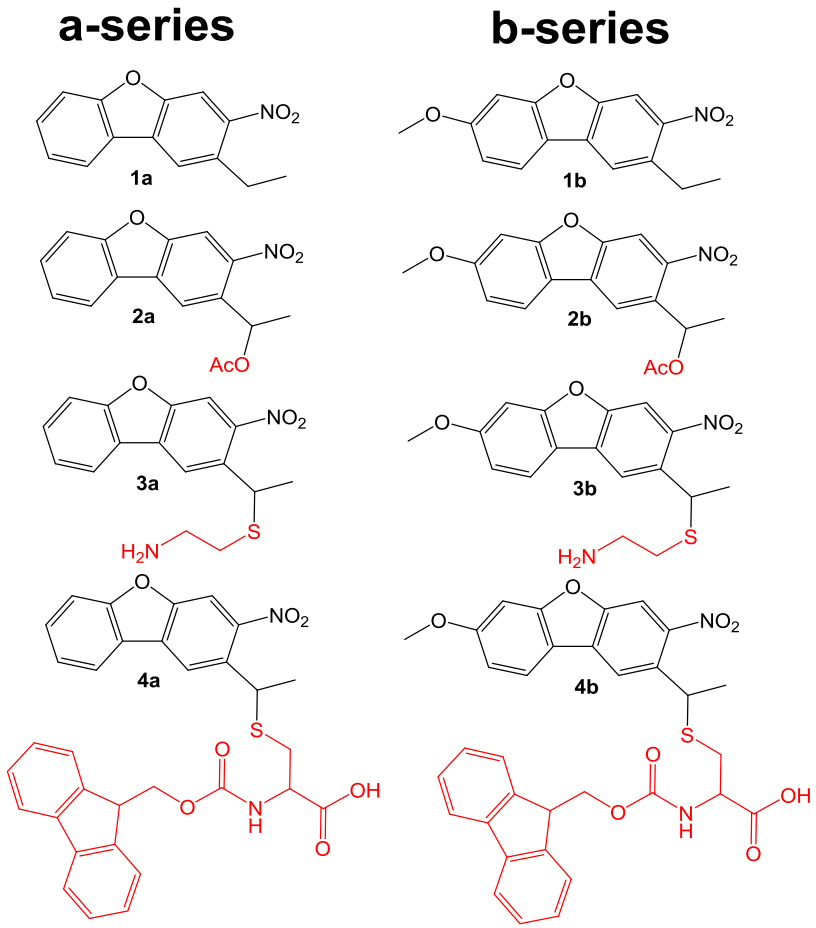

Figure 4.1: Compounds used in this work. The portions highlighted in red denote the leaving group.

To facilitate comparison, the compounds using the unmodified NDBF photocage are labeled the 'a-series' compounds and those using the methoxy modified NDBF photocage are labeled the 'b-series' compounds. The measured 1PA spectra and the one and two-photon induced dissociation rates of compounds **3a**, **3b**, **4a**, and **4b** have been previously reported or discussed in Chapter 3.[185,193] Some of the results are reproduced here to facilitate comparison between different leaving groups. The compounds were

synthesized by Dr. Feng Xu in collaboration with the Distefano Research Group at the University of Minnesota.

4.2 – EXPERIMENTAL

4.2.1 – Broadband 2PA Cross Section Measurements

One-photon absorption (1PA) spectra were measured in a 1 cm quartz cuvette using a Cary 4000 UV-Vis spectrometer. All compounds were solvated in DMSO or d6-DMSO. The broadband 2PA spectra were measured using a previously reported technique based on an ultrafast pump/probe experimental setup.[116] Briefly, a homebuilt amplified Ti:Sapph based laser system generated a pulsetrain with a 1 kHz rep rate.[188] The pulses were centered at 810 nm with a FWHM of 30 nm. The output of this laser was split into two beams. The time delay between the two pulses was controlled by a pair of mechanical stages. Waveplate/polarizer pairs were used to set the polarization of each pulse parallel to each other and attenuate the power of both pulses. A continuum from 450 nm to 750 nm was generated by focusing one beam into a 2 mm thick sapphire crystal. Both beams were then independently focused into and crossed within the sample which was contained in a 3 mm path length quartz cuvette (Starna 23-3.45-Q-3). Each pulse had a Gaussian temporal profile and was measured to be 70 fs (FWHM) at the sample. The diameter of the 810 nm beam was imaged at the sample using a Logitech c170 webcam and the width was measured to have a $1/e^2$ halfwidth of ~150 μm. Pulse energy ranged from 5 uJ to 30 uJ. The continuum beam was measured to have a diameter of ~120 μm ($1/e^2$ halfwidth) with a pulse energy of 53 nJ at the sample. After passing through the sample, the white light was dispersed and detected on a linear 256 pixel photodiode array. To improve the signal to noise, each group of six pixels was averaged

to create an array of ~42 effective pixels and a resolution of 6 nm per effective pixel. The conversion from the change in optical density (delta OD) to cross section was done using p-hydroxyacetophenone as a 2PA external standard. The conversion was the same as used in Chapter 3.

4.2.2 – Measurement of 405 nm 2PA Cross Section

2PA cross sections at 405 nm were measured using the method reported in Chapter 3. Briefly, an 810 nm laser pulse was split into two beams. The two parallel polarized beams were both centered at 810 nm and had a FWHM of 25 nm with a pulse duration of 87 fs. The diameter of one beam was around 400 μm ($1/e^2$ halfwidth) and had a pulse energy that ranged from 2.5 μJ to 30 μJ. The second beam had a diameter of around 130 μm ($1/e^2$ halfwidth) with an average pulse energy of 30 nJ. Neutral density filters were placed after the sample to attenuate the intensity of the second beam. The resultant pump-probe signal was integrated over time and the 2PA cross section was determined using the same procedure as the broadband measurements, using the average of 6 pixels from 807 nm to 812 nm as the time integrated absorption signal for the calculation. The 2PA standard used in these studies was Rhodamine B (Rhodamine 610).[100]

4.2.3 – Dissociation Experiments

To determine the two-photon induced dissociation rates of each compound, a 1 kHz laser pulse with a pulse power between 68−76 mW was used to initiate dissociation. The pulse was centered around 810 nm with a FWHM of 12 nm. Each pulse was Gaussian in time with a FWHM of 80 fs. This setup has been described in detail.[185] The beam was focused into the sample using a 35 cm focusing lens. 30 uL samples were contained in a quartz

microcuvette (Starna 16.10-Q-10/Z15, 1 mm × 1 mm sample window, 10 mm path length) and irradiated 15 cm after the focal plane of the lens. The irradiated samples were analyzed by HPLC-UV for a series of increasing exposure times.

The dissociation rates were measured by Taysir Bader in our collaboration with the Distefano Research Group at the University of Minnesota.

4.2.4 – Computational Methods

The methods for calculating 1PA and 2PA cross sections are the same as reported in Chapters 2 and 3. Briefly, the structure of each compound was optimized in Gaussian 16[146] using DFT with the B3LYP[147–149] functional, the 6-31G(d) basis set[150,151], and an IEFPCM solvent model for DMSO.[152] The Dalton quantum chemistry program[153] was used to calculate the excitation energies and one and two-photon cross sections. The calculations of 2PA cross section assumed two parallel, linearly polarized photons and were rotationally averaged over an isotropic distribution of molecular orientations. Natural Transition Orbitals (NTOs) were generated in Gaussian to visualize the orbitals involved in the transitions for each compound.[192]

4.3 – RESULTS

The 1PA spectra and two-photon induced dissociation of **3a**, **4a**, and **4b** have been previously reported are reproduced here for comparison and reference.[185,193]

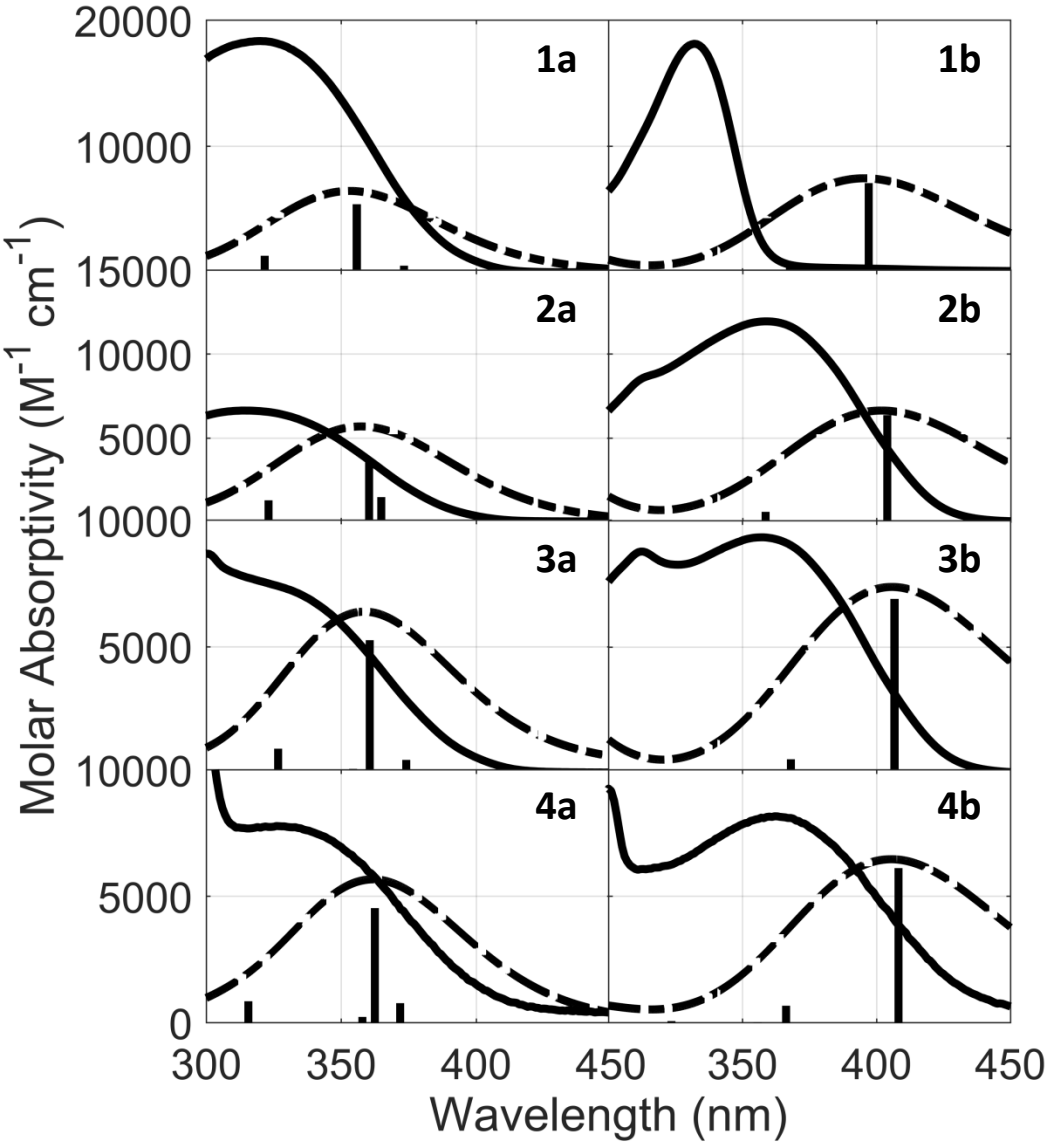

Figure 4.2: Measured and calculated 1PA spectra of the 8 compounds. The solid trace is the measured spectrum, the vertical bars represent the calculated transitions, and the dashed line is a convolution over the calculated transitions.

Figure 4.2 presents the one-photon absorption spectra of the 8 compounds. The a-series compounds all exhibited broad absorption in the UV region from <300 nm to 400 nm and had an absorption maxima around 325 nm. The b-series compounds also exhibited broad absorption in the UV region from 300 nm to 450 nm with the exception of **1b,** which had

a maximum at 332 nm that quickly falls to zero at 375 nm. Compounds **2b**, **3b**, and **4b** had an absorption maximum around 360 nm. The compounds without leaving groups, **1a** and **1b,** had a large and roughly equal molar absorptivity at their maxima, ~18,000 $M^{-1}cm^{-1}$. The compounds with acetate leaving groups exhibited differing levels of absorption. Compound **2a** had a maximum molar absorptivity of 6630 $M^{-1}cm^{-1}$ and **2b** had an absorptivity nearly double that, 11940 $M^{-1}cm^{-1}$. Both cysteamine containing photocages had roughly the same absorptivity with **3a** increasing to higher energy and **3b** having a maximum of 9340 $M^{-1}cm^{-1}$. Compounds **4a** and **4b** had roughly the same absorptivity at their respective maxima of around 8000 $M^{-1}cm^{-1}$.

For the compounds with leaving groups, the calculated molar absorptivities were on average, 30% lower than the measured values. The calculated transitions were redshifted by an average of ~40 nm when compared to the measured absorption maxima. The molar absorptivity of the control compounds, **1a** and **1b**, were on average 60% lower than the measured values. The calculated absorption maximum for **1a** was ~30 nm redshifted from the measured absorption maximum. Compound **1b** had a calculated absorption maximum that is redshifted from the measured maximum by ~70 nm.

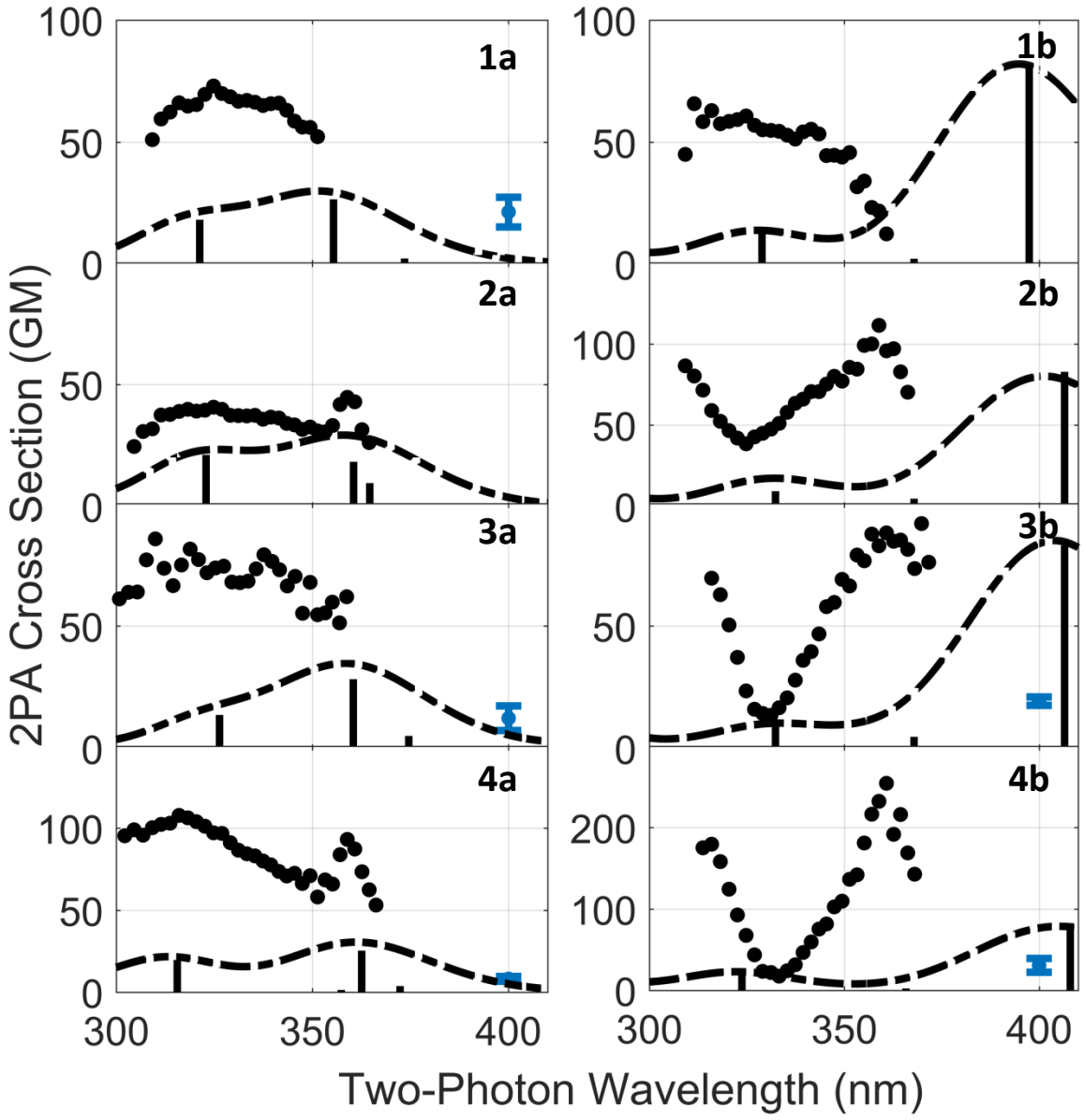

Figure 4.3: Measured and calculated 1PA spectra of the 8 compounds. The solid trace is the measured spectrum, the vertical bars represent the calculated transitions, and the dashed line is a convolution over the calculated transitions.

The measured and calculated 2PA cross sections of each compound within the window of interest are presented in Figure 4.3. The a-series compounds exhibited broad absorption over the probed range of 300 nm to 370 nm and absorption maxima around 330 nm. The maximum 2PA cross section for these compounds ranged from just under 50 GM to just

over 100 GM with **4a** exhibiting the largest cross section, 108 GM. Compounds **2a** and **4a** both showed the presence of an additional absorption peak at 360 nm. The shape of the spectrum for the b-series compounds is markedly different than for the a-series. Compounds **2b**, **3b**, and **4b** each had an absorption minimum at 330 nm with increasing absorption to the high and low energy ends of the spectrum and an absorption maximum around 360 nm. The cross sections of **2b** and **3b** were 110 GM and 90 GM respectively. Compound **1b** however, exhibited a very similar spectrum to that of **1a** with an absorption maximum around 330 nm and a max cross section of 61 GM.

Compound	Cross Section (GM)
1a	21.3 ± 6.1
1b	<8.2
2a	<8.2
2b	<8.2
3a	12.3 ± 5.0
3b	19.3 ± 1.7
4a	8.2 ± 1.4
4b	30.8 ± 8.3

Table 4.1: 2PA cross section values at 405 nm.

Table 1 presents the 2PA cross section at 405 nm for each compound. The 2PA cross section at 405 nm of **1b**, **2a** and **2b** were below the detection limits for our experimental setup, ~8 GM. The lowest measured cross section was 8.2 GM for **4a**. The measurements at 405 nm (two-photon equivalent) extended the range probed and facilitated comparisons to the dissociation experiments which were measured using an 810 nm light source.

Figures B1-B8 show the power dependence for the 2PA cross sections measurements for each compound. The cross sections for each compound depended linearly on the power

of the 810 nm pump pulse as expected for a two-photon excitation involving one photon each from the pump and probe beams.

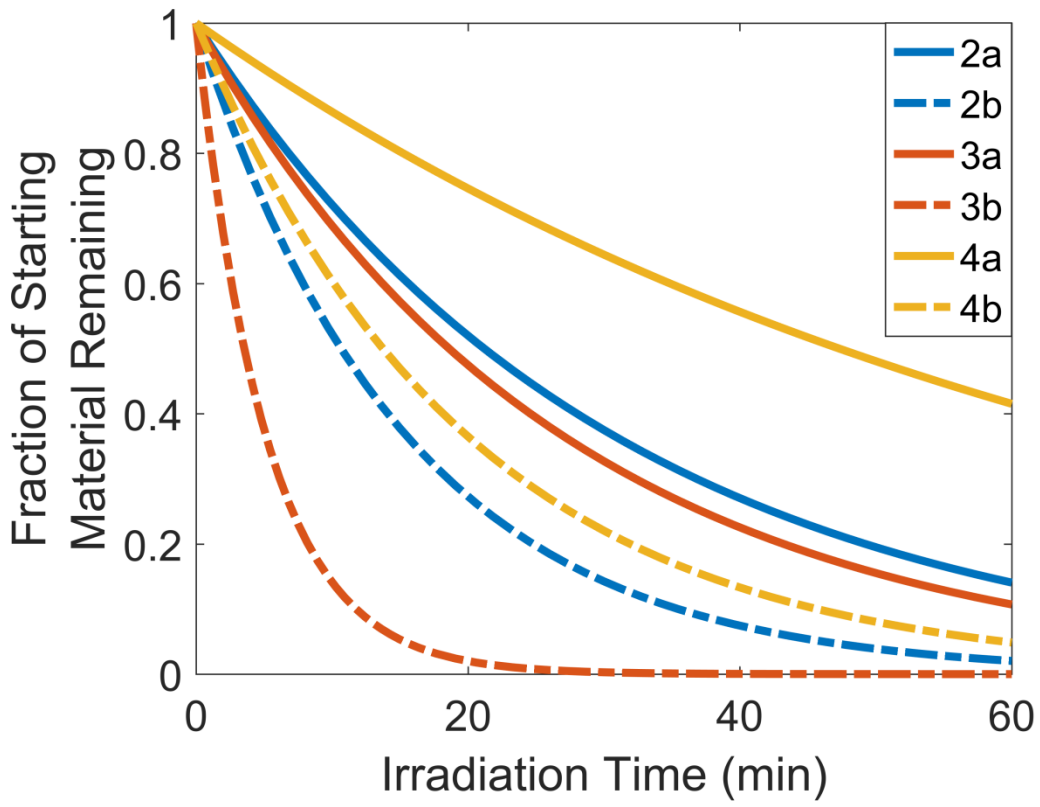

Figure 4.4: Two-photon induced dissociation over time using 810 nm light.

Figure 4.4 presents the rate of dissociation for the compounds with leaving groups. A general trend is that the b-series compounds dissociated faster than the a-series compounds. The compounds with the cysteamine leaving group, **3a** and **3b** dissociated the fastest compared to the others in their respective series and the compounds with cys-FMOC leaving groups dissociated the slowest.

4.4 – DISCUSSION

4.4.1 – Nature of the 1PA and 2PA Transitions

For each of these 8 compounds, the first, second, and third transitions dominated the spectra within measured window from 300 nm to 400 nm. These transitions are from the HOMO, HOMO-1, HOMO-2, and HOMO-3 to the LUMO (Figures B9-B17) and are characterized as involving orbitals delocalized across the conjugated π system of the NDBF core with a few orbitals from some compounds exhibiting electron density on the leaving groups. For **1a**, **1b**, **2a**, and **2b** the dominant transitions are characterized by being mostly from the HOMO or HOMO-1 orbitals to the LUMO and are from orbitals evenly distributed across the NDBF core to orbitals delocalized across the core, but with electron density shifted towards the nitro group. Compounds **3a**, **4a**, and **4b** are dominated by transitions from the HOMO-1 to the LUMO. These orbitals are characterized as being similar to the orbitals for **1a**-**2b**. While the dominant transition for **3b** is also from the HOMO-1 to LUMO orbitals, the HOMO-1 orbital for this compound is characterized as having substantial electron density on both the NDBF core and on the cysteamine leaving group. Many of the higher energy transitions for each of these compounds also had contributions from orbitals with electron density on the leaving group. These orbitals do not greatly influence the 1PA spectra because only one of the lower energy transitions dominate the spectra for these compounds. For many of the a-series compounds, however, the 2PA spectra within the measured window are influenced by both the lower and higher energy transitions. At 405 nm, the cross section for both series is not significantly influenced by the leaving group with the exception of **3b**.

Within the measured spectral window, we assign the strongest calculated transition(s) as being responsible for the measured 1PA and 2PA spectra. For the a-series compounds, the tail of the transitions at ~360 nm and ~370 nm are assigned as being responsible for the 2PA cross section at 405 nm because those transitions are closest in energy to 405 nm and exhibit the strongest absorption. No strong transition lower in energy than 405 nm was predicted that is >10% the strength of the 360 nm transition for any compound. For the b-series compounds, the dominant transition closest to 405 nm is assigned as being responsible for the 2PA cross section at 405 nm.

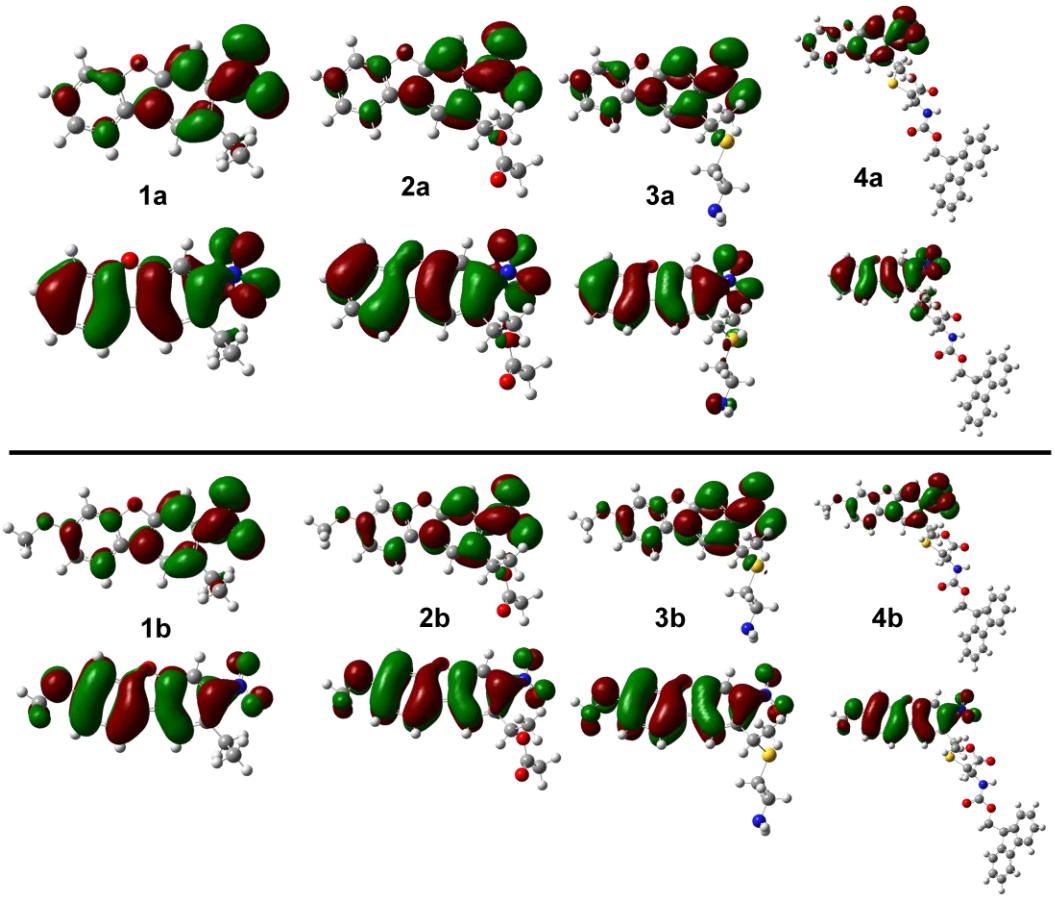

Figure 4.5: Ground state and excited state NTOs for the dominant transition for each compound.

Figure 4.5 presents the ground state and excited state NTOs for the strongest calculated transition of each compound within the window of interest. For each compound, the dominant transition is characterized as being a π to π* transition to and from orbitals delocalized across the conjugated NDBF core with electron density shifting towards the nitro group. The shift in electron density is likely due to the electron withdrawing ability of the nitro group as well as the electron donating ability of the methoxy group in the case of the b-series compounds. The NTOs for each compound show little to no electron density on the leaving groups. This is consistent with what has been previously published about the NDBF system and indicates that the choice of leaving group does not greatly influence the nature of 1PA and 2PA transitions for these NDBF systems.[129]

Differences in the amount of charge transfer for the dominant transitions between the compounds could contribute to the differences seen in the cross section and absorption maxima for the 1PA and 2PA spectra. The degree of charge transfer character of a transition can be determined by using a procedure reported by Peach *et. al.* and is evaluated by determining the orbital overlap between the ground and excited state orbitals.[173] This quantity is symbolized as Λ, and ranges between 0 and 1 with 1 being a local excitation with total overlap between ground and excited state electron density and 0 being a charge transfer excitation with no overlap between ground and excited states orbitals. Table 4.2 gives the values of Λ for the dominant transitions of each compound.

Compound	**1a**	**1b**	**2a**	**2b**	**3a**	**3b**	**4a**	**4b**
Λ	0.5806	0.5140	0.5195	0.4965	0.4918	0.4821	0.4933	0.4873

Table 4.2: Orbital overlap of the dominant transition in each compound.

With each leaving group, the b-series compounds exhibited slightly more charge transfer character than the a-series compounds, likely due to the additional electron-donating methoxy group on the NDBF core. The values for each compound indicated that the dominant transitions had a significant degree of charge transfer character, with **1a** having the least. Even though the compounds had very similar charge transfer character to one another, modest differences in the degree of charge transfer could be a contributor to the modest differences seen in the 1PA and 2PA cross sections of between the compounds.

4.4.2 – Comparison of 2PA Cross Sections and Dissociation

The absorption cross section is not the only factor in evaluating the effectiveness of a photocage. The overall dissociation quantum yield also plays role and influences the overall dissociation rate. Several variables factor into the overall dissociation quantum yield of a photocage after it absorbs light such as the fraction of photocages that initially dissociate and the fraction that geminately recombine after dissociating. The 2PA cross sections for these compounds differ by up to a factor of two, however the nature of the absorption changes very little between the compounds. The observed trends in the strength of the 2PA cross section at 405 nm and in the overall dissociation rates were different for these compounds. There was also no consistent correlation between the strength of 2PA cross section or dissociation rate and the bonding motif of the leaving group, whether bonded through oxygen or sulfur. Comparing the dissociation rates of the compounds within their respective series, **3a** and **3b**, with cysteamine leaving groups, were observed to dissociate faster than the compounds with the other leaving groups by a factor of 3-4. However, these compounds did not exhibit the highest 2PA cross section at 405 nm within their respective series.

Comparing **2a** and **2b** with **3a** and **3b**, respectively, the larger overall dissociation rate of the compounds with cysteamine leaving group could be due to the differing bonding motifs between the two different leaving groups. The acetate and cysteamine leaving groups are of a similar size/mass, but one is bonded through a carbon-oxygen bond and the other through a carbon-sulfur bond. The carbon-sulfur bond, being weaker than the carbon oxygen bond, could explain the difference in the dissociation rates. When compared to the compounds with the cys-FMOC leaving groups, though also bonded through a carbon-sulfur bond, the cys-FMOC leaving group is 4-5 more massive. Comparing **2a** and **2b** with **4a** and **4b**, the larger mass of **4a** and **4b** could compete with the weaker C-S bond, lowering the overall dissociation rate.

There is no evidence of strong contributions to the absorption spectrum or dissociation from any of the leaving groups which suggests the dynamics of dissociation are similar. One possible reason for the difference in observed trends between 2PA cross section and two-photon induced dissociation rate could be differences in either the fraction of photocages that initially dissociate or the geminate recombination fraction between the compounds. The compounds with the cys-FMOC leaving groups dissociate with a slower overall rate than the other compounds within their respective series but **4b** features the largest absorption cross section at 405 nm. As previously mentioned, the size of the cys-FMOC leaving group could be a factor. Immediately following dissociation, a leaving group and the photocage it was attached to are still within proximity to one another for a time until diffusion naturally separates them or recombination of the two occurs. The larger leaving groups could hinder cage escape and subsequent diffusion, decreasing the fraction of molecules which remain dissociated. Not only is it possible

that the geminate recombination fraction could be larger for larger compounds, but the fraction of molecules that initially dissociate could be as well. Larger leaving groups, like cys-FMOC, have more degrees of freedom decreasing the fraction that dissociate prior to vibrational relaxation via transfer to the surrounding solvent. With more degrees of freedom, the molecule can better distribute the energy gained from the absorbed light after internal conversion. These factors could be the reason for the low overall dissociation rate for **4a** and **4b**.

4.5 – CONCLUSION

Few studies have been published investigating the effect that the leaving group has on the absorption and dissociation properties of photocage systems. In this work, the 2PA cross sections and two-photon induced dissociation rates of 4 NDBF based photocage-leaving group systems were measured and compared to the previously measured 2PA cross sections of 2 compounds with other leaving groups. The different leaving groups exhibited 2PA cross section differences of up to a factor of four with only minor shifts seen in their absorption maxima. Compared to the photocage without a leaving group, the absorption spectrum had as much as a 50 nm shift to longer wavelengths and decreased in strength by up to a factor of 2. Differences in the dissociation rate of up to a factor of 4 were measured between the photocages. Compounds with leaving groups of similar size/mass featured different dissociation rates due to leaving group bonding motif, with the weaker C-S bond dissociating faster than C-O. For both the a-series and b-series compounds, the largest leaving group, cys-FMOC, dissociated the slowest. This was true

even for **4b** which was measured to have the highest 2PA cross section at the wavelength of dissociation. This points to differences in the dissociation dynamics, such as a lower fraction of photocages that initially dissociate and/or a greater fraction of photocages/leaving groups that recombine after dissociation. The dynamics of dissociation will be proved in future works.

Chapter 5

The Dynamics of Dissociation in NDBF-Based Photocages

5.1 - INTRODUCTION

Dissociation in the condensed phase is complex and often involves many factors that influence the rate of dissociation such as viscosity and the dissociation product mass/size.[220–225] The overall dissociation rate, R_{diss}, for a photocage is proportional to its dissociation cross section, δ_{diss}, which is a representation of how well a photocage absorbs light and uses that energy to break the bond between photocage and leaving group.[27,30] The dissociation cross section is dependent on two quantities, the absorption cross section, σ_{Abs}, and the overall dissociation quantum yield, ϕ_O. In Chapters 3 and 4, it was demonstrated that the trend in the strength of the 2PA cross section for the photocages studied did not follow the trend in overall dissociation rate of those compounds. Compounds which exhibited comparatively higher 2PA cross sections were found to have comparatively lower dissociation rates and vice versa. This suggested that the dynamics of dissociation, namely the overall dissociation quantum yield, is different between the compounds studied. Both the choice of leaving group and modification of the structure of the photocage were found to influence the dissociation dynamics. Directly probing the dissociation dynamics of a photocage is key to predicting how well

that photocage can be applied in different situations and with different samples. The quantum yield of initial dissociation and the fraction of molecules that geminately recombine both play a role in determining the overall dissociation quantum yield, and thus, the overall dissociation rate for a photocage. The overall dissociation quantum yield is the fraction of photocages that remain dissociated after absorbing light and the quantum yield of initial dissociation, ϕ_I, refers to the fraction of photocages that initially release their leaving groups after absorbing light. The geminate recombination fraction, ϕ_R, refers to the fraction of leaving groups that recombine with their photocage after dissociation. Equation 5.1 shows the quantities that influence the dissociation cross section, and thus, the overall dissociation rate.

$$R_{diss} \propto \delta_{diss} = \sigma_{Abs} * (\phi_I - \phi_R) \qquad (5.1)$$

The dissociation dynamics of photocages are not well known and apart from one-photon induced dissociation quantum yields and overall dissociation rates, they are rarely reported. The extent to which the structure of the photocage and the leaving group, such as the leaving group bonding motif, leaving group size, or modifications made to the structure of the photocage, have on the dissociation dynamics is not well understood. In order to design photocages that exhibit large 2PA cross sections and fast overall dissociation rates, an understanding of not only absorption, but also the dissociation dynamics is needed. Some of the factors that influence the dynamics of dissociation can be probed. This chapter describes an initial investigation into the dissociation dynamics. One of the factors of the dissociation dynamics, the amount of photocages that initially release their leaving groups after absorption occurs, was measured and compared to

different photocages and to a photocage with different leaving groups. The structures of the compounds used in this chapter are shown in Figure 5.1.

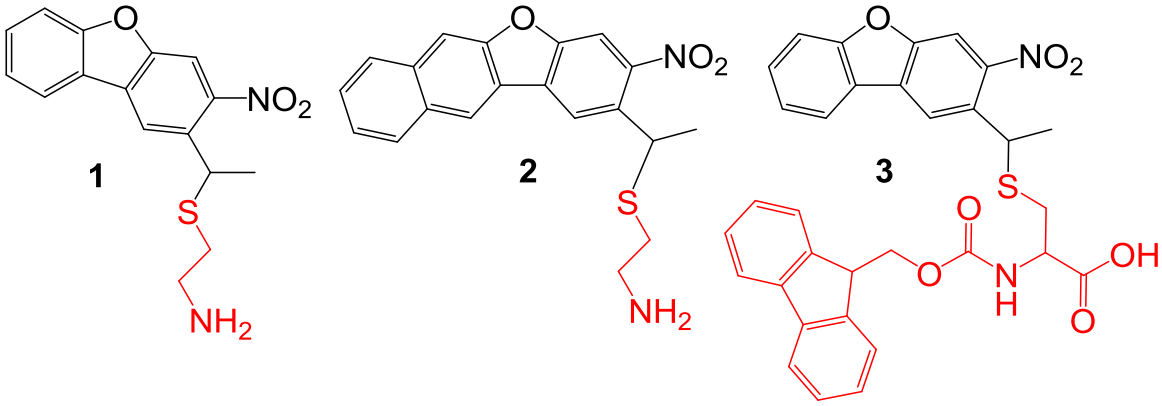

Figure 5.1: Compounds used in this chapter. Red denotes the leaving group.

In order to probe the dynamics of dissociation, a spectroscopic handle for the dissociation process needed to be identified. Figure 5.2 shows the calculated 1PA spectrum of the undissociated and dissociated form of **1**. (These calculations were performed using the method described in Chapter 2 of this dissertation.)

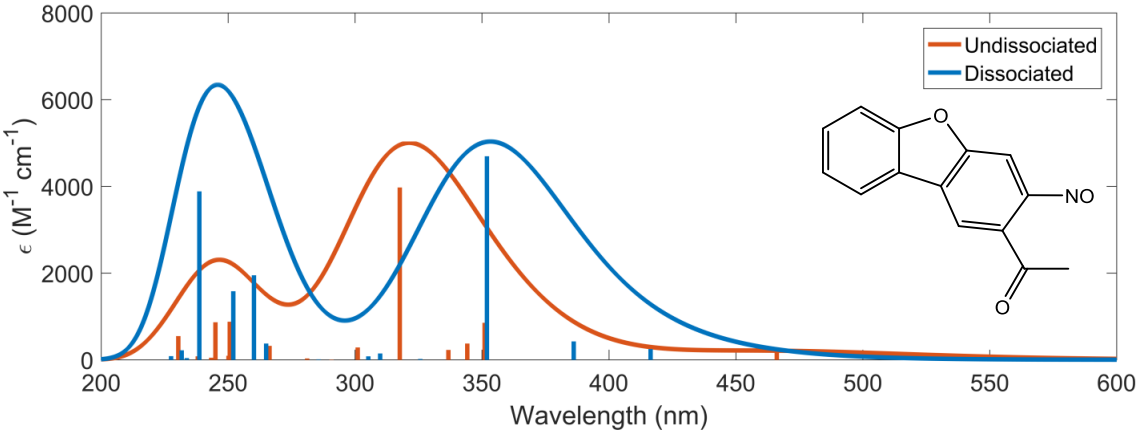

Figure 5.2: Calculated 1PA spectra of the undissociated and dissociated forms of **1**. The dissociated form of **1** is included.

Much of the absorption for these compounds occurs to shorter wavelengths than 400 nm. In previous investigations, such as those in Chapters 3 and 4, a sapphire crystal was used to generate a continuum probe with wavelengths from 750 nm to 450 nm. For this initial investigation, to reach a wavelength that features a large difference in the absorption spectrum between the dissociated and undissociated compounds, a CaF_2 crystal was used which extended the range we can probe to 350 nm.

At 365 nm, the spectrum for the dissociated form of **1** features a calculated molar absorptivity of more than double that for the undissociated form. This wavelength represented an ideal handle for where to probe the dissociation dynamics. When the 405 nm pump pulse interacts with the sample and initiates dissociation, the absorption of the sample is calculated to increase. The difference in absorption before and after irradiation is proportional the amount of dissociation. Since the 1PA spectra don't significantly change from leaving group to leaving group and only slight shifts in spectra are seen between **3** and **1**, it is expected that the OD of **2** and **3** will also change similarly to **1**.

5.2 – EXPERIMENTAL

The samples were all contained in a 3 mm path length quartz cuvette (Starna 23-3.45-Q-3) and dissolved in d6-DMSO. The solution for **1** had a concentration of 1.855 mM, **2** had a concentration of 0.48 mM, and **3** had a concentration of 0.68 mM. The OD for each solution was: 0.23 for **1**, 0.41 for **2**, and 0.24 for **3**.

The technique of measuring the amount of initial dissociation is based on a standard pump/probe setup. A homebuilt Ti:sapph based laser was used to generate 810 nm pulses

at a 1 kHz repetition rate. The pulses were Gaussian in profile and had a FWHM of 12 nm and had a pulse duration of 90 fs, as determined by autocorrelation. After exiting the laser, the pulses were split in two, a 'pump' pulse and a 'probe' pulse, and where sent to separate mechanical delay stages which controlled the relative time each pulse reached the sample. The pump went through a BBO which generated 405 nm light and was mechanically chopped to 500 Hz. The probe pulse was focused into a 2 mm thick CaF_2 crystal which generated a continuum from ~350 nm to 750 nm. The CaF_2 crystal was circularly translated to prevent photodamage from the high light intensity, while maintaining a constant crystal axis. Waveplate/polarizer pairs were used to attenuate the power of each pulse and to set the relative polarization of the beams parallel to one another. The pump had an energy per pulse of 400 nJ and a beam diameter of 420 μm (Gaussian FWHM). The probe had a pulse energy of 1.6 uJ and a beam diameter of 165 μm (Gaussian FWHM). The beams were focused and crossed in the sample. After passing through the sample, the probe light was spectrally dispersed and detected on a linear 256 pixel photodiode array. The change in optical density, ΔOD, of the sample with and without the pump present was measured for each time delay.

Using this setup, the amount of photocages that initially dissociate was determined by measuring the absorption of the sample before and after dissociation occurred. It is expected, due to the calculated increase in OD, that the pump/probe spectra will feature a ΔOD that is above baseline and exhibit a very slow decay, due to the creation of the dissociation product.

5.3 – RESULTS & DISCUSSION

A large, non-resonant scattering signal was detected from the solvent. This signal was only detected when the pulses were overlapped (± 500 fs) and decayed to baseline when outside of the pulse overlap. This scattering signal made it difficult to detect the initial change in absorption around time zero and thus, monitor the early time dynamics. Figure 5.3 shows the pump/probe plots for each compound.

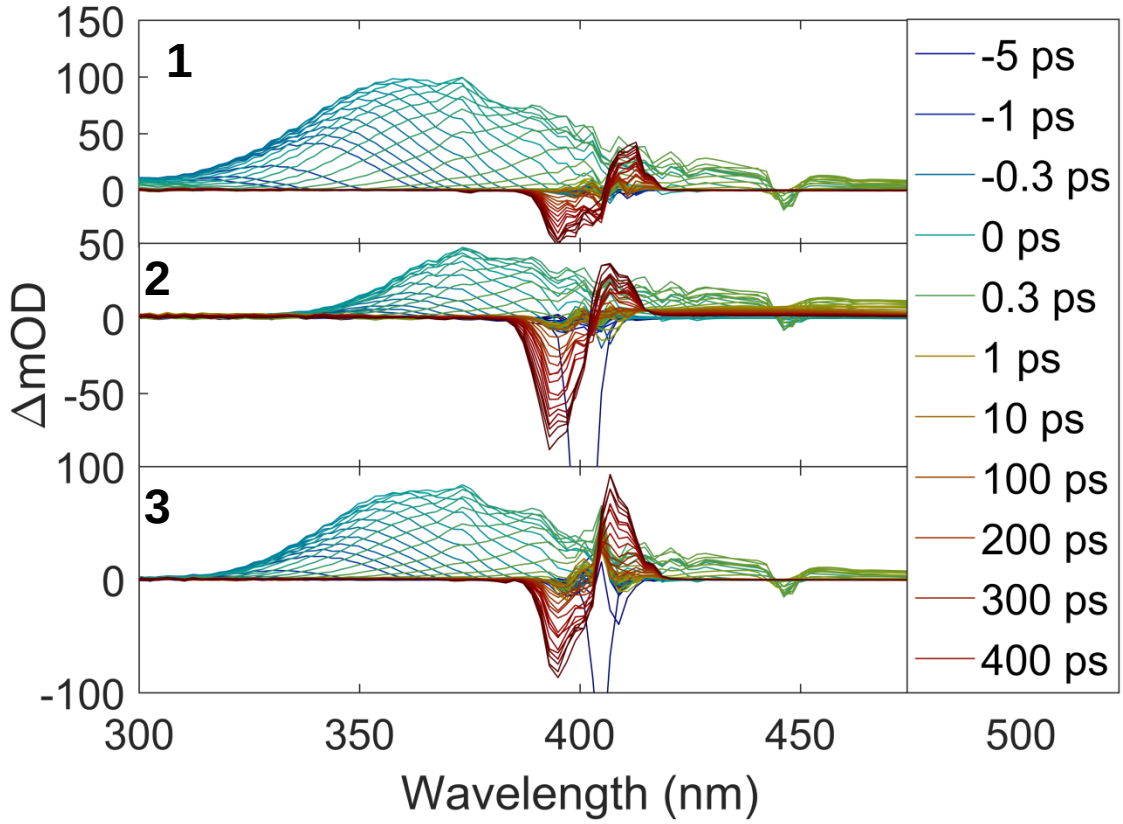

Figure 5.3: Pump/Probe spectra of **1**-**3**.

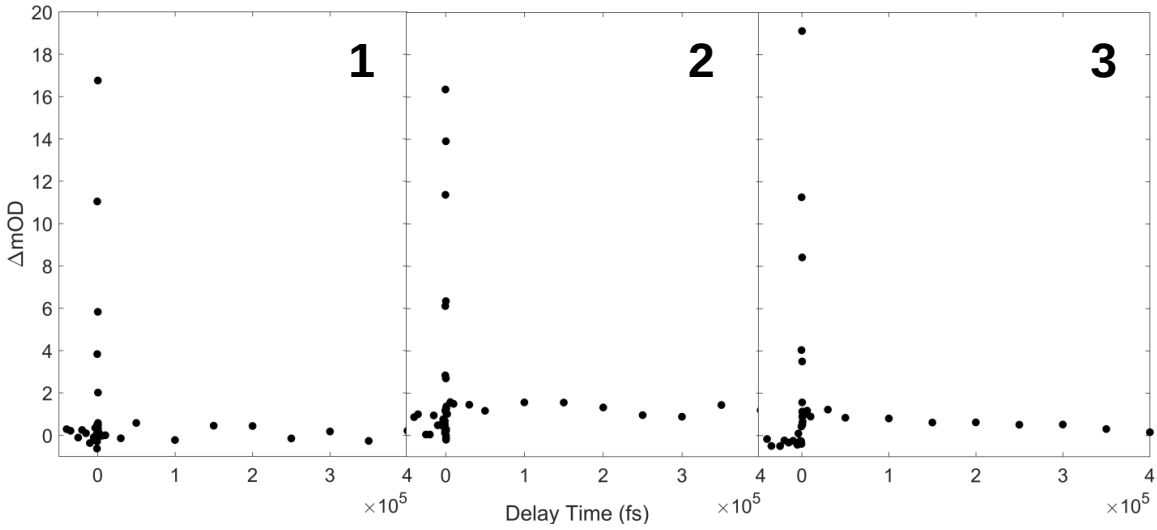

Figure 5.4: ΔOD of each compound over time at a probe wavelength of 365 nm.

Figure 5.4 shows the ΔOD of each compound over time. The signal from the dissociated compounds decay slowly over time so the ΔOD of the sample from 500 fs to 30 ps was averaged to determine the amount of photocages initially dissociated. To correct for differences in solution optical density and to facilitate comparison, the amount of photocages initially dissociated per photon absorbed, *I*, was determined using Equation 5.2.

$$\frac{A}{10^{-OD}*\frac{P*\lambda}{h*c}} = I \qquad (5.2)$$

In Equation 5.2, *A* is the amount of photocages that initially dissociate, *OD* is the optical density of the solution, *P* is the power of the pump pulse, λ is the wavelength of the pump, and *h* and *c* are Plank's constant and the speed of light, respectively. By calculating *I* for each compound, the amount of initial dissociation for each compound can be compared.

Table 5.1 gives the cross section at 405 nm, the overall dissociation rate, and *I* for these three compounds. Each of these quantities is normalized to **1**.

Compound	**σ_{Abs}(405)**	**Dissociation Rate**	***I***
1	1	1	1
2	3.72	2.25	4.33
3	0.67	0.40	6.22

Table 5.1: Normalized cross section at 405 nm, overall dissociation rate, and *I* for **1**-**3**. Each quantity is normalized to **1**.

Compared to **1**, **2** exhibits a cross section at 405 nm that is nearly 4 times greater, a 2 times greater dissociation rate, and nearly a 4 times greater amount of photocages dissociating per photon absorbed. Compound **3**, when compared to **1** on the other hand, features a cross section that is 2/3 as large, a dissociation rate smaller by more than a factor of 2, but the amount of photocages that dissociate per photon absorbed is over six times greater.

Compared to **1**, **2** features a larger $\sigma_{Abs,}$ dissociation rate, and *I*. The enhancement of these quantities for **2** is due to the additional phenyl ring on the chromophore backbone, extending the conjugation. It was not expected that the amount of initial dissociation would be significantly larger for **2** than **1**. This is because **2** has additional degrees of freedom due to its larger size than **1**, allowing for the absorbed energy to be more distributed and less of a chance to break the bond between leaving group and photocage. It is possible, however, that the additional conjugation on **2** stabilizes the photocage dissociation product, leading to a slight lowering of the energy needed to break the bond.

Compared to **1**, the cross section and dissociation rate for **3** are both smaller, but *I* is disproportionately larger. This difference in observed trends indicates that the other

factors are influencing the dissociation dynamics, namely the fraction of photocages which recombine. In Chapter 3 it was hypothesized that the size of a leaving group could influence its dissociation dynamics, with larger leaving groups theorized to have lower initial dissociation quantum yields and higher recombination fractions due to having more degrees of freedom and slower diffusion through solution, respectively. The influence of molecule size on recombination rate has been studied previously.[226,227] This hypothesis further was supported by the lower overall dissociation rate of **3** compared to **1**.

Not only is it possible that the size of the leaving group is influencing the dissociation dynamics for these compounds, but the size of the photcage could be as well. This is evidenced by comparisons of **1** and **2**. Compound **2** has more than a four times greater amount of photocages that initially dissociate compared to **1**, but the overall dissociation rate is only a bit over twice as fast as the dissociation rate for **1**. This indicates that the recombination rate is higher for **2** than for **1**. The cause for this difference is the extra phenyl ring in **2**. While both **1** and **2** have the same leaving group, **2** has a larger photocage. After dissociation, it is possible that the photocage dissociation product, being larger, moves through solution slower, spending more time near the dissociated leaving group and increasing the chance for recombination.

It was not expected that **3** would have a larger initial dissociation, due to having more degrees of freedom to distribute the absorbed light energy. In a statistical dissociation on the ground electronic surface, a larger number of degrees of vibrational freedom will reduce the rate of dissociation, and thereby reduce the initial dissociation yield as it becomes less competitive with other relaxation channels. With this new measurement of

the initial dissociation for these compounds, it can be concluded that the geminate recombination fraction is implicated as another important factor to consider when comparing leaving groups. The slow decay, over nanoseconds, of the signal from the dissociated compounds could reflect the amount of recombination occurring. Directly probing this in the future will further our understanding on how the structure of the chromophore and leaving group influence the overall dissociation rates of photocages.

5.4 – CONCLUSION

This chapter presented a prefatory investigation into whether the dynamics of dissociation can be probed and, if so, what information they can tell us about the NDBF photocage system. It was determined that even with a lower overall dissociation rate, a compound can exhibit a larger fraction of photocages which initially dissociate. This stresses the importance of understanding how molecular design changes the overall dissociation rate by influencing all of the factors that make up the dissociation cross section, with no one factor dominating the rate.

While this was only an initial study into the dissociation dynamics of photocages, it offers clear evidence that the details of the dissociation dynamics cannot be ignored when building a complete understanding of overall 2PA dissociation efficiency in photocages. In this dissertation, the methods for measuring the absorption cross section, the overall dissociation rate, and the fraction of photocages that initially dissociate were described. To complete the picture of how structure affects the photophysical properties of photocages, further investigations should be undertaken to also measure the fraction of

compounds that recombine after dissociation. With a complete understanding of how structural modification of photocages and leaving groups affect all of these factors, more efficient photocages that exhibit fast dissociation, low recombination rates, large quantum yields of dissociation, and large 2PA cross sections can be synthesized.

Chapter 6

Computational Investigation of Future Photocages of Interest

Throughout this dissertation, computational predictions were used to supplement experiment. In Chapter 2, the methods used to predict one and two-photon spectra were tested for accuracy against sets of test molecules. It was determined that the B3LYP functional calculated 2PA cross sections that were in good agreement with experimental observation. Chapter 3 investigated the effect that additional electron withdrawing groups and extending the conjugation of the NDBF core had on the photophysical properties of the system. Calculations using B3LYP were used to determine the nature of the transitions. It was found that the modifications did not change the nature of the dominant transitions of the NDBF system. The investigations presented in Chapter 4 used calculations to determine the role that the leaving group had on the properties of the NDBF photocage and it was found that different leaving groups had a modest effect on the size of the 2PA cross section. This chapter aims to apply the information learned about these computational methods, their accuracy and utility, and use computational prediction to test several hypotheses on how structure may enhance absorption properties. The results are intended to help guide future new directions in NDBF photocage development.

The structures (Figures 6.1-6.3) studied were chosen to investigate four hypotheses:

1. A dimeric form of the NDBF chromophore will enhance it its 2PA cross section with the amount of enhancement dependent on the degree of electronic coupling between the two chromophoric units.
2. Replacing the heteroatom of the central five-membered ring with N, S, or C will change the amount of light that is absorbed and shift the wavelength where it will absorb.
3. A change in the donor-π-acceptor (D-π-A) motif of the NDBF system to an acceptor-π-acceptor (A-π-A) motif will increase the 2PA cross section.
4. The inclusion of a second electron acceptor group near the leaving group will increase the 2PA cross section.

As a point of reference and for comparison to the hypothesized structures, the calculated 2PA cross sections of the unmodified NDBF photocage and the methoxy modified NDBF photocage, both with the cysteamine leaving group, (**1** and **2** in Chapter 3) are reproduced in Figure 6.1. The two-photon absorption cross section of each compound was calculated using the methods described in Chapter 2.

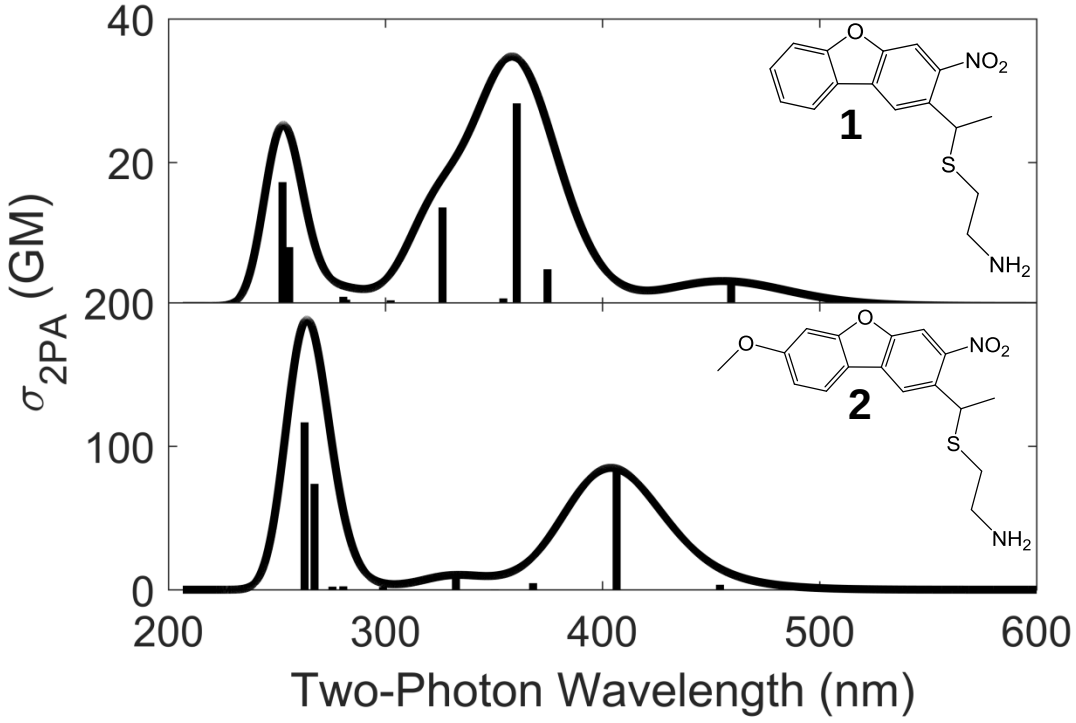

Figure 6.1: Calculated 2PA cross sections of the unmodified (top) and methoxy modified (bottom) NDBF photocages with the cysteamine leaving group.

6.1 – HYPOTHESIS 1: NDBF DIMERS

It has been demonstrated previously that in conjugated organic molecules, dimers can exhibit greatly enhanced 2PA cross sections when compared to their monomeric counterparts.[228,229] Based on this, we chose to explore dimers of the NDBF chromophore with the proposed structures in Figure 6.2. The degree of electronic coupling between the two units is of primary interest with the prediction that the more the electronic coupling between the monomers, the greater the 2PA cross section. By using different conjugated and non-conjugated linkers, the effect that the coupling between monomeric units has on enhancing the 2PA cross section can be determined.

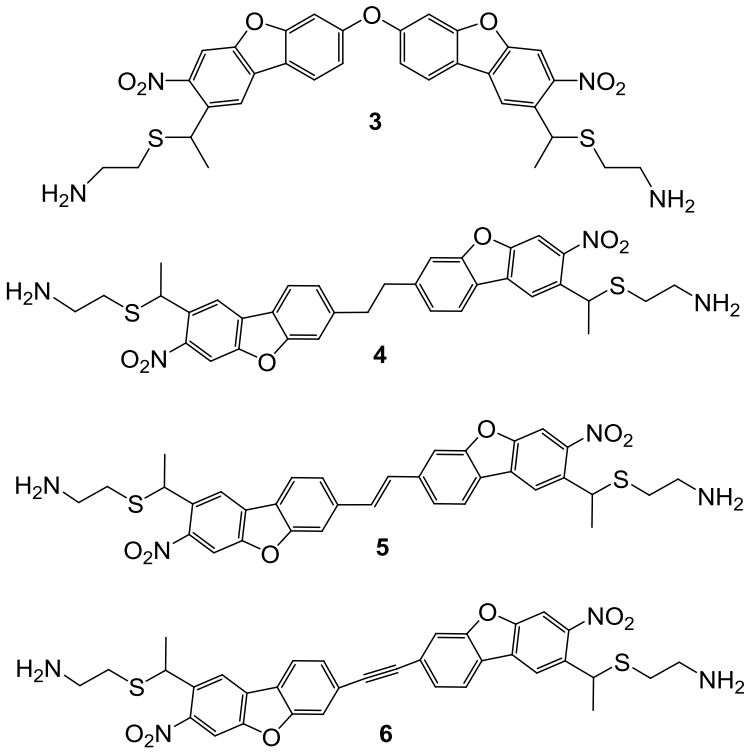

Figure 6.2: Compounds used to test Hypothesis 1.

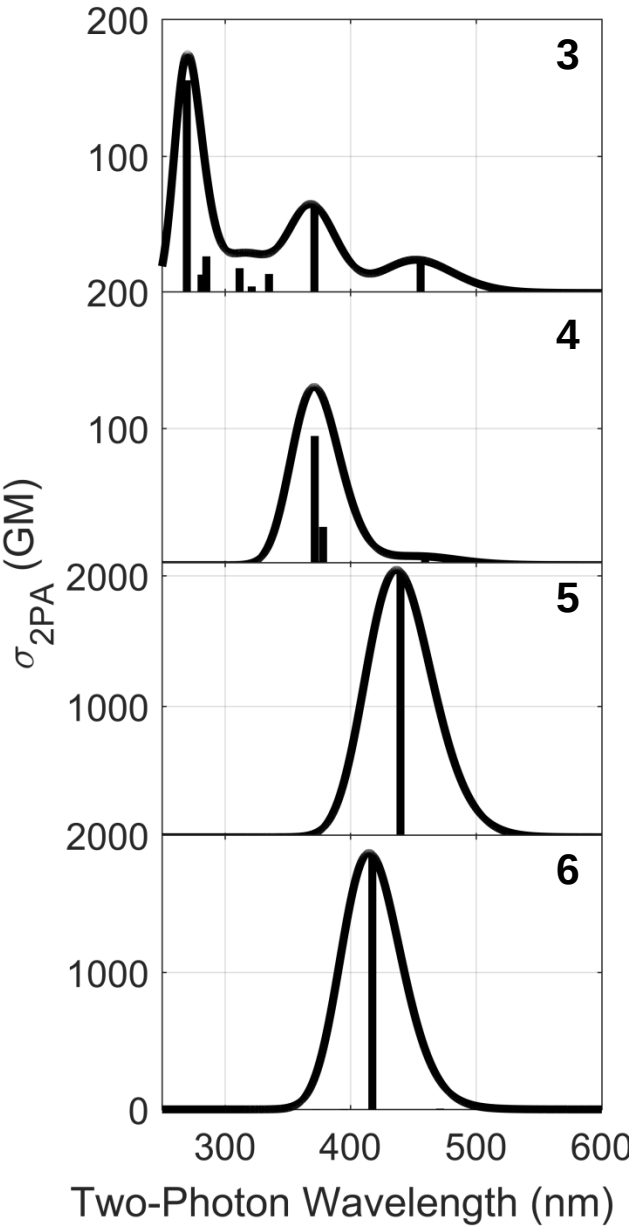

Figure 6.3: Calculated 2PA spectra of **3**-**6**.

Figure 6.3 presents the calculated 2PA spectra of **3**-**6**. Compound **3** exhibits three absorption peaks at 270 nm, 370 nm, and 455 nm, respectively, with a calculated maximum cross section of 173 GM at 270 nm. Compound **4** has a single peak at 370 nm with a cross section of 200 GM. Compounds **5** and **6** have a cross section nearly an order

of magnitude higher than **3** and **4** at their peaks, around 2000 GM at 435 nm and 415 nm, respectively.

The 2PA spectra of **3-6** suggest that the degree of conjugation/electronic coupling between two linked NDBF units has a significant impact on the calculated 2PA cross section. With less electronic coupling between the two attached chromophores in the case of compounds **3** and **4**, the 2PA cross sections are similar to **1**. However, when the two are connected via a conjugated linker such as through an alkene or alkyne, the 2PA cross section is increased by an order of magnitude and the spectrum is redshifted by as much as 60 nm. Figure 6.4 shows the ground state and excited state NTOs for the largest transitions of the four molecules within the spectral region of interest.

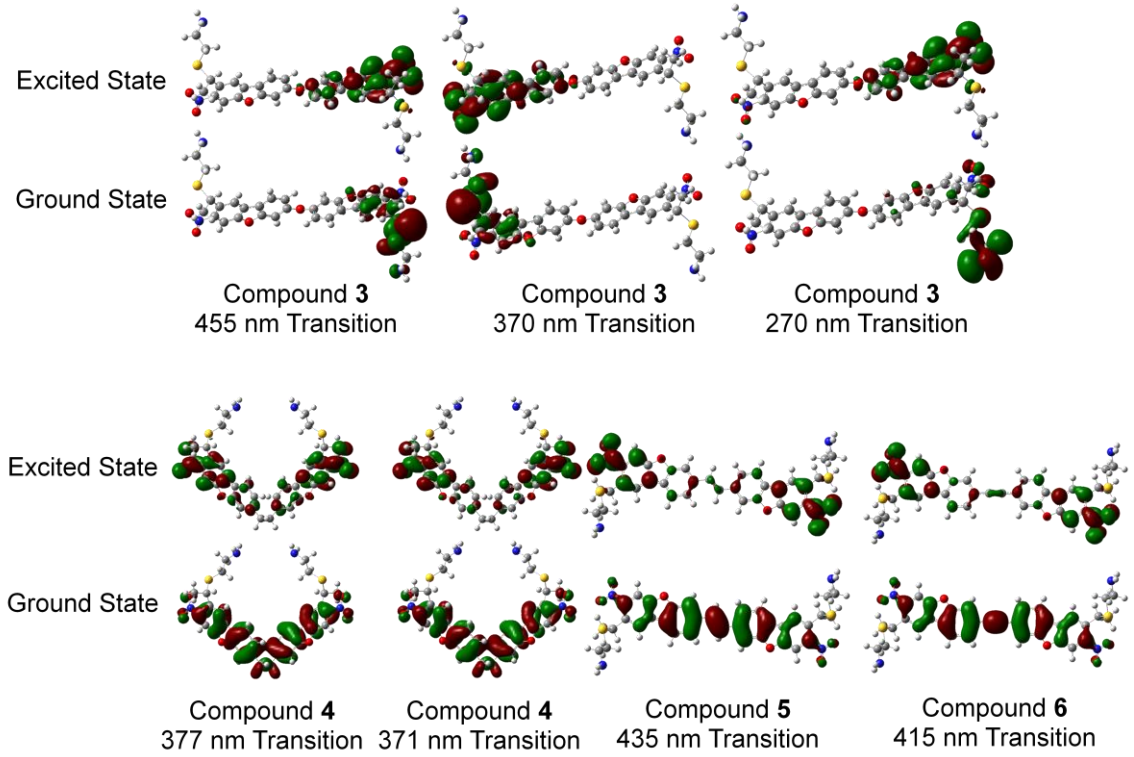

Figure 6.4: NTOs for the major transitions of compounds **3-6**.

Analysis of the NTOs in Figure 6.4 indicated that the transitions for **3** are from ground states distributed across the photocage backbone and leaving group of one of the NDBF units to excited states delocalized across the backbone of that same NDBF unit with little electron density on the leaving group. The lack of electron density across both NDBF units in the same ground or excited state NTOs for compound **3** reflects that the electronic coupling between the two photocage units is low. The NTOs for the transitions of compound **4** indicate a different character. The ground states of both major transitions show electron density located across the photocage backbone of both NDBF units. The excited states show the same, but with the density shifted to be more localized around each nitro group and less density around the alkane linker. The NTOs indicate involvement of both NDBF units during the same transition. This was unexpected because, like **3**, there is no conjugation between the two monomers and little coupling through the alkane linker. Even though the electron density is shared between the two monomers, no significant increase in the 2PA cross section is observed. The different nature of the transitions between compounds **3** and **4** is the cause of the differences seen in the 2PA spectra between these molecules with three distinct peaks being present in the spectrum for compound **3** while one is present in the spectrum for compound **4**. The nature of the transitions for compounds **5** and **6** are very similar to each other. The ground states are characterized by electron density delocalized across the backbone of the two NDBF units and the excited states are characterized by electron density distributed across the backbone, but shifted towards both nitro groups with less density located around the linkers. The large increase in 2PA cross section exhibited in compounds **5** and **6** when compared to the cross section of **1** and **2** are due to the extended conjugation

of these compounds. Because of the conjugated alkene and alkyne linkers, there is much more electronic coupling between the two monomers, increasing its 2PA cross section. The use of NDBF dimers, when joined via a conjugated linker, greatly increase the 2PA cross section and redshift the two-photon absorption maxima when compared to the reference compounds **1**, and **2**.

6.2 – HYPOTHESIS 2: CHANGING THE CENTRAL HETEROATOM

Two-photon absorption cross section enhancement by changing heteroatoms has been reported previously.[230] In a study by Zheng *et. al.*, the effect of nitrogen and sulfur heteroatoms on the 2PA cross section of bis(diarylaminostyryl) chromophores found that compounds with sulfur heteroatoms had a cross section twice that of compounds that featured nitrogen heteroatoms. We computationally investigated the impact that changing the heteroatom of the central ring of NDBF has on its 2PA cross section. The heteroatom was changed from oxygen to sulfur, nitrogen, and carbon. Figure 6.5 presents the structures used to test this hypothesis. For **9**, the deprotonated form was used because the conjugation was similar to the other compounds and better facilitated comparison with the other photocages. The fully protonated form of **9 (**fluorene) was not used because the upper portion of the central 5-membered ring is not conjugated unlike in the other compounds in the series.

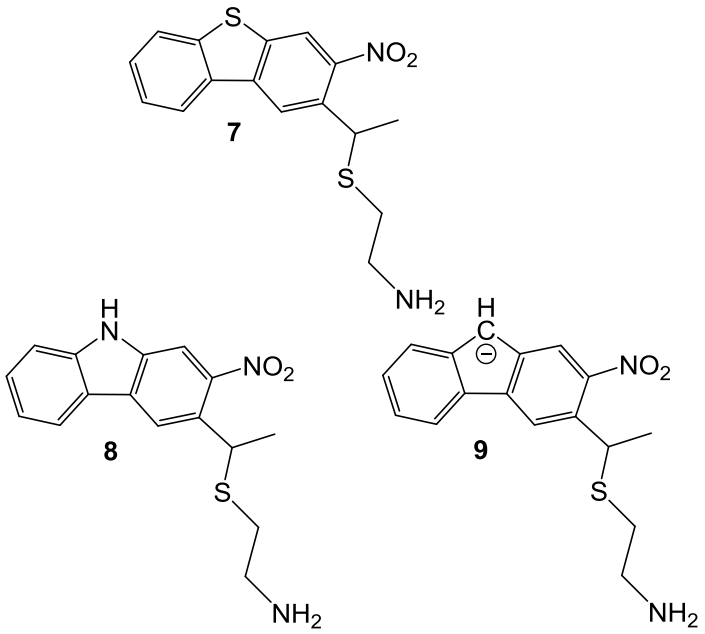

Figure 6.5: Structures used to test Hypothesis 2 with different heteroatoms on the central ring.

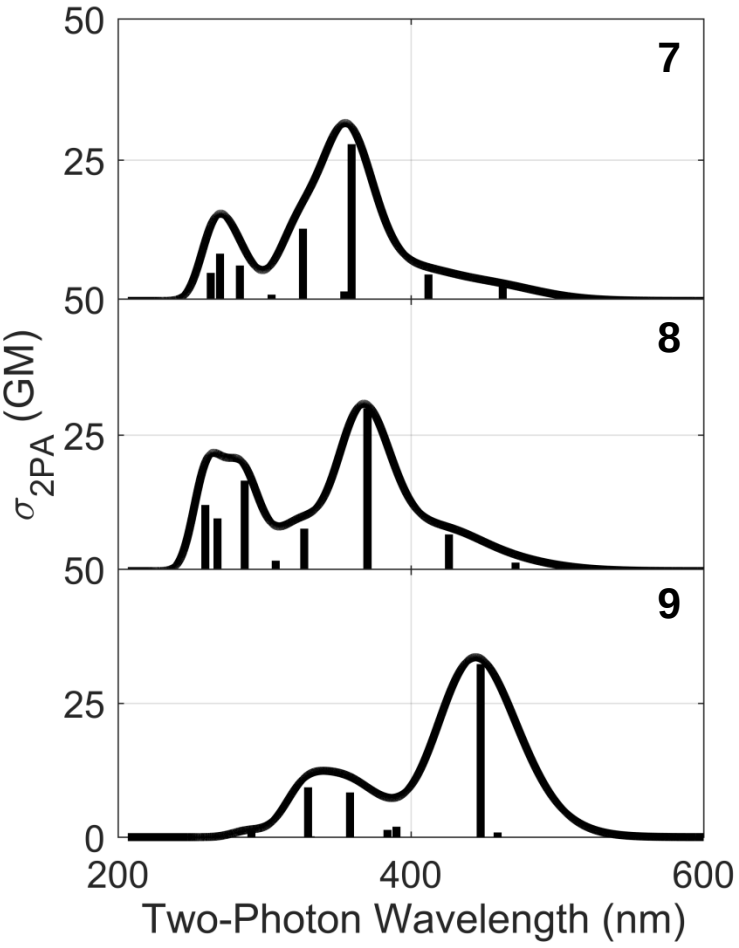

Figure 6.6: Calculated 2PA spectra of **7-9**.

Figure 6.6 presents the 2PA spectra for **7-9**. The spectra each contain two distinct peaks. Compounds **7** and **8** are very similar and have a peak around 260-270 nm and another around 360 nm while the peaks of **9** are shifted from the other compounds to longer wavelengths by ~80-90 nm. The maximum cross sections of the compounds are all ~30 GM, with the lower energy peak being the larger of the two.

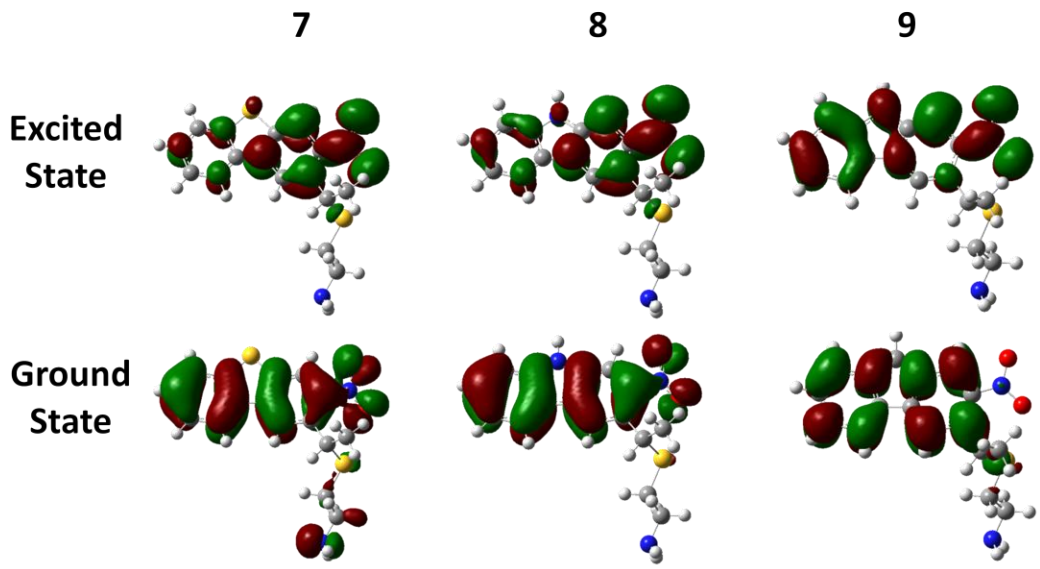

Figure 6.7: NTOs for the strongest transition for **7**-**9**.

Replacing the oxygen of the central ring of NDBF with sulfur or nitrogen does not greatly change the maximum 2PA cross section when compared to **1**. However, when carbon is used as the heteroatom to create a photocage backbone, which contains a fluorenyl anion, the 2PA spectrum is redshifted by up to 100 nm. Figure 6.7 shows the NTOs for **7**-**9**. The dominant transitions for **7** and **8** are similar in nature to **1** with an oxygen heteroatom. The ground and excited states are characterized by electron density being delocalized across the NDBF backbone with the excited state having density shifted more towards the nitro group. Compound **9** differs in that the ground state has much less electron density on the nitro group and a stronger shift in electron density to the nitro group in the excited state. These differences in the nature of the transition are likely due to the extra negative charge on the heteroatom changing the electronic structure of the molecule. This is observed through comparison of the NTOs for these compounds and is likely what gives rise to the observed redshift of the 2PA maxima.

The choice of heteroatom causes only modest differences in the size of the 2PA cross section, but, in the case of **7**, the deprotonated carbon caused a shift in the 2PA maximum by 75 nm.

6.3 – HYPOTHESES 3 & 4: DIFFERENT ELECTRON DONATING AND ELECTRON ACCEPTING MOTIFS

Various combinations of electron donors and electron acceptors connected via π-conjugated bridges have been reported to increase 2PA cross sections.[162,231,232] Such combinations include D-π-A, D-π-D, and A-π-A, where D is an electron donating group and A is an electron accepting group. It is hypothesized that by adding a nitrile group opposite the nitro group on the NDBF chromophore will enhance the 2PA cross section by creating an A-π-A motif, **10** (Figure 6.8). Likewise, it is proposed that the 2PA cross section will be enhanced by increasing the electron accepting character of the NDBF chromophore by adding a second electron withdrawing group near the leaving group, **11**, (Figure 6.8).

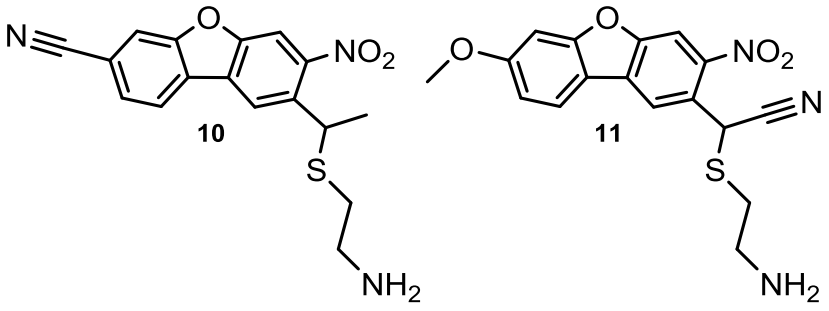

Figure 6.8: Compounds used to test hypotheses 3 and 4.

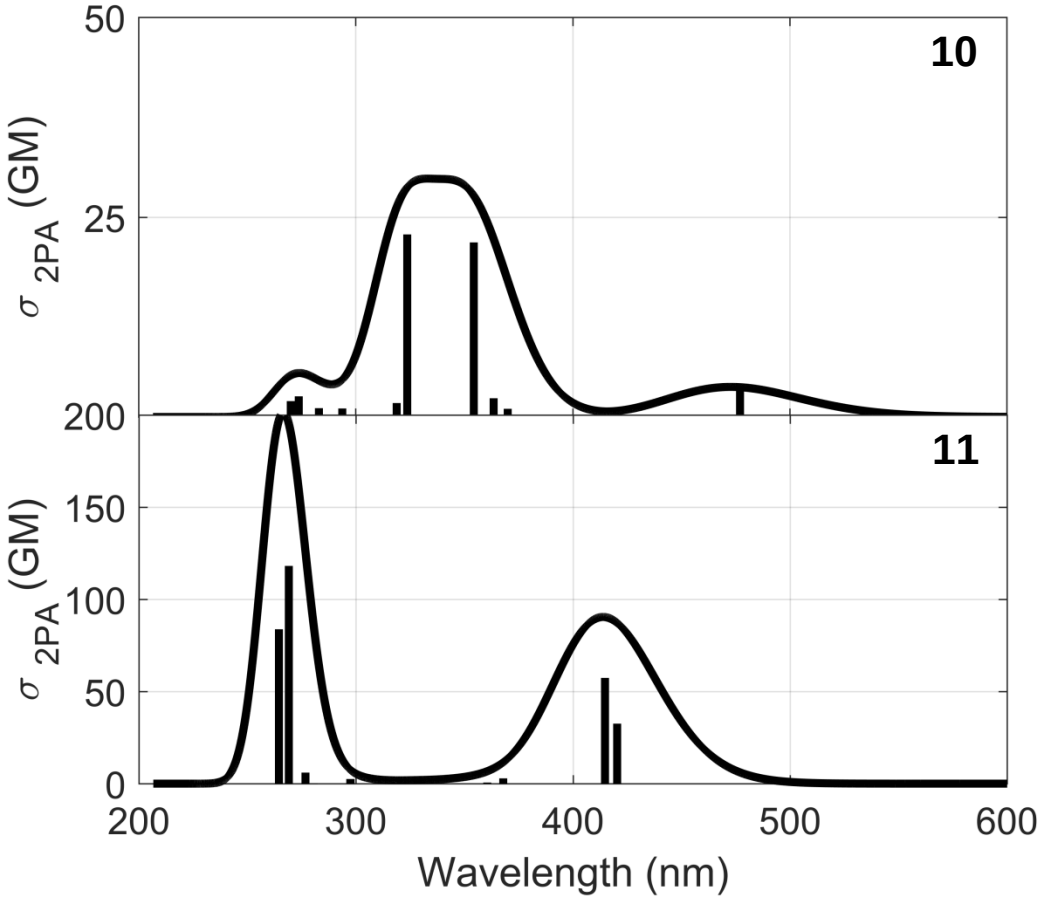

Figure 6.9: Calculated 2PA spectra of **10** and **11**.

Figure 6.9 presents the 2PA spectra of **10** and **11**. Two absorption peaks are present in the spectrum of **10**, one at 475 nm with a cross section of ~5 GM and another at ~350 nm with a cross section of 28 GM. Compound **11** also has two peaks, one at 275 nm with a cross section of 200 GM and another one at 415 nm with a cross section of around 90 GM.

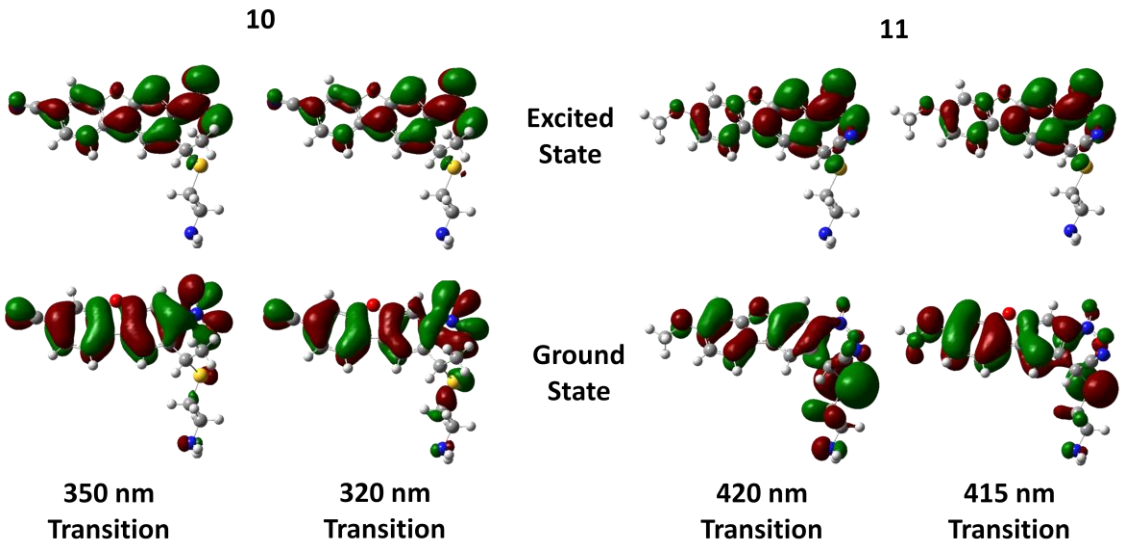

Figure 6.10: NTOs for relevant transitions for **10** and **11**.

Changing the D-π-A motif of the NDBF photocage to an A-π-A motif, as in the case of compound **10**, does not increase its 2PA cross section when compared to **1** nor does it shift the spectrum substantially. Compound **10** is calculated to absorb at similar wavelengths to **1** and features similar absorption cross sections. This points to A-π-A motifs for the NDBF molecule having little to no effect on the 2PA cross section. Compound **10** exhibits not only similar absorption spectra as **1**, but also exhibits similar NTOs (Chapter 3) indicating that the A-π-A motif does not influence the nature of the dominant transitions for NDBF.

Comparing the calculated 2PA spectrum for **11** with the 2PA spectrum for **2**, the addition of a second acceptor group near the leaving group does not increase the calculated 2PA cross section of the NDBF photocage or shift the spectrum. The NTOs (Figure 6.10) for the transitions at ~415 nm in **11** show that the ground state for both of these transitions are characterized as being delocalized across both the NDBF backbone and the leaving

group. The excited state for these transitions are characterized by electron density delocalized across the backbone, but shifted more towards the nitro group and less density on the leaving group. Compared to the NTOs for **2** (Chapter 3), **11** exhibits much more influence from the leaving group, but the 2PA cross section and absorption maxima are similar. The similar 2PA cross sections of **10** and **11** when compared to **1** and **2**, respectively, as well as the similar transition nature, indicates that an A-π-A motif and additional electron accepting groups near the leaving group do not significantly increase or redshift the 2PA cross section of the NDBF photocage.

6.4 – CONCLUSION

When considering molecular design for future photocages, photocage dimers coupled via a conjugated linker offers the greatest enhancement of the 2PA cross section. In this chapter, it was demonstrated that extending the conjugation across a dimer (**3**-**6**) has the ability to increase the 2PA cross section by an order of magnitude. An attempt to construct an A-π-A motif or adding extra electron acceptors near the leaving group (**10** & **11**) did not show much in the way of increasing the 2PA cross section and didn't substantially shift the absorption spectra to longer wavelengths. It is reasonable to conclude that, in their current forms, such structures would offer little benefit to photocaging applications with most leaving groups. Exchanging the heteroatom of NDBF for other elements showed no significant difference in the strength of the 2PA cross section, but the use of a carbon anion significantly shifted the spectrum to longer wavelengths. The use of nitrogen and carbon atoms in the five-membered ring opens up

the intriguing possibility of further synthetic modification such as additional electron donating/accepting groups or extended conjugation while retaining the same 2PA cross section

This chapter focused on calculating the 2PA cross section of compounds which could exhibit stronger absorption. However, ability of these compounds to dissociate and the dynamics of that dissociation were not investigated. Likewise, this chapter makes no inferences as to the synthetic accessibility of the proposed compounds. The results of this chapter suggest that the dimer of NDBF, due to the greatly increased 2PA cross section and the fact that it carries two leaving groups, possibly increasing the dissociation yield, should be synthetically pursued and the focus of further investigation. Additional NDBF compounds featuring different heteroatoms should also be pursued as the additional sites for modification open up new possibilities for modification of the photophysical properties of the NDBF photocage.

Appendix A

This appendix contains additional information, plots, and data regarding Chapter 3. The dependence of the two-photon signal on the power of the pump pulse is shown to be linear. Figures A1-A4 give the power dependence for **1-4**.

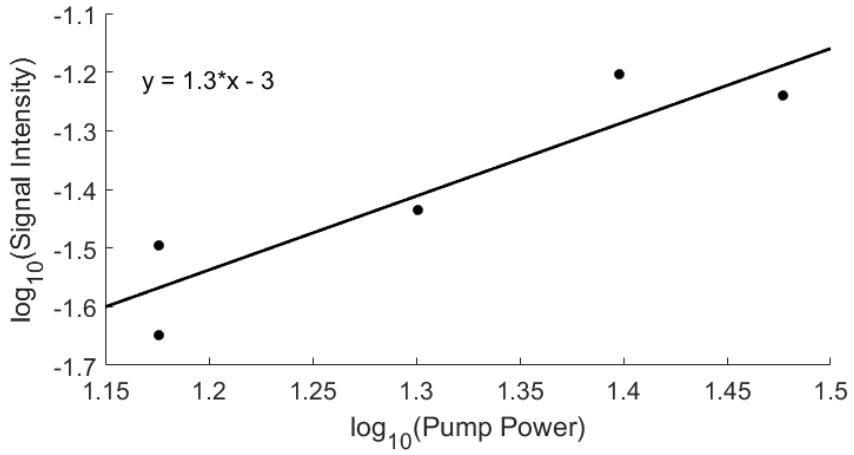

Figure A1: Power dependence for compound **1**.

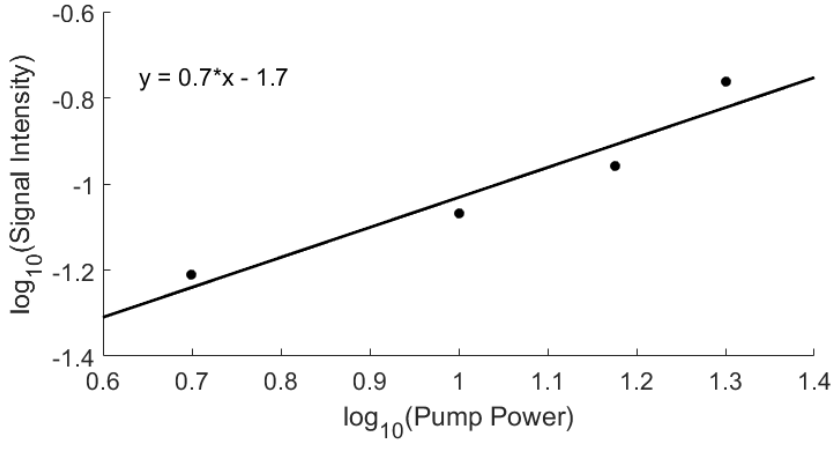

Figure A2: Power dependence for compound **2**.

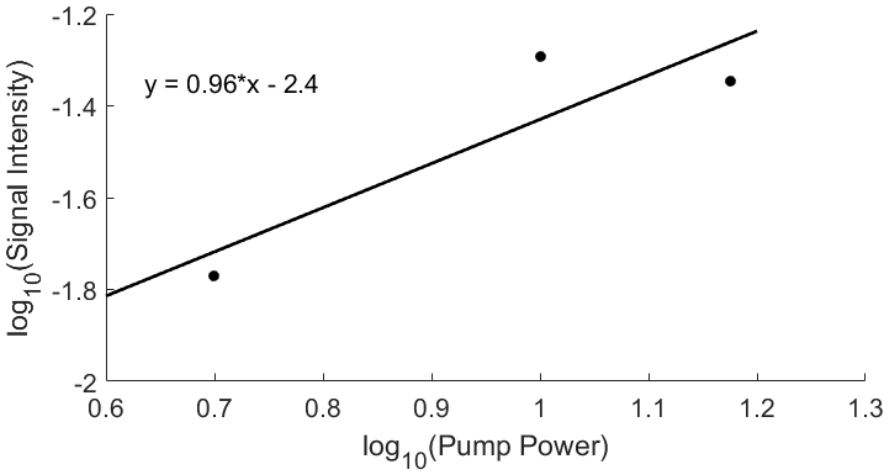

Figure A3: Power dependence for compound **3**.

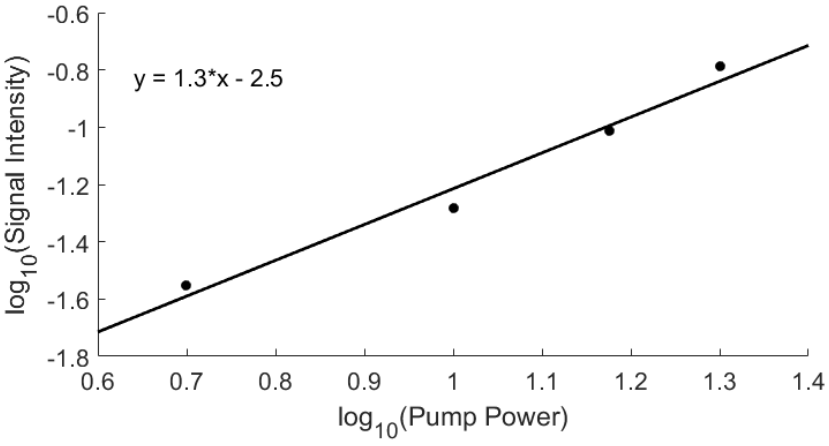

Figure A4: Power dependence for compound **4**.

Figures A5-A12 give the orbital contributions and energies of each transition and show the orbital diagrams for the orbitals involved in each transition. The energies of each orbital are given in eV and are relative to the HOMO.

Transition	Orbital Contributions	Energy (eV)	Wavelength (nm)
1		2.698	458
	H --> L		
	H-3 --> L		
2		3.314	373
	H-1 --> L		
	H-2 --> L		
	H-3 --> L		
	H-4 --> L		
3		3.439	359
	H-1 --> L		
	H-2 --> L		
	H-3 --> L		
	H-5 --> L		
	H-7 --> L		
4		3.5	353
	H-1 --> L		
	H-2 --> L		
	H-3 --> L		
5		3.796	326
	H-5 --> L+1		
	H-1 --> L		
	H-3 --> L		
	H-5 --> L		
	H-7 --> L		
6		4.101	301
	H-1 --> L+1		
	H-4 --> L		
7		4.404	281
	H --> L+1		
	H-6 --> L		
	H-7 --> L		
	H-8 --> L		
	H-9 --> L		
	H-10 --> L		
	H-9 --> L+1		
8		4.416	280
	H-7 --> L		
	H-8 --> L		
	H-9 --> L		
	H --> L+1		
	H --> L+2		

9		4.851	255
	H --> L+2		
	H --> L+3		
	H-1 --> L+2		
	H-1 --> L+1		
	H-2 --> L+1		
	H-3 --> L+1		
	H-3 --> L+2		
10		4.913	251
	H-5 --> L		
	H-6 --> L		
	H-7 --> L		
	H-1 --> L+1		
	H-2 --> L+1		
	H-3 --> L+1		
	H --> L+2		

Figure A5: Orbital contributions to the calculated transitions for **1**. H = HOMO and L = LUMO.

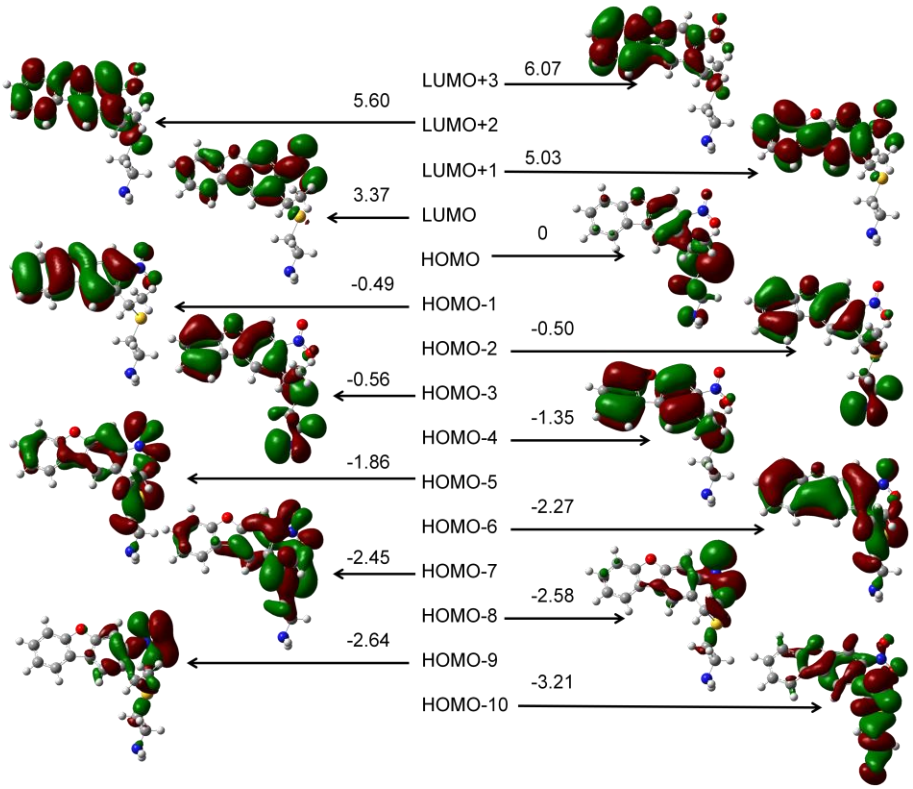

Figure A6: Molecular orbitals involved in the first 10 calculated transitions of **1**.

Transition	Orbital Contributions	Energy (eV)	Wavelength (nm)
1		2.731	453
	H --> L		
	H-1 --> L		
2		3.049	406
	H --> L		
	H-1 --> L		
3		3.368	367
	H-2 --> L		
	H-3 --> L		
4		3.537	350
	H-2 --> L		
	H-3 --> L		
	H-5 --> L		
	H-6 --> L		
5		3.73	331
	H-6 --> L+1		
	H-2 --> L		
	H-3 --> L		
	H-4 --> L		
	H-5 --> L		
	H-6 --> L		
	H-7 --> L		
6		4.151	298
	H-4 --> L		
	H-5 --> L		
	H --> L+1		
7		4.415	280
	H-9 --> L+1		
	H-9 --> L		
	H-8 --> L		
	H-6 --> L		
8		4.497	275
	H-1 --> L+1		
	H --> L+1		
	H --> L+2		
9		4.64	266
	H-1 --> L+1		
	H-1 --> L+2		
	H-4 --> L		
	H-5 --> L		
	H-6 --> L		

	H --> L+1		
10		4.719	262
	H-9 --> L		
	H-8 --> L		
	H-6 --> L		
	H-5 --> L		
	H-3 --> L+1		
	H-2 --> L+1		
	H-1 --> L+1		
	H-1 --> L+2		

Figure A7: Orbital contributions to the calculated transitions for **2**. H = HOMO and L = LUMO.

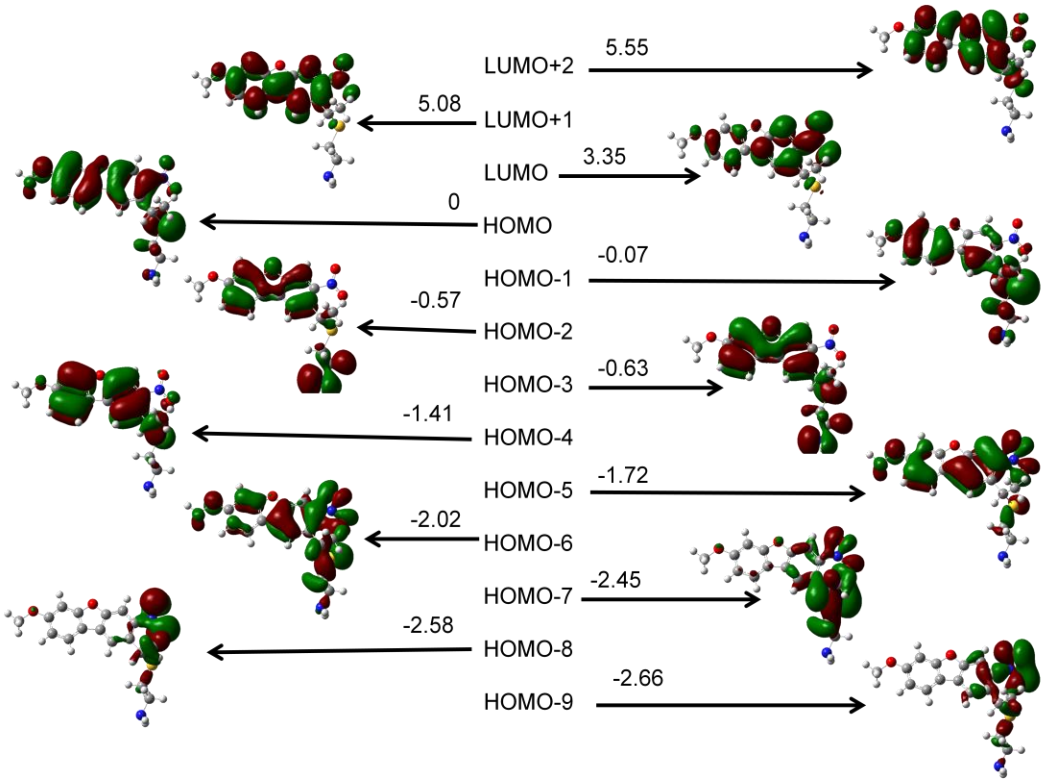

Figure A8: Molecular orbitals involved in the first 10 calculated transitions of **2**.

Transition	Orbital Contributions	Energy (eV)	Wavelength (nm)
1		2.703	458
	H --> L		
2		3.156	392
	H-1 --> L		
	H-2 --> L		
	H-3 --> L		
3		3.342	370
	H-1 --> L		
	H-2 --> L		
	H-3 --> L		
	H-6 --> L		
4		3.503	353
	H-2 --> L		
	H-3 --> L		
	H-6 --> L		
5		3.756	329
	H-6 --> L+1		
	H-1 --> L		
	H-3 --> L		
	H-6 --> L		
	H-7 --> L		
	H-8 --> L		
	H-9 --> L		
6		4.011	308
	H-2 --> L		
	H-4 --> L		
	H-5 --> L		
	H-1 --> L+1		
7		4.269	289
	H-4 --> L		
	H-5 --> L		
8		4.409	280
	H --> L+1		
	H-5 --> L		
	H-9 --> L		
	H-10 --> L		
	H-11 --> L		
9		4.423	279
	H-11 --> L		
	H --> L+1		
10		4.665	265

H-6 --> L
H-7 --> L
H-2 --> L+1
H-3 --> L+1
H-1 --> L+1

Figure A9: Orbital contributions to the calculated transitions for **3**. H = HOMO and L = LUMO.

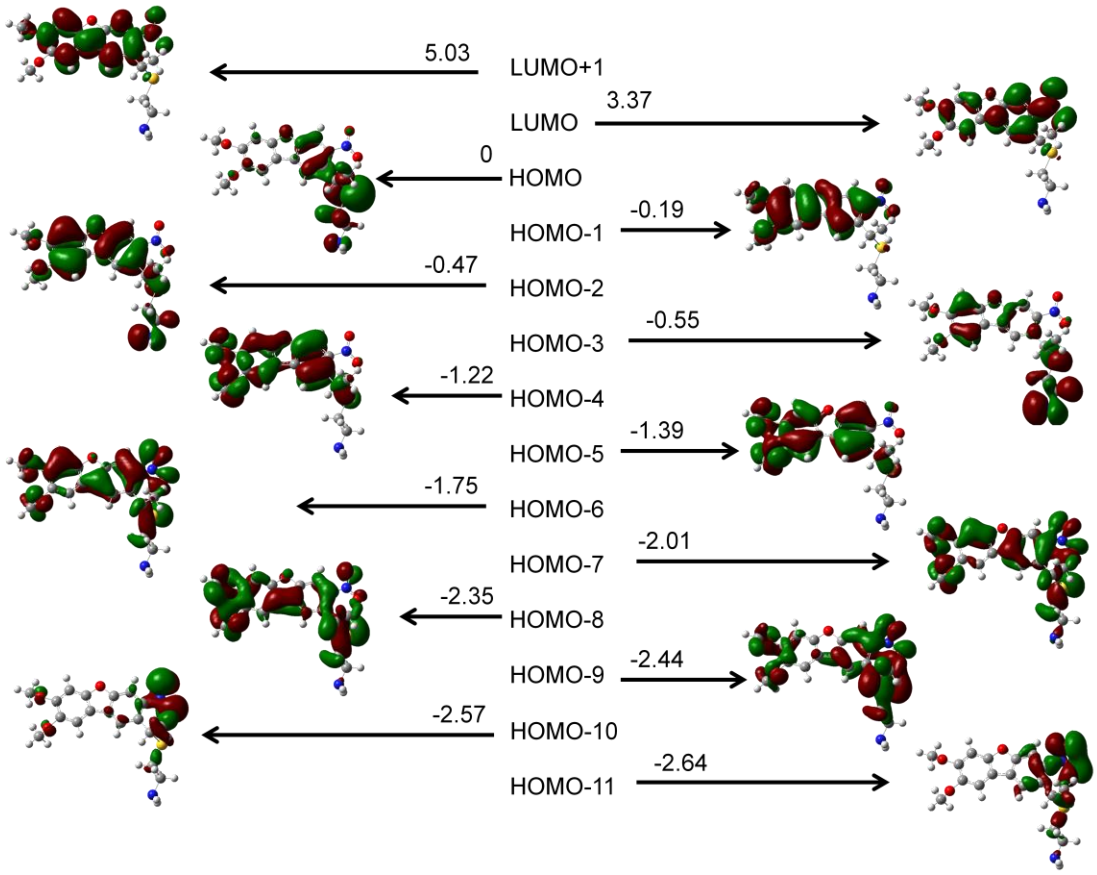

Figure A10: Molecular orbitals involved in the first 10 calculated transitions of **3**.

Transition	Orbital Contributions	Energy (eV)	Wavelength (nm)
1		2.624	471
	H --> L		
	H-1 --> L		
2		2.738	452
	H --> L		
	H-1 --> L		
3		3.324	372
	H --> L+2		
	H --> L		
	H-2 --> L		
	H-6 --> L		
4		3.439	359
	H-3 --> L		
5		3.375	366
	H-7 --> L+1		
	H-5 --> L		
	H-6 --> L		
	H-7 --> L		
	H-8 --> L		
	H-9 --> L		
6		3.795	326
	H-2 --> L		
	H-5 --> L		
	H-6 --> L		
	H-7 --> L		
	H-2 --> L+1		
	H-7 --> L+1		
7		3.946	313
	H --> L+1		
	H --> L+2		
	H-1 --> L+1		
	H-2 --> L+2		
8		4.171	296
	H --> L+1		
	H-1 --> L+2		
	H-1 --> L+1		
9		4.349	284
	H-2 --> L+1		
	H --> L+2		
10		4.388	282
	H-10 --> L		

H-10 --> L+1
H-9 --> L
H-5 --> L
H-2 --> L+1

Figure A11: Orbital contributions to the calculated transitions for **4**. H = HOMO and L = LUMO.

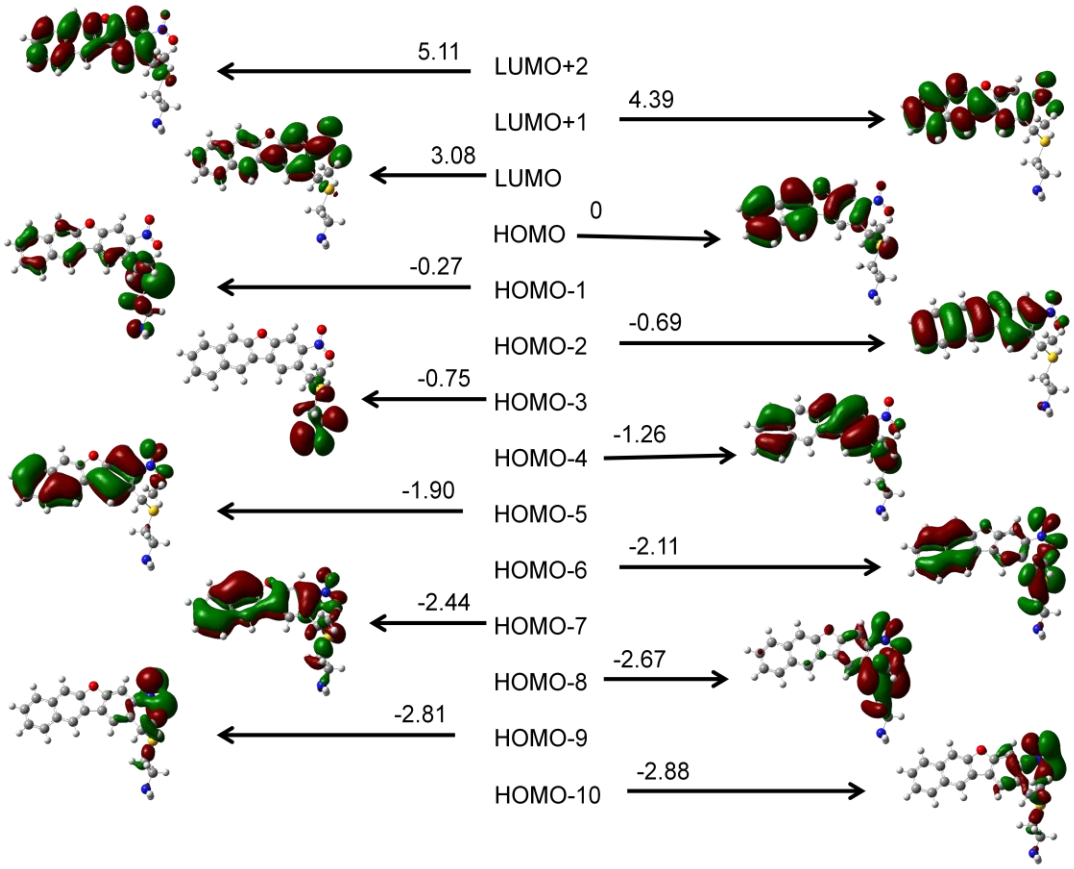

Figure A12: Molecular orbitals involved in the first 10 calculated transitions of **4**.

Figures A13- A24 show the pump probe plots of the sample and solvent and the time integrated pump probe plots for **1-4**.

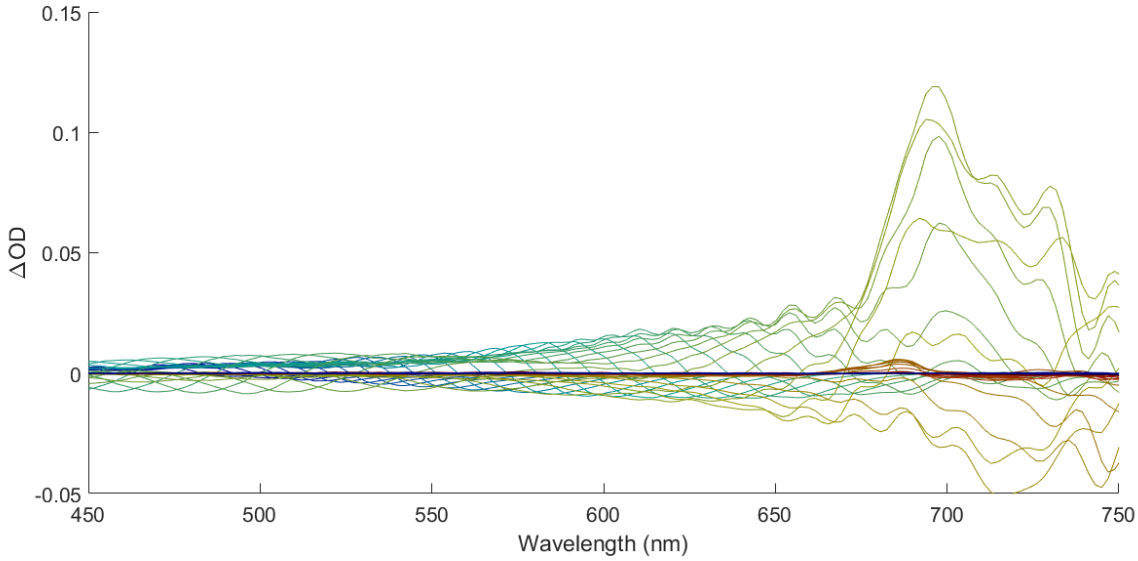

Figure A13: Full frequency pump probe sample spectrum collected during measurement of 2PA cross section for compound **1**.

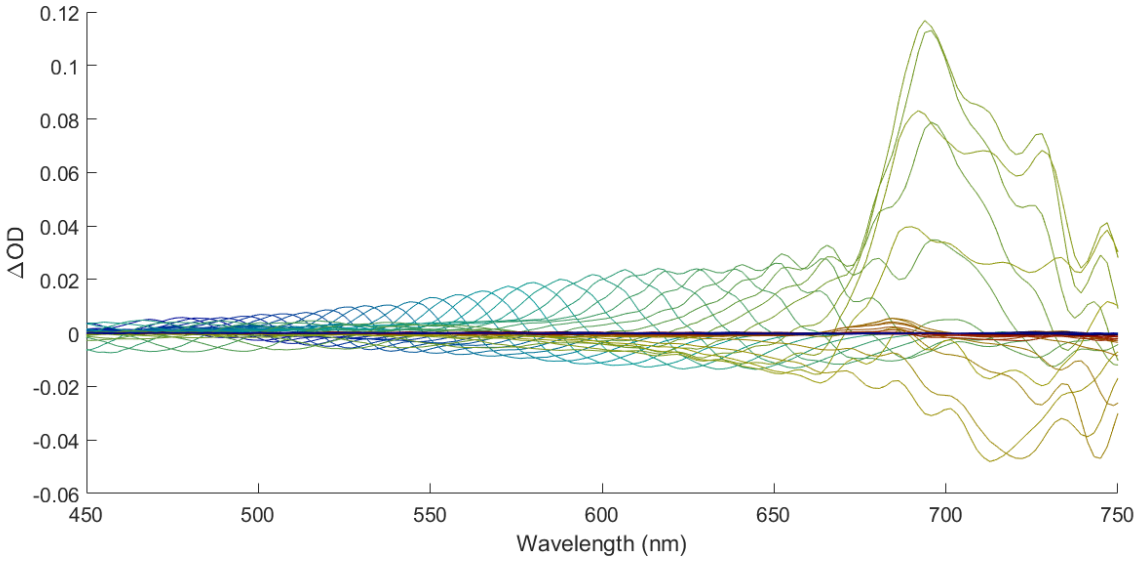

Figure A14: Full frequency pump probe solvent spectrum (d6-DMSO) collected during measurement of 2PA cross section for compound **1**.

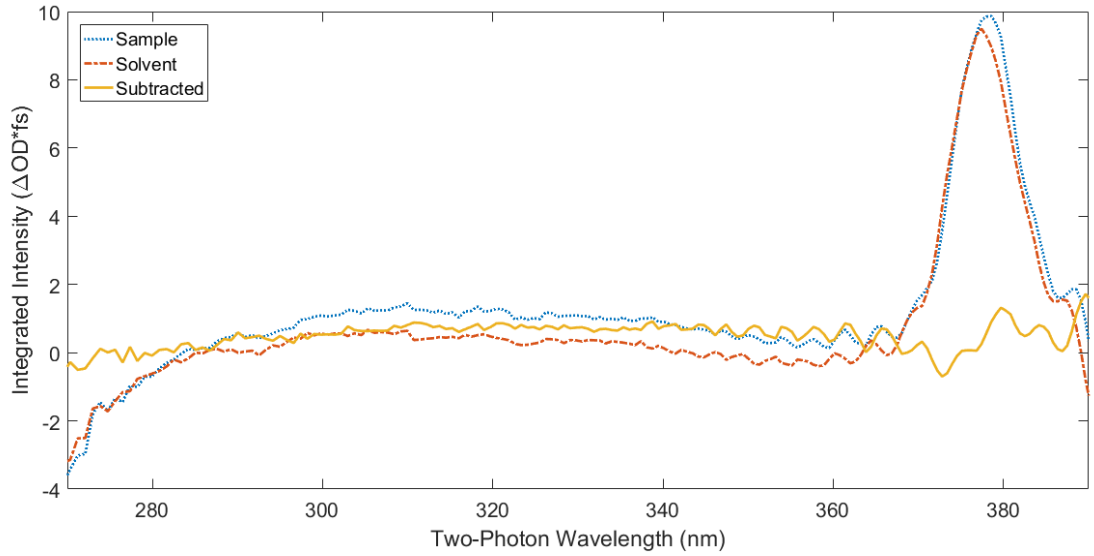

Figure A15: Integrated spectra for the sample, solvent, and the sample – solvent for compound **1**.

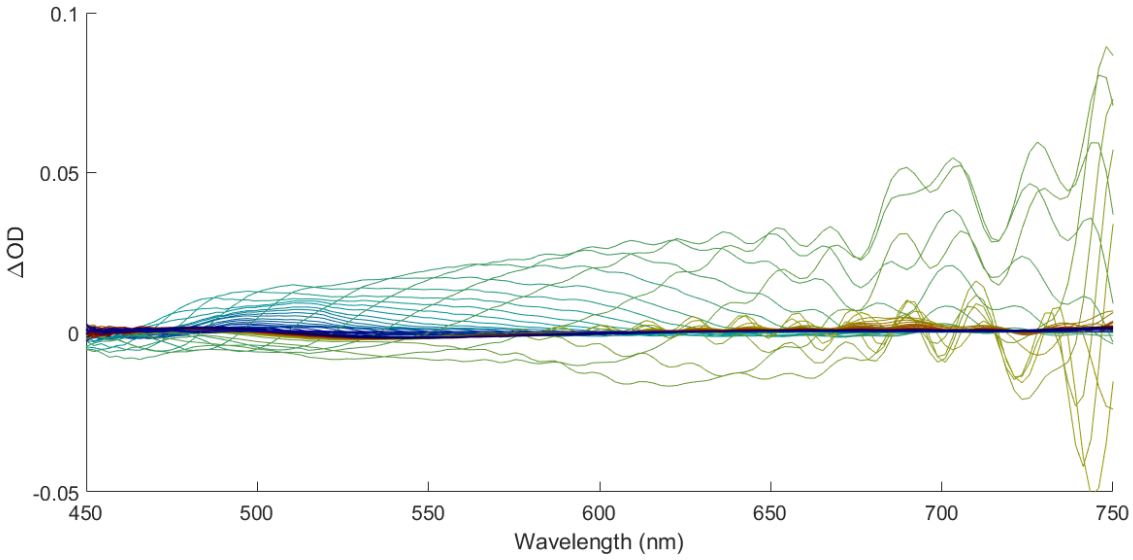

Figure A16: Full frequency pump probe sample spectrum collected during measurement of 2PA cross section for compound **2**.

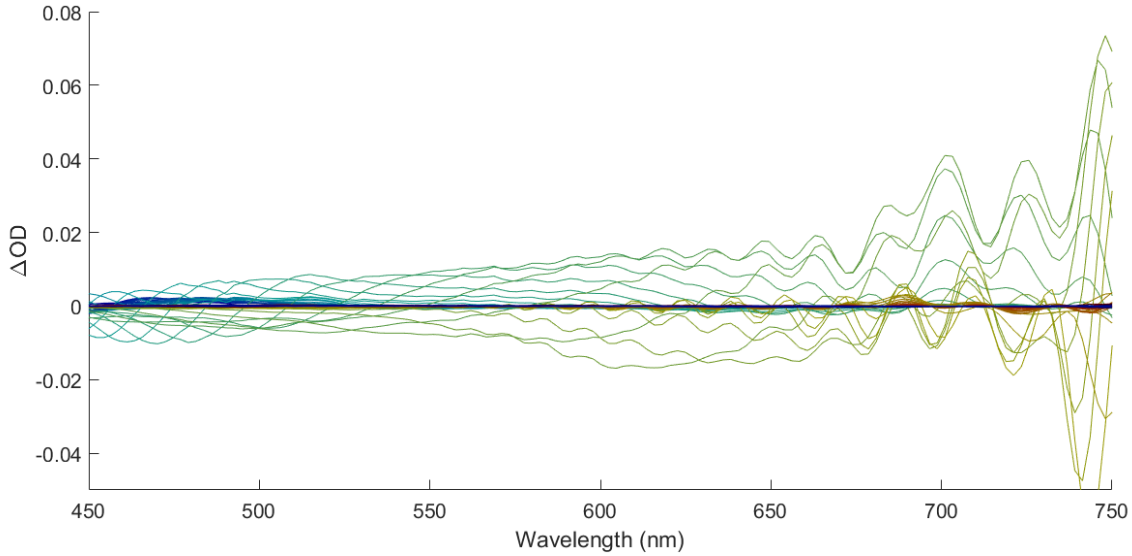

Figure A17: Full frequency pump probe solvent spectrum (d6-DMSO) collected during measurement of 2PA cross section for compound **2**.

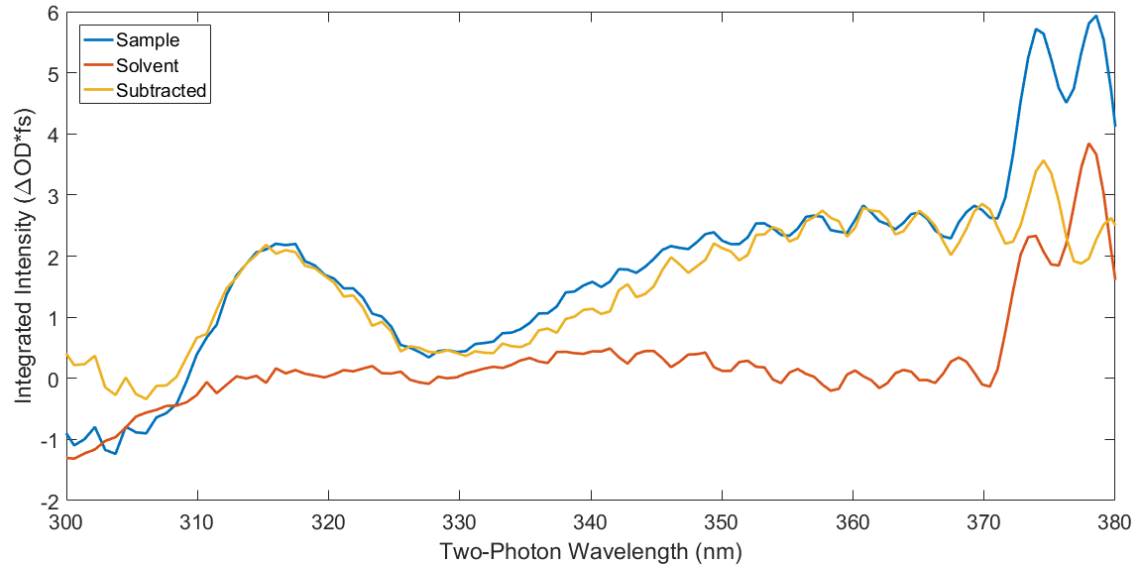

Figure A18: Integrated spectra for the sample, solvent, and the sample – solvent for compound **2**.

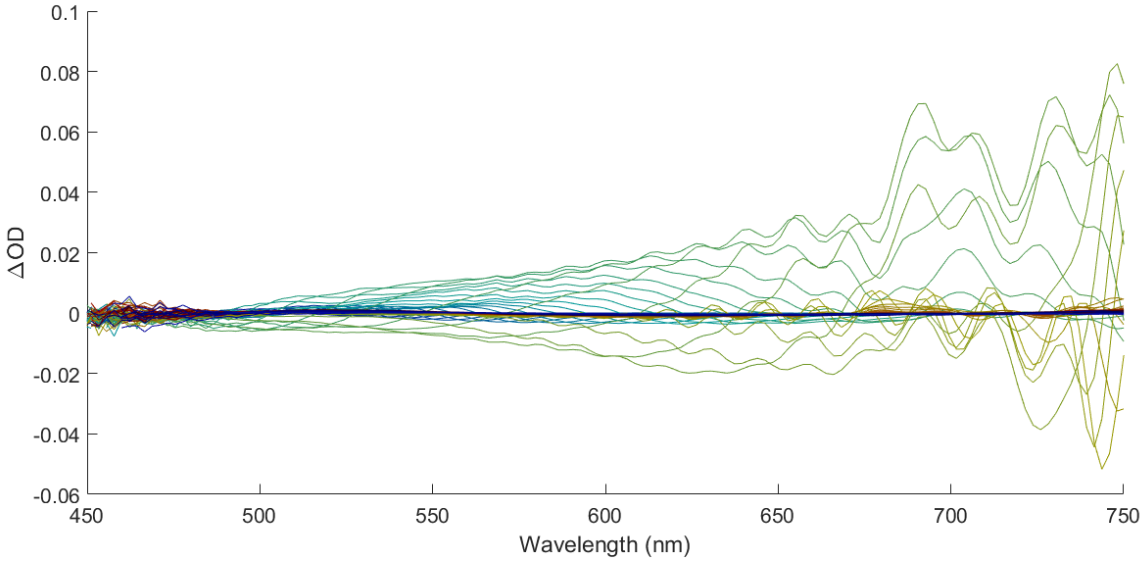

Figure A19: Full frequency pump probe sample spectrum collected during measurement of 2PA cross section for compound **3**.

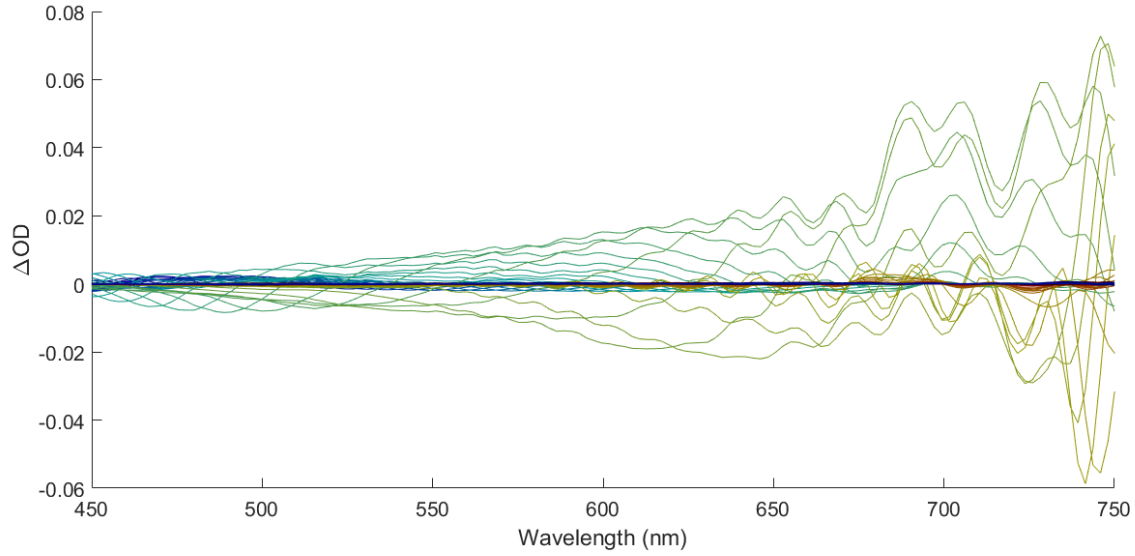

Figure A20: Full frequency pump probe solvent spectrum (d6-DMSO) collected during measurement of 2PA cross section for compound **3**.

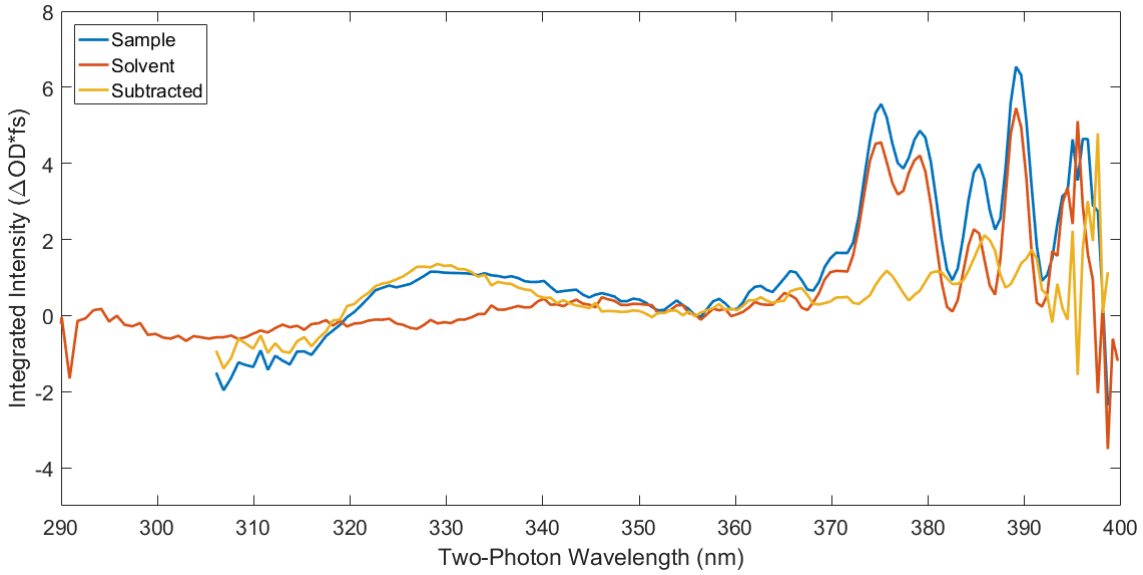

Figure A21: Integrated spectra for the sample, solvent, and the sample – solvent for compound **3**.

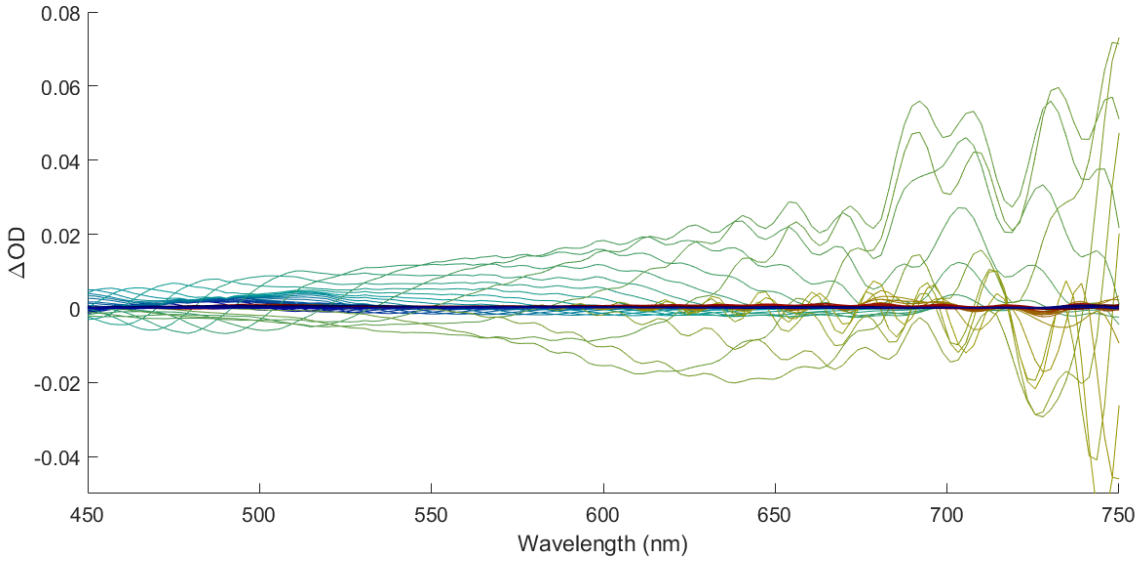

Figure A22: Full frequency pump probe sample spectrum collected during measurement of 2PA cross section for compound **4**.

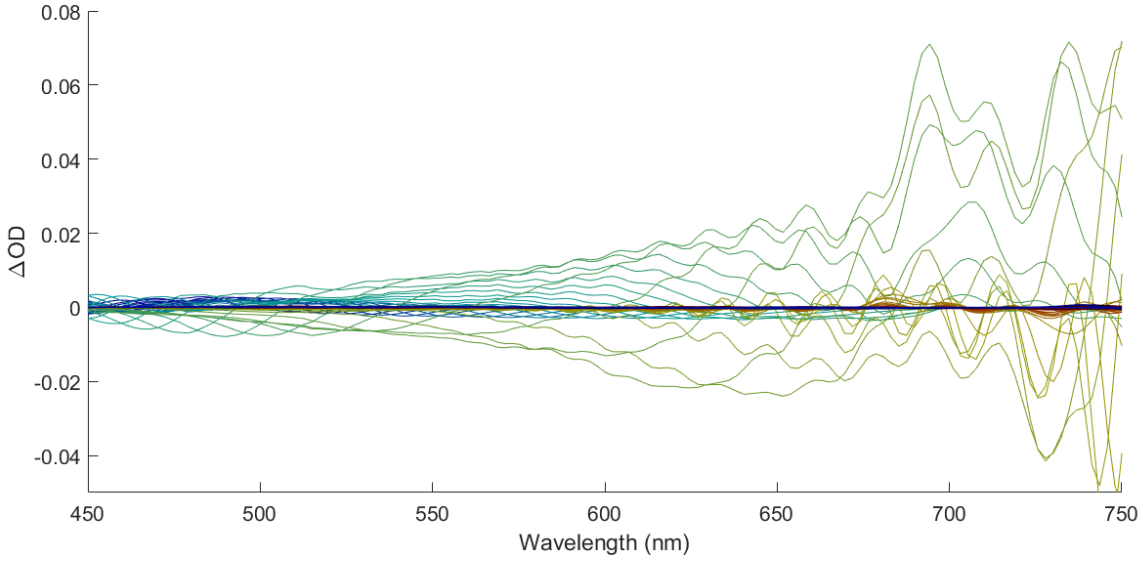

Figure A23: Full frequency pump probe solvent spectrum (d6-DMSO) collected during measurement of 2PA cross section for compound **4**.

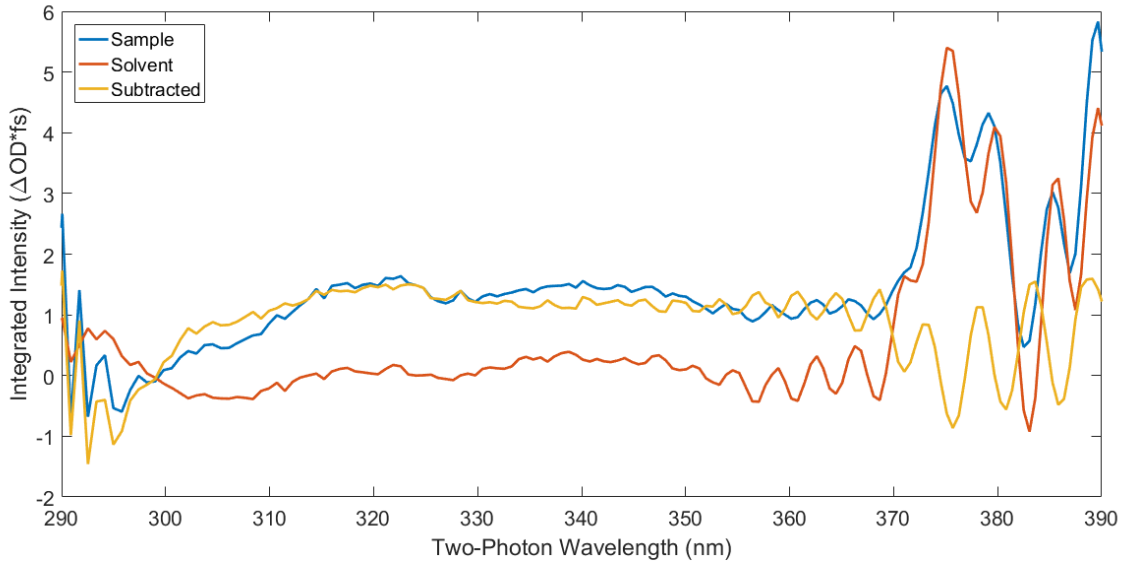

Figure A24: Integrated spectra for the sample, solvent, and the sample – solvent for compound **4**.

Relevant Cartesian coordinates of the optimized structures for each compound taken from Gaussian.

1:

C	0.588251	0.586658	0.517996
C	0.191172	1.817327	-0.07704
C	-1.11845	2.081033	-0.50183
C	-2.04291	1.072454	-0.3411
C	-1.7163	-0.16981	0.232986
C	-0.40636	-0.39107	0.663337
H	-1.37064	3.034513	-0.94534
H	-0.14759	-1.33674	1.128971
C	-3.90615	-0.08581	-0.36328
C	-5.23065	-0.45165	-0.55929
C	-5.58813	-1.73552	-0.14331
C	-4.65181	-2.60762	0.442792
C	-3.3273	-2.22041	0.630552
C	-2.94594	-0.93554	0.220559
H	-5.94473	0.227553	-1.01205
H	-4.96991	-3.59831	0.752717
H	-2.60876	-2.89705	1.082982
O	-3.36394	1.135929	-0.70789
N	1.131077	2.909707	-0.32592
O	0.676687	4.047563	-0.4796
O	2.337488	2.654714	-0.39788
C	1.959472	0.229736	1.081382
S	3.224365	-0.07628	-0.26145
C	3.533316	-1.87332	0.006508
C	4.600476	-2.36849	-0.97194
H	2.607184	-2.43652	-0.14452
H	3.869202	-2.02886	1.03844
H	4.246704	-2.22338	-1.99933
H	5.512273	-1.75881	-0.8574
N	4.822063	-3.80854	-0.76966
H	5.459605	-4.14571	-1.49039
H	5.319232	-3.94547	0.110758
H	-6.61364	-2.06691	-0.27649
C	2.479963	1.155151	2.191029
H	3.374216	0.714017	2.641971
H	1.717885	1.258009	2.973107
H	2.739123	2.148246	1.82276
H	1.834182	-0.75677	1.532675

2:

C	-1.35033	-0.61482	0.525907
C	-1.16788	-1.89103	-0.07825
C	0.082733	-2.3669	-0.50398
C	1.162227	-1.53203	-0.33289
C	1.050975	-0.25528	0.250726
C	-0.2052	0.180044	0.679585
H	0.1716	-3.34542	-0.95542
H	-0.30228	1.152774	1.151226
C	3.197518	-0.70812	-0.34306
C	4.559228	-0.57952	-0.53505
C	5.144961	0.624375	-0.10892
C	4.366277	1.64428	0.484845
C	2.995728	1.479035	0.662202
C	2.390097	0.288139	0.246333
H	5.162028	-1.35695	-0.98968
H	4.832083	2.566782	0.807836
H	2.410939	2.27118	1.119581
O	2.457288	-1.81625	-0.69833
N	-2.27476	-2.80652	-0.33502
O	-2.01504	-3.99774	-0.53834
O	-3.42777	-2.3615	-0.36364
C	-2.64086	-0.03255	1.092374
S	-3.84711	0.469292	-0.24509
C	-3.83344	2.296596	-0.00516
C	-4.79365	2.957919	-0.99603
H	-2.8218	2.684131	-0.16021
H	-4.13825	2.525494	1.022754
H	-4.46823	2.737376	-2.01936
H	-5.7992	2.520645	-0.87791
N	-4.75814	4.417408	-0.81548
H	-5.32547	4.850715	-1.54351
H	-5.2247	4.65289	0.060866
C	-3.29783	-0.85327	2.212067
H	-4.10867	-0.27172	2.661581
H	-2.55809	-1.0688	2.992681
H	-3.71192	-1.79602	1.853274
H	-2.35248	0.922761	1.536077
O	6.483906	0.716265	-0.31279
C	7.165457	1.904832	0.092202
H	7.078082	2.064382	1.172836
H	8.212213	1.745619	-0.16869

H	6.785021	2.782874	-0.44178

3:

C	-1.8358	-0.67237	0.516731
C	-1.78512	-1.96581	-0.07627
C	-0.59727	-2.56074	-0.52554
C	0.559574	-1.82631	-0.39206
C	0.57947	-0.5395	0.178443
C	-0.61917	0.014694	0.633718
H	-0.61021	-3.54818	-0.96615
H	-0.6138	0.996271	1.096978
C	2.65643	-1.1904	-0.46197
C	4.02706	-1.18516	-0.67558
C	4.726494	-0.04359	-0.27975
C	4.048729	1.064707	0.301534
C	2.67536	1.025021	0.514663
C	1.963738	-0.12107	0.134449
H	4.551422	-2.02217	-1.12207
H	2.185769	1.882722	0.964363
O	1.81136	-2.23133	-0.78569
N	-2.97993	-2.7779	-0.2963
O	-2.83834	-3.99405	-0.45963
O	-4.08238	-2.22159	-0.33553
C	-3.05472	0.029845	1.105236
S	-4.22916	0.645541	-0.21326
C	-4.03499	2.463191	0.021444
C	-4.94975	3.213478	-0.94892
H	-2.99477	2.752057	-0.15801
H	-4.29273	2.720504	1.055496
H	-4.67312	2.959563	-1.97884
H	-5.99024	2.877888	-0.80403
N	-4.76555	4.662665	-0.77613
H	-5.30459	5.148531	-1.49234
H	-5.18491	4.945303	0.110046
C	-3.77045	-0.72373	2.23599
H	-4.50924	-0.06372	2.701028
H	-3.04246	-1.016	3.002541
H	-4.28595	-1.618	1.884509
H	-2.6687	0.95282	1.543151
O	6.076122	0.001352	-0.51682
C	6.913978	-0.01376	0.654355

H	7.940812	0.027762	0.287202
H	6.711514	0.848117	1.295117
H	6.762386	-0.94206	1.217271
O	4.752724	2.179409	0.699439
C	5.197519	3.024352	-0.3756
H	4.34048	3.406723	-0.94269
H	5.726992	3.856379	0.092421
H	5.87396	2.485998	-1.04628

4:

C	-1.69948	-0.62978	0.525681
C	-1.64852	-1.94053	-0.0224
C	-0.46122	-2.55538	-0.44622
C	0.698572	-1.82133	-0.33282
C	0.717206	-0.51757	0.193576
C	-0.47897	0.05644	0.624179
H	-0.47635	-3.5573	-0.85276
H	-0.47131	1.053469	1.053201
C	2.80879	-1.20342	-0.41921
C	4.159729	-1.21017	-0.63739
C	4.887379	-0.04262	-0.27809
C	4.201322	1.092141	0.293578
C	2.799624	1.043113	0.497543
C	2.105449	-0.09821	0.143736
H	4.664104	-2.06909	-1.06791
H	2.290323	1.900824	0.927985
O	1.948954	-2.24806	-0.70792
N	-2.84681	-2.75619	-0.22035
O	-2.71027	-3.97928	-0.31805
O	-3.94298	-2.19415	-0.30777
C	-2.91871	0.094919	1.085301
S	-4.07841	0.680813	-0.2596
C	-3.8888	2.503354	-0.06205
C	-4.79457	3.231226	-1.05767
H	-2.84718	2.789633	-0.23734
H	-4.15725	2.782206	0.963654
H	-4.50812	2.954182	-2.0789
H	-5.83631	2.898581	-0.9151
N	-4.61216	4.683991	-0.91606
H	-5.14316	5.153185	-1.64918
H	-5.04112	4.987003	-0.04132

C	-3.64885	-0.62379	2.229431
H	-4.38503	0.05426	2.671999
H	-2.92936	-0.90317	3.008676
H	-4.17055	-1.52178	1.896974
H	-2.53053	1.027071	1.501303
C	6.295027	0.039291	-0.4699
C	4.960156	2.246974	0.642251
C	6.99282	1.172774	-0.12018
C	6.319773	2.288861	0.441747
H	6.811989	-0.81457	-0.90015
H	4.439398	3.098837	1.072206
H	6.884354	3.176363	0.712563
H	8.067318	1.216792	-0.27416

Relevant orbital energies of each compound in Hartree taken from Dalton. The bold numbers denote HOMO and LUMO.

1:

-88.85242404	-19.22123367	-19.18786790	-19.18567688	-14.57688717
-14.30637194	-10.26399509	-10.25806713	-10.25682654	-10.22888813
-10.22827970	-10.21799726	-10.21711318	-10.20960568	-10.20748481
-10.20458690	-10.20083604	-10.20021419	-10.19905511	-10.19836593
-10.19221091	-10.17284067	-7.92714604	-5.89150475	-5.88797437
-5.88115749	-1.23256084	-1.12149027	-1.05721372	-0.89737547
-0.87984586	-0.87005807	-0.82669015	-0.82098162	-0.77756289
-0.77082035	-0.75756932	-0.73982753	-0.70293714	-0.67423092
-0.65216061	-0.63886077	-0.61067119	-0.60417007	-0.59507489
-0.57371774	-0.56314135	-0.54118258	-0.52844769	-0.51918921
-0.50864365	-0.49910244	-0.48689251	-0.47537528	-0.47435835
-0.46522462	-0.45552266	-0.45281036	-0.44725785	-0.43557959
-0.42990785	-0.42154087	-0.41478223	-0.40160912	-0.38661532

-0.38060636 -0.37162056 -0.36784458 -0.36687991 -0.36249030

-0.35468238 -0.35089966 -0.34095377 -0.32019919 -0.31785864

-0.31307927 -0.30635812 -0.29144916 -0.27265981 -0.24354486

-0.24131155 -0.24092195 **-0.22295031** **-0.09921951** -0.03825912

-0.01711341 0.00002150 0.02132675 0.04661325 0.06243436

0.08583246 0.09220624 0.09888815 0.11103201 0.12108995

0.13457549 0.13676346 0.14409194 0.14818446 0.15504162

0.16202067 0.16316926 0.17300534

2:

-88.85202530 -19.21999557 -19.18516958 -19.18475320 -19.18283602

-14.57443287 -14.30629762 -10.26367509 -10.26214159 -10.26006835

-10.25429221 -10.23050043 -10.22784904 -10.22754297 -10.21748959

-10.21516086 -10.20749910 -10.20470763 -10.20444080 -10.20275302

-10.19988681 -10.19384871 -10.19267193 -10.17230799 -7.92671907

-5.89107770 -5.88754814 -5.88073693 -1.22959190 -1.12016602

-1.07412326 -1.05398454 -0.89570745 -0.87972369 -0.86963532

-0.82594939 -0.81996575 -0.77741533 -0.77378314 -0.76203765

-0.73972317 -0.72219997 -0.68427695 -0.67324082 -0.64998934

-0.64226872 -0.61171559 -0.59718890 -0.59470482 -0.57394340

-0.56130791 -0.53985255 -0.53066604 -0.52405108 -0.51482714

-0.50860641 -0.48851509 -0.48592083 -0.47716259 -0.47508496

-0.46809188 -0.46056189 -0.45865859 -0.45540668 -0.44147569

-0.43860687 -0.42781834 -0.41533171 -0.41415360 -0.41197766

-0.39823055 -0.38385408 -0.38072473 -0.37589964 -0.36662516

-0.36312518 -0.36070190 -0.35444165 -0.34097913 -0.33699924

-0.33627419 -0.31832405 -0.31533893 -0.31075122 -0.29475360

-0.28404982 -0.27272139 -0.24376061 -0.24167793 -0.22330879

-0.22066983 **-0.09758078** -0.03397127 -0.01660038 0.00163028

0.02715517 0.04825886 0.06288166 0.08593676 0.09139560

0.09915629 0.11123771 0.11165578 0.12246583 0.13538891

0.13683711 0.13862090 0.14456345 0.14920251 0.15892797

0.16260841

3:

-88.85236305 -19.22218009 -19.18711352 -19.18486752 -19.17086510

-19.16721151 -14.57621816 -14.30631735 -10.26402090 -10.26040896

-10.25729024 -10.25625102 -10.24911345 -10.22878607 -10.22815658

-10.22387926 -10.22306371 -10.21874949 -10.21693930 -10.20934689

-10.20904540 -10.20455013 -10.20205628 -10.20015337 -10.19967859

-10.17272024 -7.92707845 -5.89143634 -5.88790698 -5.88109241

-1.23172680 -1.12247828 -1.06792427 -1.05629386 -1.04594245

-0.89723930 -0.87978551 -0.87030711 -0.82680834 -0.82072964

-0.77805712 -0.77271924 -0.76295080 -0.74140483 -0.71798484

-0.69803101 -0.67597566 -0.67282082 -0.65142993 -0.63368301

-0.61427104 -0.59782262 -0.59544253 -0.57491097 -0.56143563

-0.54324042 -0.53376913 -0.52563874 -0.51952688 -0.51003200

-0.49179413 -0.48758922 -0.48322255 -0.47985011 -0.46797795

-0.46443036 -0.46139258 -0.45815434 -0.45316848 -0.45111569

-0.44334441 -0.43762001 -0.43149847 -0.42664054 -0.41930817

-0.41458829 -0.40267502 -0.39119658 -0.38023877 -0.37295077

-0.36719768 -0.36448772 -0.36315891 -0.35493204 -0.35412561

-0.34203459 -0.34085441 -0.31971270 -0.31713286 -0.31255054

-0.30913078 -0.29670425 -0.28696134 -0.27383192 -0.26771643

-0.24291503 -0.24019349 -0.22965488 **-0.22281413** **-0.09892392**

-0.03797086 -0.01727582 -0.00050596 0.02105810 0.04664658

0.06235738 0.08171102 0.08617776 0.09536459 0.11041146

0.11365285 0.12042188 0.12916665 0.13328061 0.13645179

0.14260141 0.14588602 0.14840668 0.15143860

4:

-88.85275406 -19.21936877 -19.18862159 -19.18653016 -14.57751512

-14.30637423 -10.26558135 -10.25821140 -10.25799704 -10.22974661

-10.22878520 -10.21927427 -10.21695808 -10.21099011 -10.21067289

-10.20823401 -10.20466295 -10.20431094 -10.20364413 -10.20038758

-10.19686727 -10.19060154 -10.19052314 -10.18917992 -10.18825733

-10.17315676 -7.92748067 -5.89183990 -5.88830781 -5.88149069

-1.23335837 -1.11961064 -1.05810399 -0.89841057 -0.88427599

-0.87986176 -0.84125762 -0.82457655 -0.81659736 -0.78395529

-0.77368973 -0.76304115 -0.74330157 -0.72882273 -0.70362099

-0.67438941 -0.65448805 -0.64645914 -0.61566070 -0.61156950

-0.60322002 -0.59437087 -0.57240736 -0.56748439 -0.54354139

-0.53339699 -0.52749621 -0.51712547 -0.50854314 -0.49369463

-0.48643101 -0.47493997 -0.46809958 -0.46507105 -0.46058542

-0.45919635 -0.45279303 -0.44068211 -0.43762516 -0.42763198

-0.42286276 -0.41871814 -0.41493255 -0.40226583 -0.39412265

-0.38829267 -0.37938113 -0.36791372 -0.36674764 -0.36573662

-0.35475769	-0.35294733	-0.34199877	-0.33923919	-0.33813973
-0.32060625	-0.31814013	-0.31273281	-0.30429705	-0.29245402
-0.28444914	-0.26102928	-0.24247969	-0.24014861	-0.22452271
-0.21474301	**-0.10151640**	-0.05324274	-0.02708814	-0.00996293
0.00603021	0.02642904	0.04542566	0.06179599	0.08542625
0.09363832	0.09946534	0.10083339	0.11017905	0.11555880
0.12410190	0.12712091	0.14265833	0.14886391	0.15214345
0.15246198				

Conversion of 2PA absorption to 2PA cross section:

Equation 3.1 was derived from Equation A1 which is used to convert from integrated two-photon absorption signal to 2PA cross section.[116,191]

$$\sigma_{2PA} = \frac{\ln(10)*\hbar*\omega_{pu}}{E_{pu}*l*f_{xy}*N_{sol}} * \int A_{2PA}(\tau)d\tau \qquad \text{(A1)}$$

In Equation A1, σ_{2PA} is the 2PA cross section (in GM, 10^{-50} cm^4·s·molecules^{-1}), $\hbar$ is the reduced Planck's constant ($1.054571817\times10^{-34}$ J·s), ω_{pu} is the frequency of the pump photons (in s^{-1}), E_{pu} is the energy of the pump (in J), l is the path length in (cm), N_{sol} is the number density of the solute/sample (in molecules·cm^{-3}), $\int A_{2PA}(\tau)d\tau$ is the time integrated 2PA signal in s, f_{xy} is the pump/probe overlap factor determined by Equation A2.

$$f_{xy} = \frac{2}{\pi*\sqrt{(w_{pu_x})^2+(w_{pr_x})^2}*\sqrt{(w_{pu_y})^2+(w_{pr_y})^2}} \qquad \text{(A2)}$$

Where w_{pu} and w_{pr} are the 1/e^2 halfwidths of the Gaussian pump (*pu*) and probe (*pr*) pulses. The *x* and *y* subscripts denote the halfwidths of the plane orthogonal to light propagation.

Appendix B

Power dependence plots of each compound showing a linear dependence of the signal on the power of the pump.

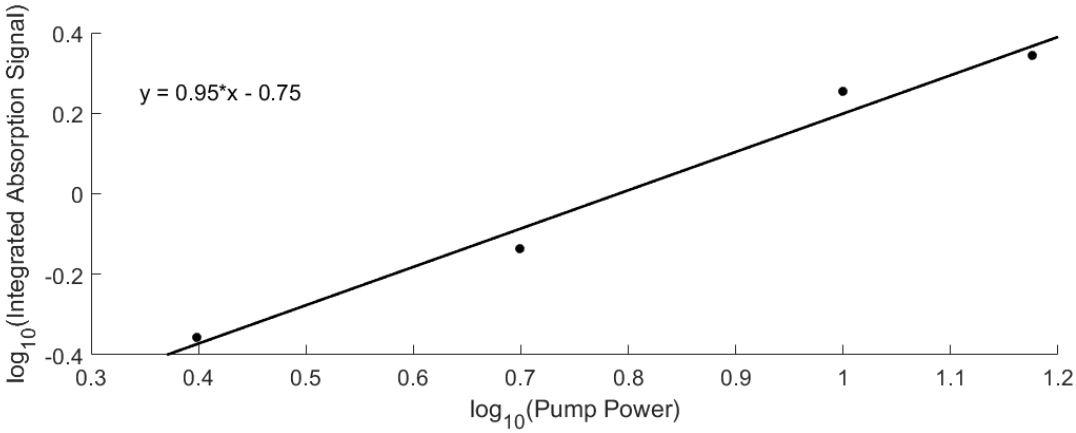

Figure B1: Power dependence plot for **1a**.

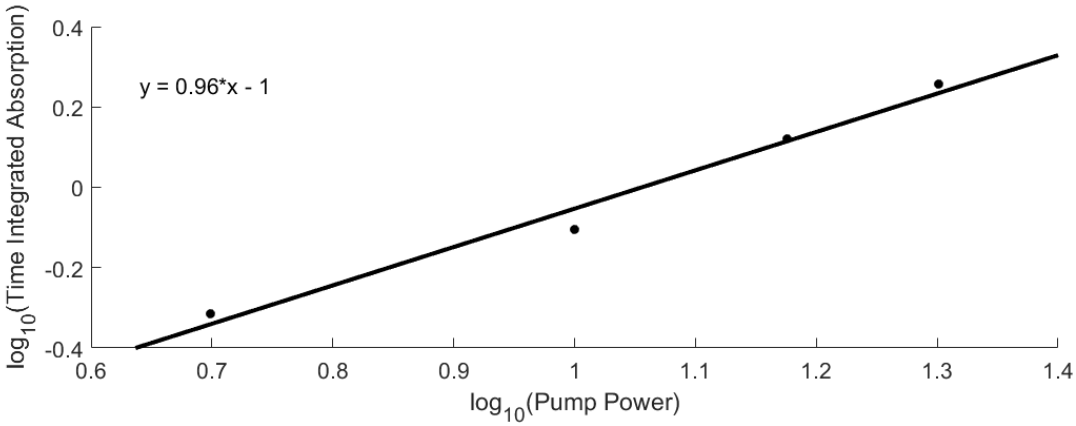

Figure B2: Power dependence plot for **1b**.

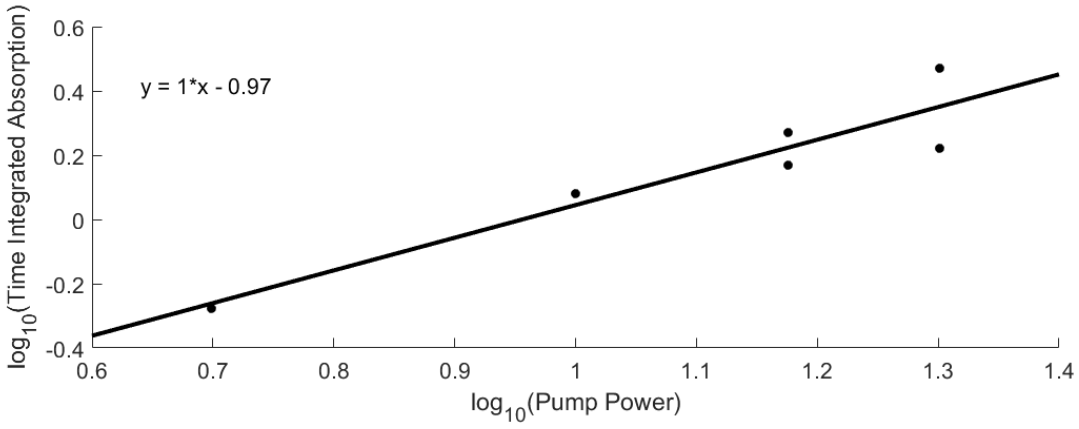

Figure B3: Power dependence plot for **2a**.

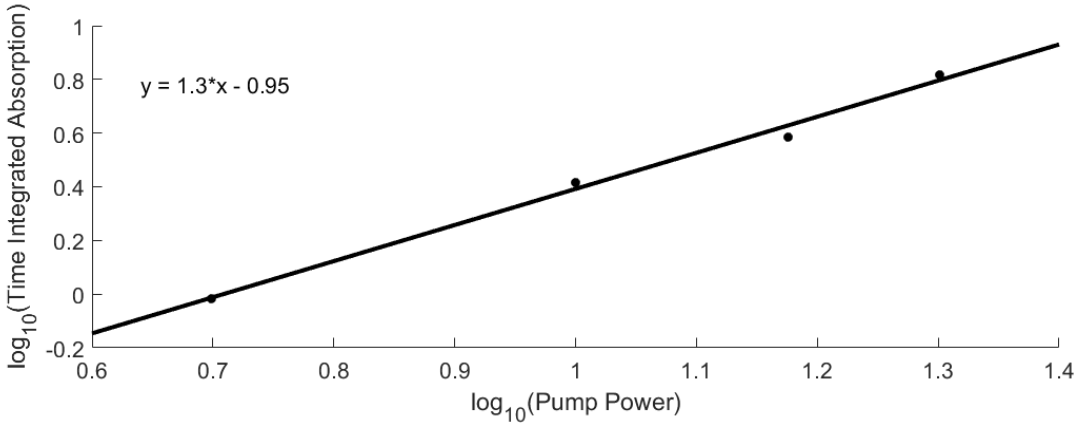

Figure B4: Power dependence plot for **2b**.

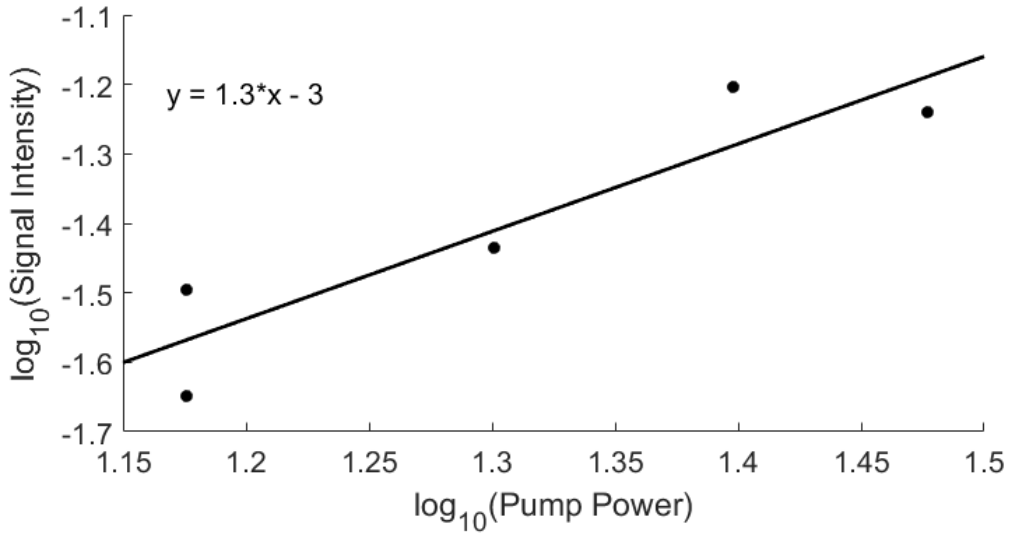

Figure B5: Power dependence plot for **3a**.

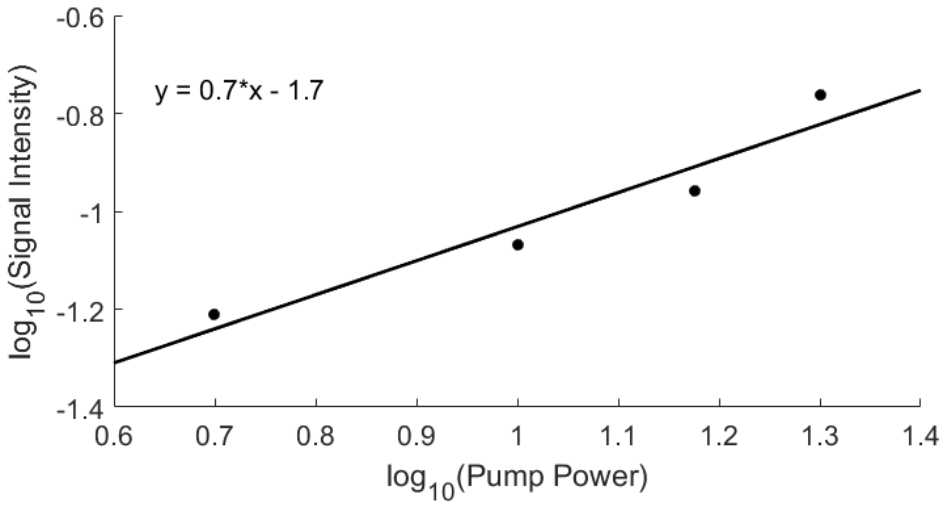

Figure B6: Power dependence plot for **3b**.

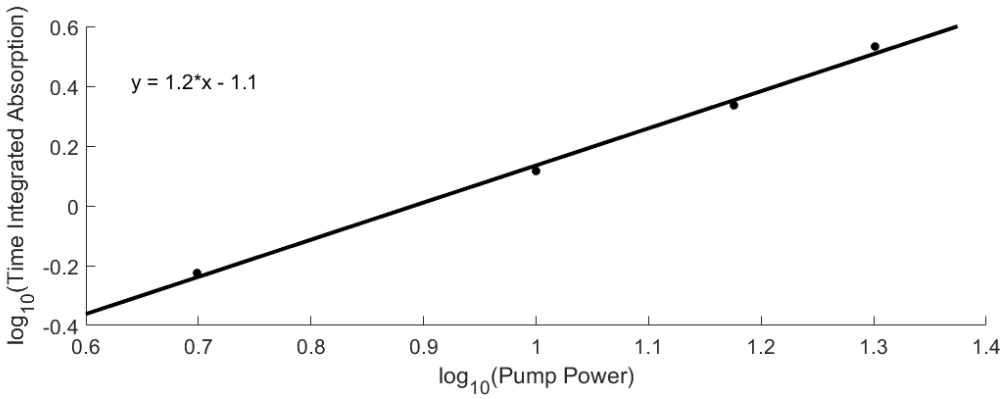

Figure B7: Power dependence plot for **4a**.

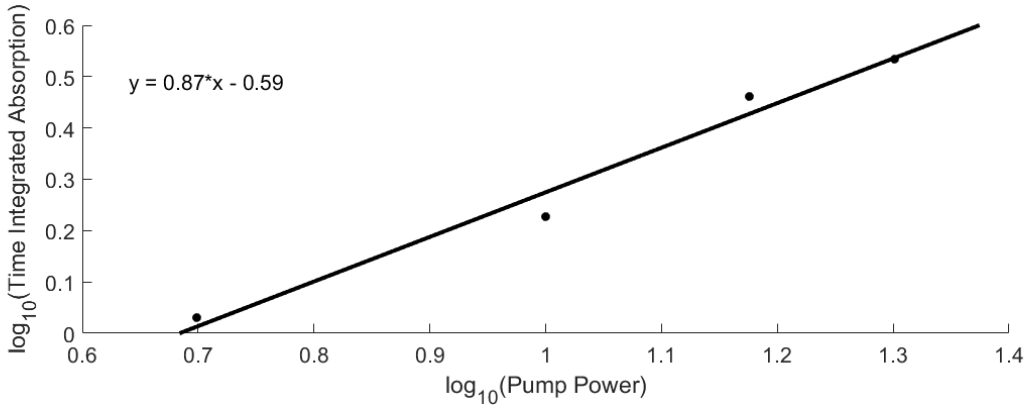

Figure B8: Power dependence plot for **4b**.

Table of orbital contributions to the first 10 transitions of each compound. H = HOMO and L = LUMO.

Compound								
	1a	2a	3a	4a	1b	2b	3b	4b
1	3.32 eV H L	3.40 eV H L H-1 L	2.70 eV H L	3.05 eV H L	3.12 eV H L	3.07 eV H L	2.73 eV H L H-1 L	3.04 eV H-1 L
2	3.49 eV H-1 L	3.44 eV H L H-1 L	3.31 eV H-1 L H-2 L H-3 L	3.33 eV H-1 L H-2 L	3.37 eV H-1 L	3.46 eV H-1 L	3.05 eV H L H-1 L	3.09 eV H L
3	3.86 eV H-3 L	3.84 eV H-4 L	3.44 eV H-1 L	3.42 eV H-1 L H-2 L	3.77 eV H-3 L H-4 L	3.73 eV H-3 L H-4 L H-5 L H-6 L	3.37 eV H-2 L H-3 L	3.39 eV H-2 L
4	4.15 eV H-2 L	4.21 eV H-2 L	3.50 eV H-2 L H-3 L	3.47 eV H-4 L	4.21 eV H-2 L	4.25 eV H-2 L	3.54 eV H-2 L H-3 L	3.49 eV H-4 L
5	4.40 eV H-5 L H-6 L	4.29 eV H-3 L H-8 L	3.80 eV H-5 L	3.82 eV H-3 L	4.40 eV H-5 L H-6 L	4.30 eV H-3 L H-8 L	3.73 eV H-5 L H-6 L	3.83 eV H-10 L H-13 L
6	4.83 eV H-1 L+1 H-2 L+2	4.55 eV H-3 L H-8 L	4.10 eV H-4 L	3.93 eV H-4 L H-10 L	4.66 eV H L+1	4.54 eV H L+1 H-8 L	4.15 eV H-4 L	3.87 eV H-3 L
7	5.00 eV H-1 L+1	4.83 eV H-1 L+1	4.40 eV H L+1 H-9 L	4.00 eV H-5 L	4.78 eV H-3 L H-4 L	4.61 eV H-3 L H-8 L H L+1	4.41 eV H-9 L	4.04 eV H-5 L
8	5.18 eV H-3 L H-4 L	4.88 eV H-5 L	4.42 eV H L+1 H-9 L	4.14 eV H-5 L H-6 L	4.85 eV H-1 L+1 H L+2	4.77 eV H L+2 H-1 L+1 H-4 L H-5 L	4.50 eV H L+1 H-1 L+1	4.19 eV H-6 L H-7 L
9	5.54 eV H L+2 H-1 L+2	4.93 eV H L+1	4.85 eV H-3 L+1 H-2 L+1 H L+2	4.30 eV H-5 L H-6 L	5.27 eV H-1 L+1 H L+2	4.83 eV H L+2 H-5 L H-1 L+1	4.64 eV H L+1 H-1 L+1	4.34 eV H-6 L H-7 L
10	5.62 eV H-1 L+2 H-1 L+3 H-2 L+1	5.21 eV H-4 L H-6 L	4.91 eV H-2 L+1 H L+2 H-6 L H-7 L	4.41 eV H-13 L H-15 L	5.43 eV H L+3	4.93 eV H-6 L	4.72 eV H-5 L H-6 L	4.41 eV H-14 L H-15 L

Figure B9: Orbital contributions to each transition for each compound. For each transition, the energy is given. Ground state to excited state orbital contributions for each transition are also given.

Orbital diagrams for each compound. The energy for each orbital is in eV and is relative to the HOMO.

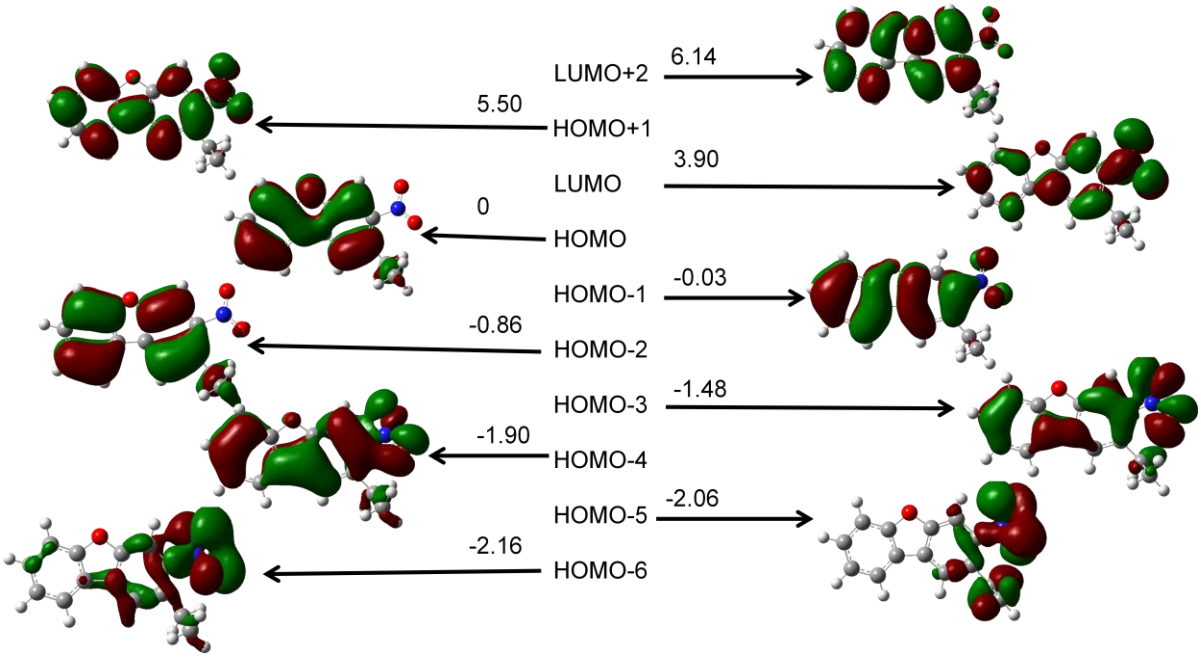

Figure B10: Relevant orbitals for **1a**.

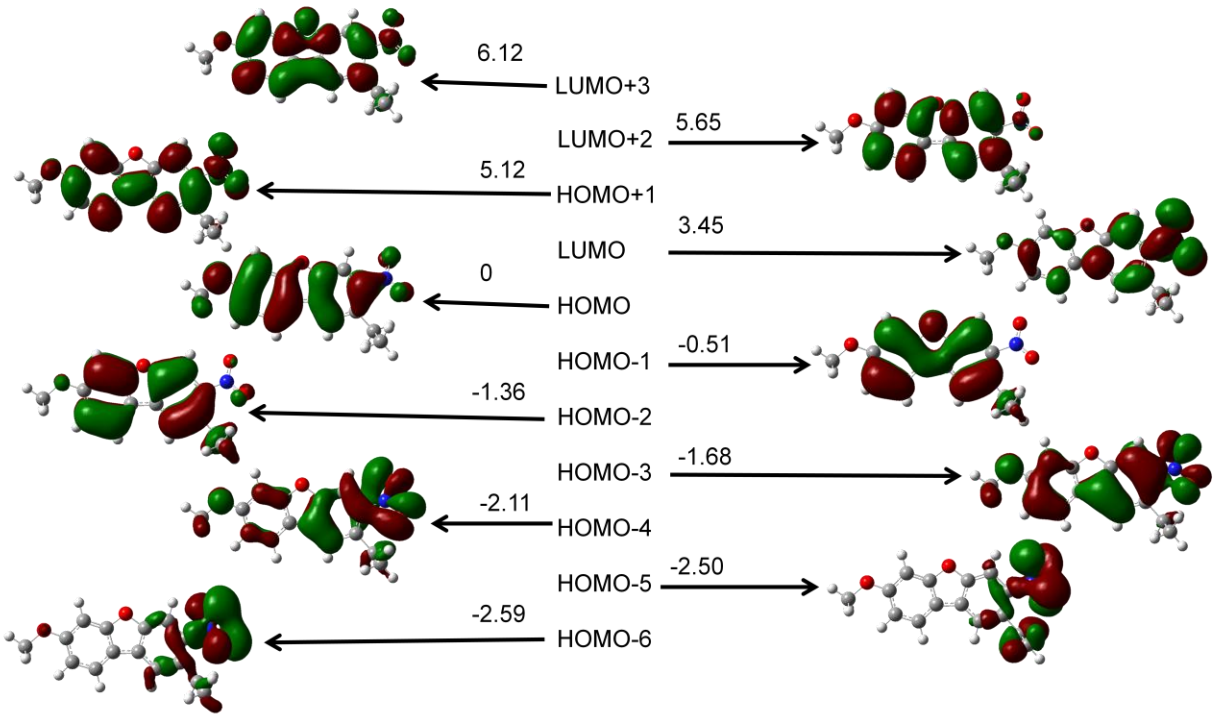

Figure B11: Relevant orbitals for **1b**.

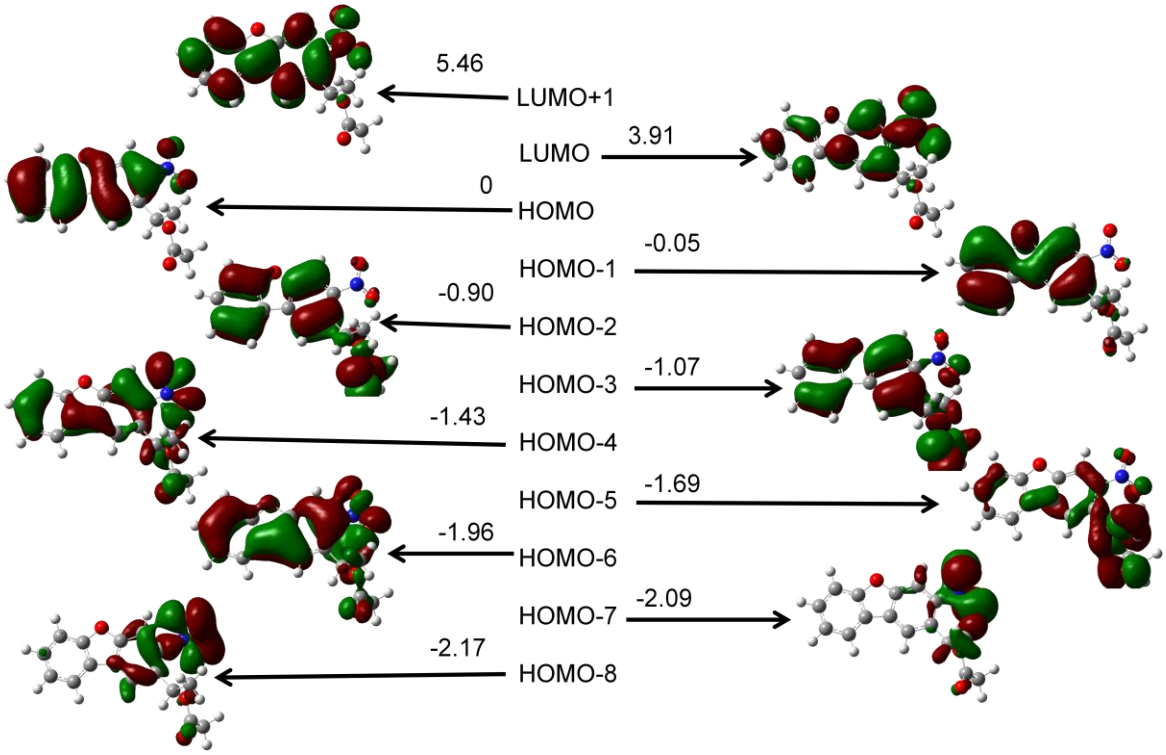

Figure B12: Relevant orbitals for **2a**.

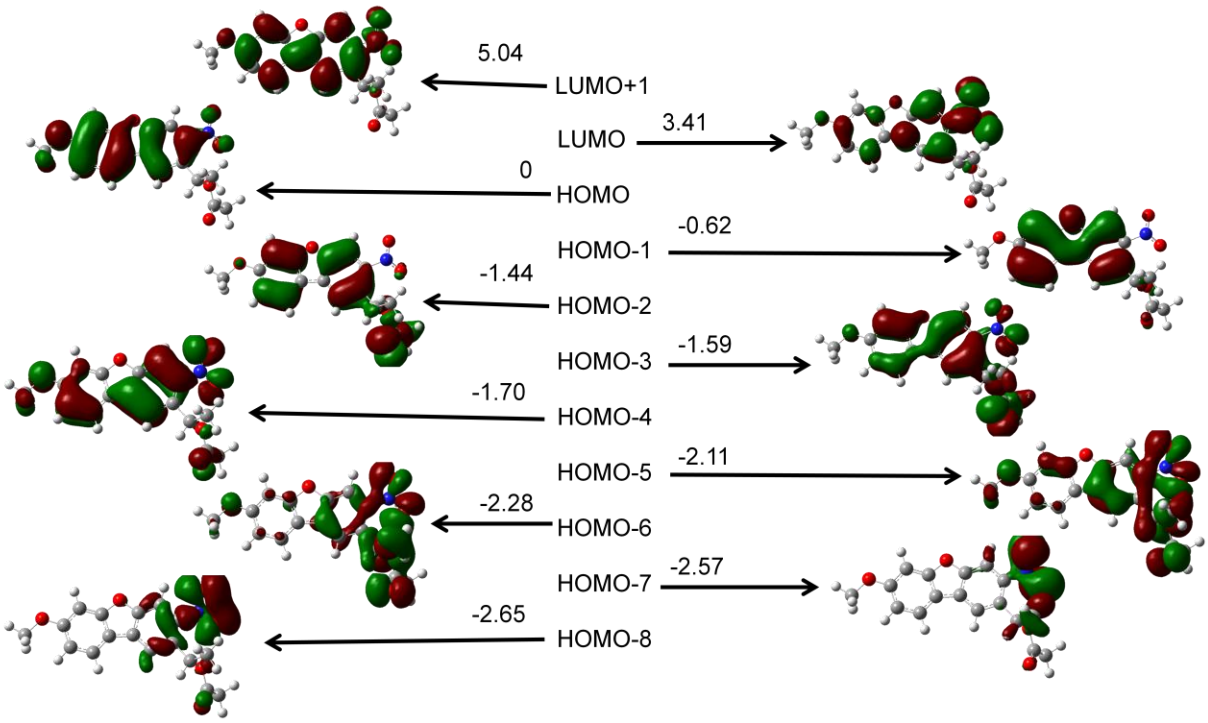

Figure B13: Relevant orbitals for **2b**.

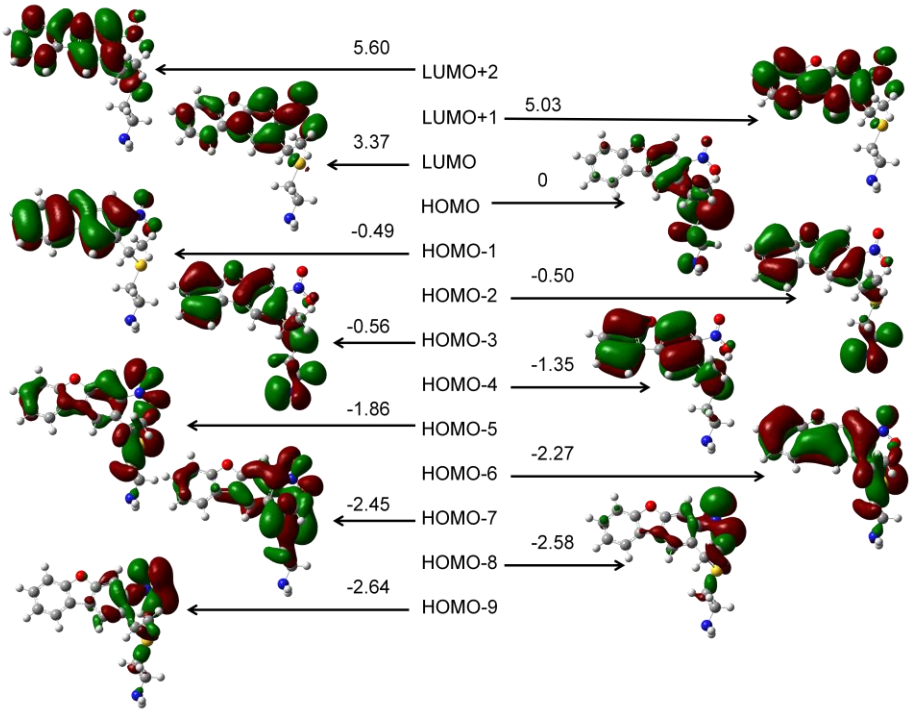

Figure B14: Relevant orbitals for **3a**.

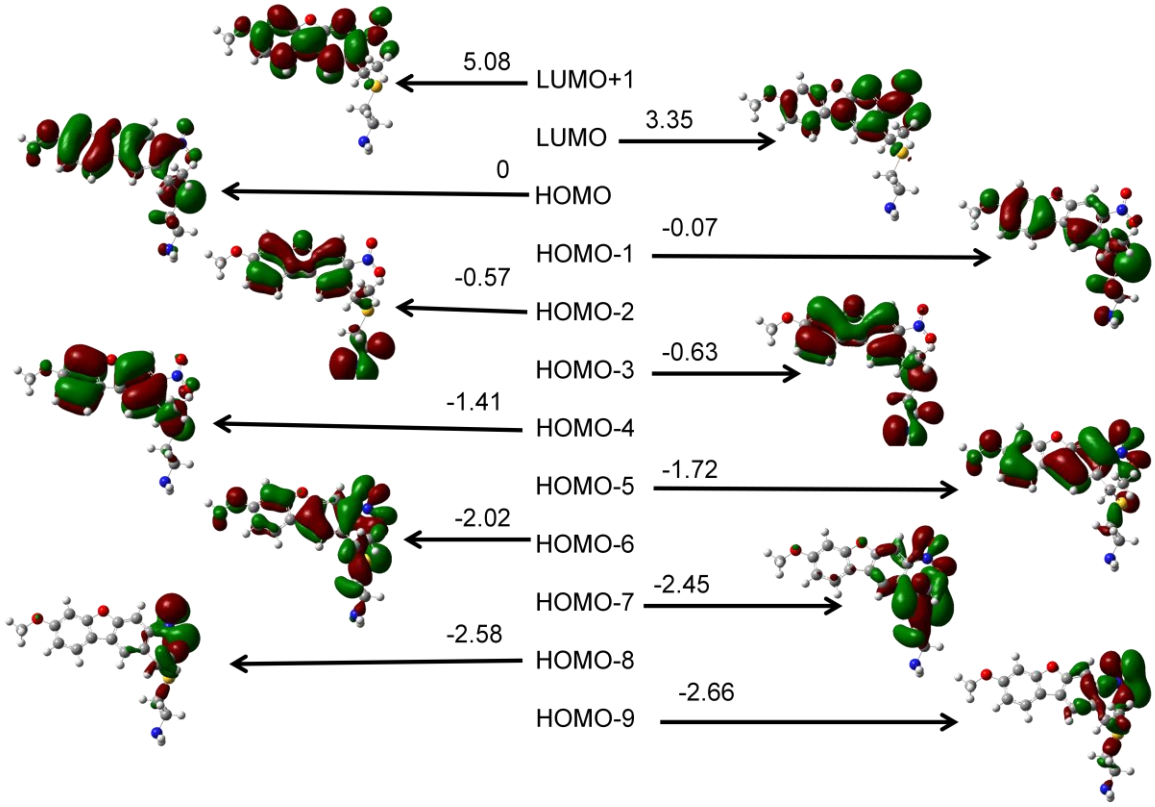

Figure B15: Relevant orbitals for **3b**.

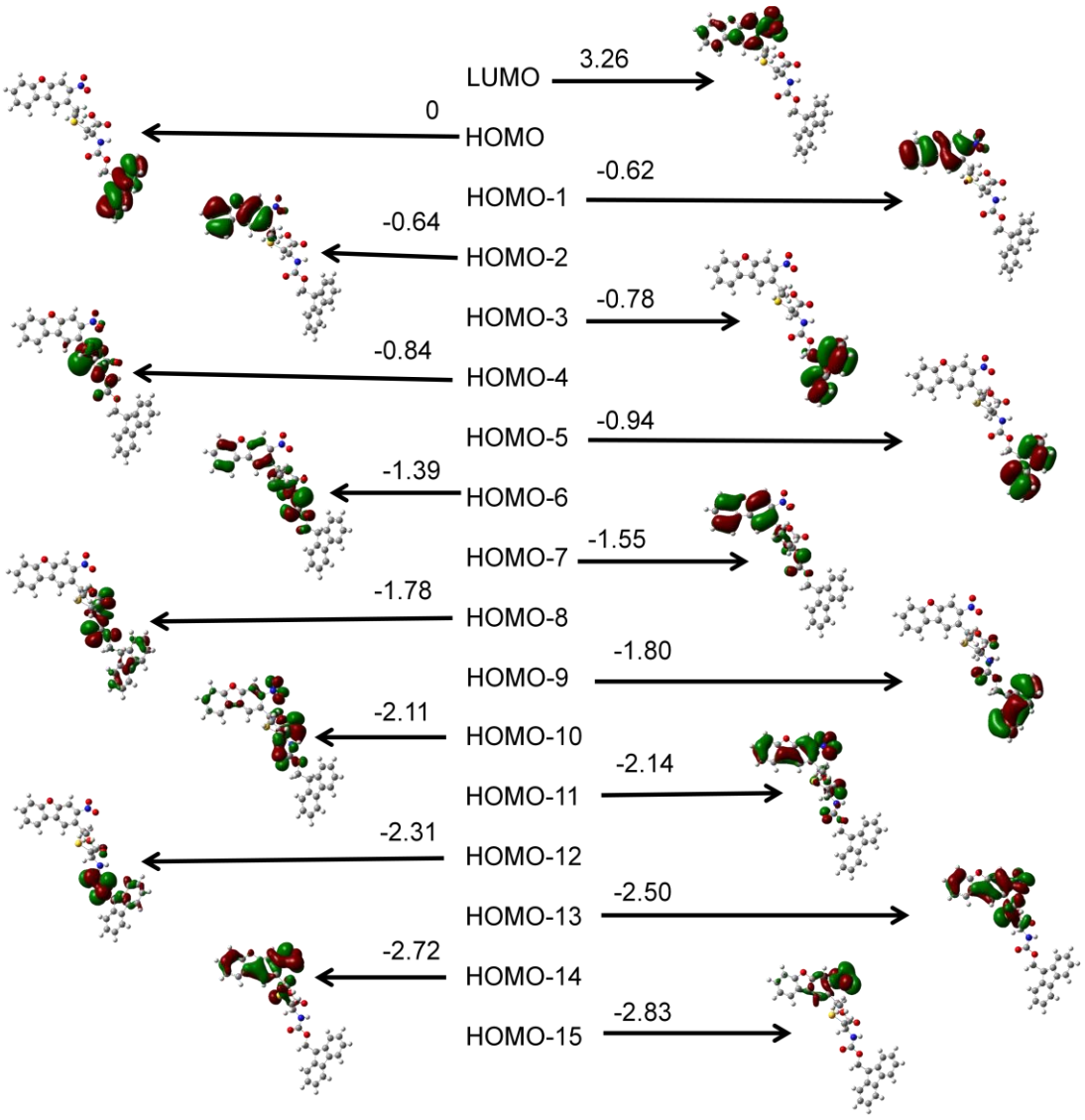

Figure B16: Relevant orbitals for **4a**.

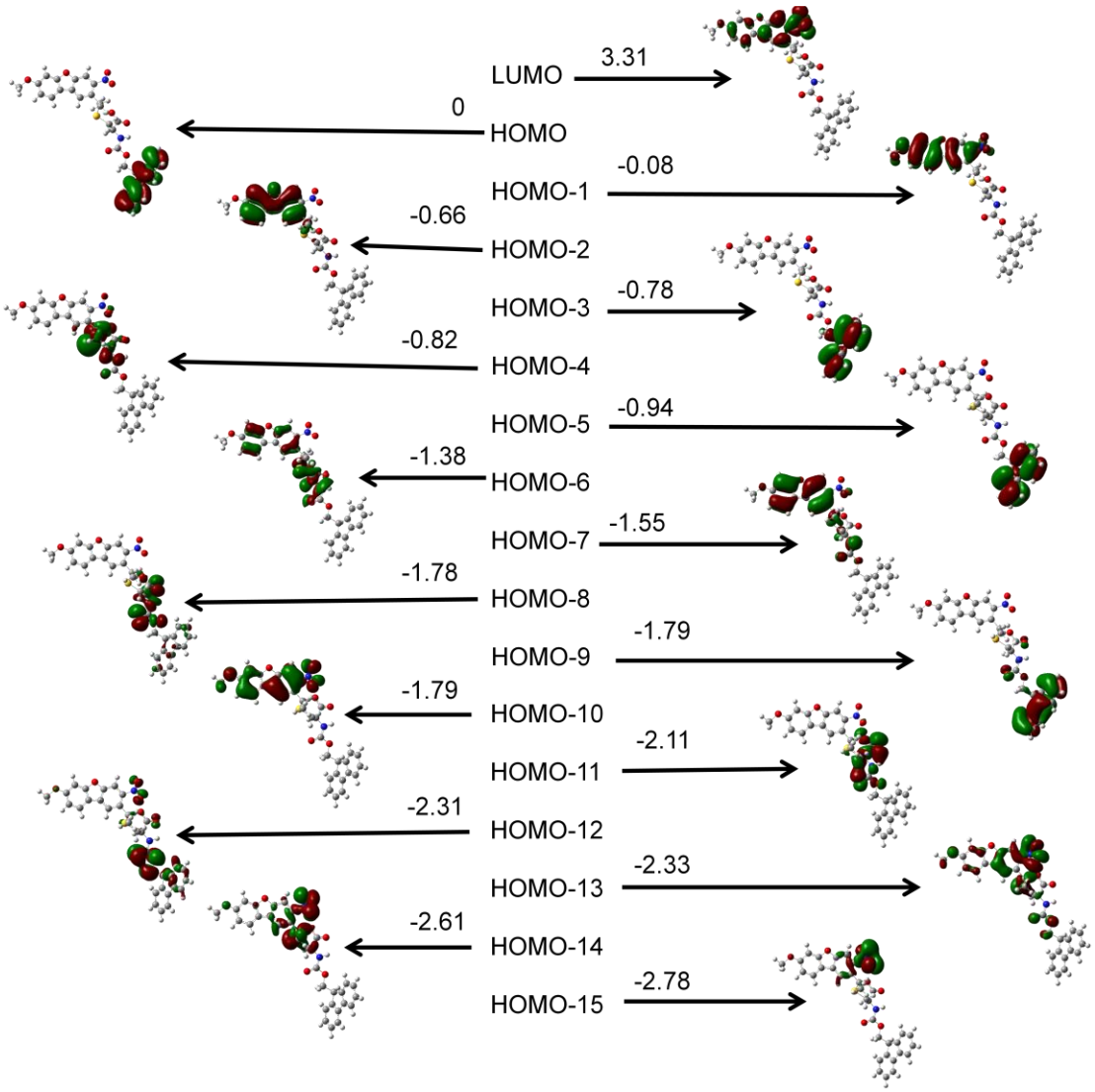

Figure B17: Relevant orbitals for **4b**.

Pump probe spectra and time integrated spectra of the sample and solvent. The solvent subtracted spectrum is also included.

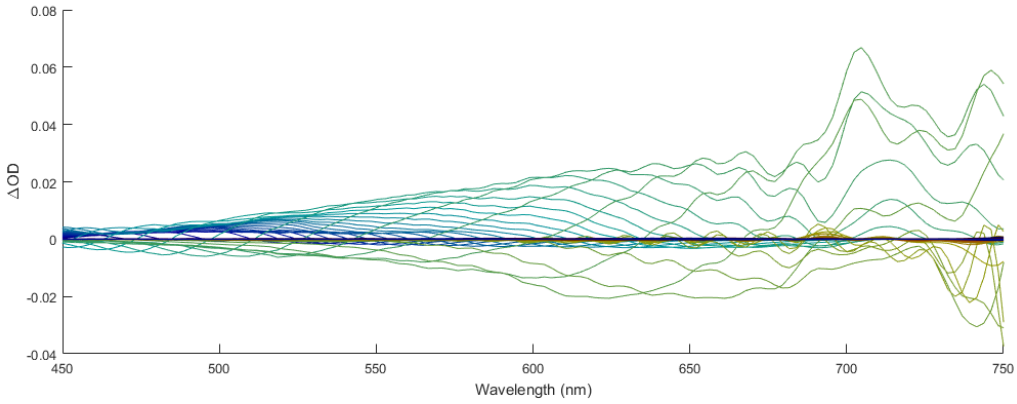

Figure B18: Full frequency pump probe sample spectrum collected during measurement of 2PA cross section for compound **1a**.

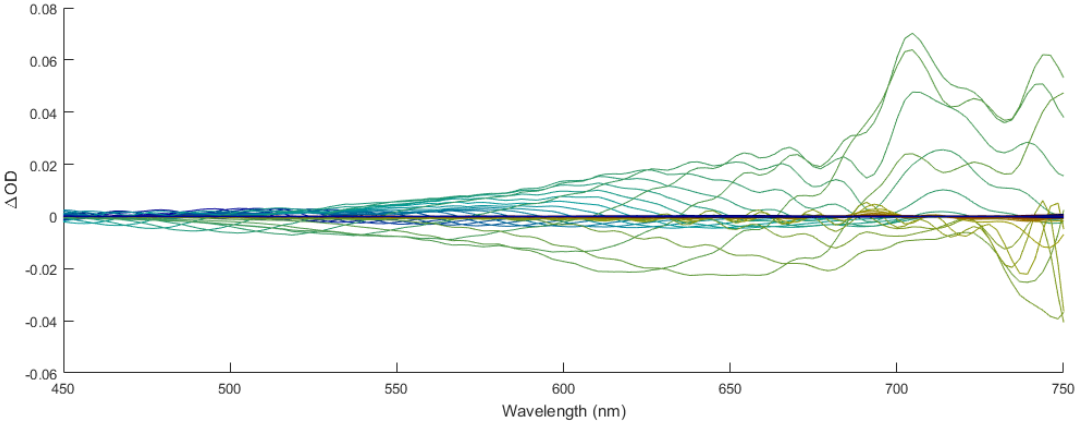

Figure B19: Full frequency pump probe solvent spectrum (d6-DMSO) collected during measurement of 2PA cross section for compound **1a**.

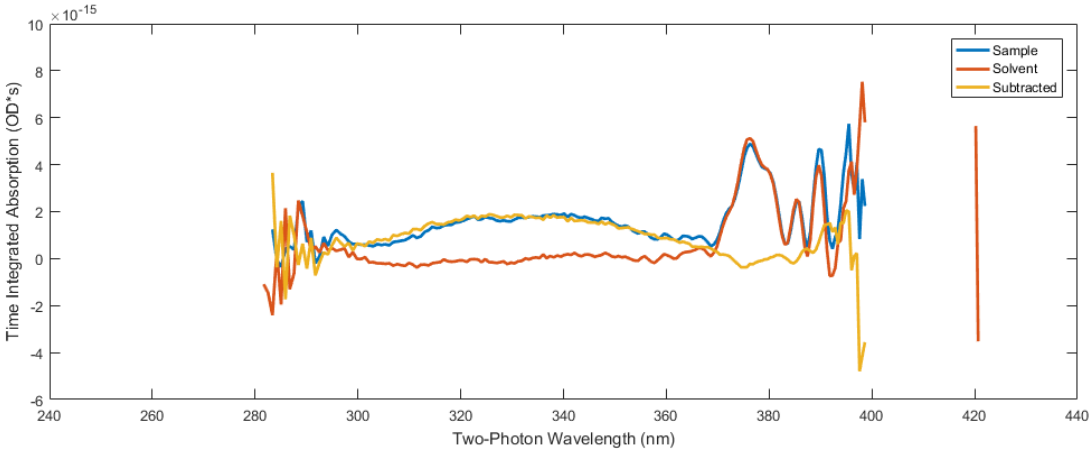

Figure B20: Time integrated spectra of the sample and solvent for **1a**.

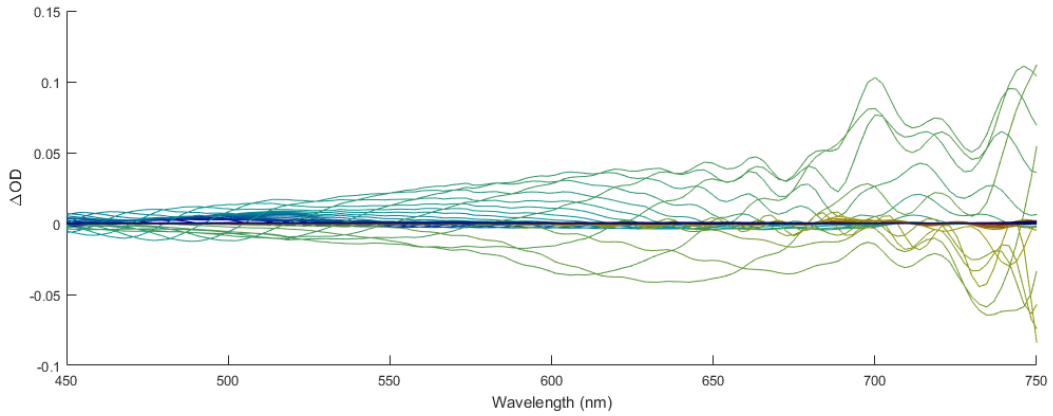

Figure B21: Full frequency pump probe sample spectrum collected during measurement of 2PA cross section for compound **1b**.

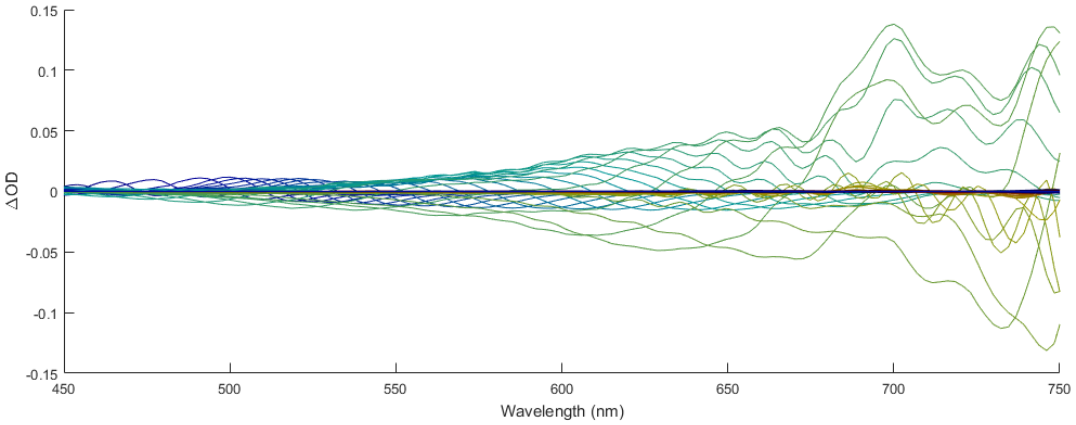

Figure B22: Full frequency pump probe solvent spectrum (d6-DMSO) collected during measurement of 2PA cross section for compound **1b**.

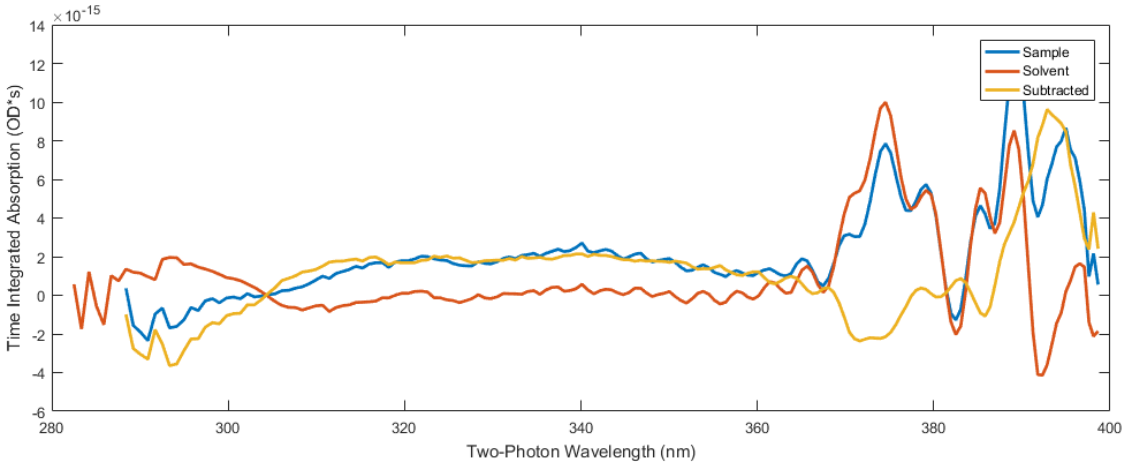

Figure B23: Time integrated spectra of the sample and solvent for **1b**.

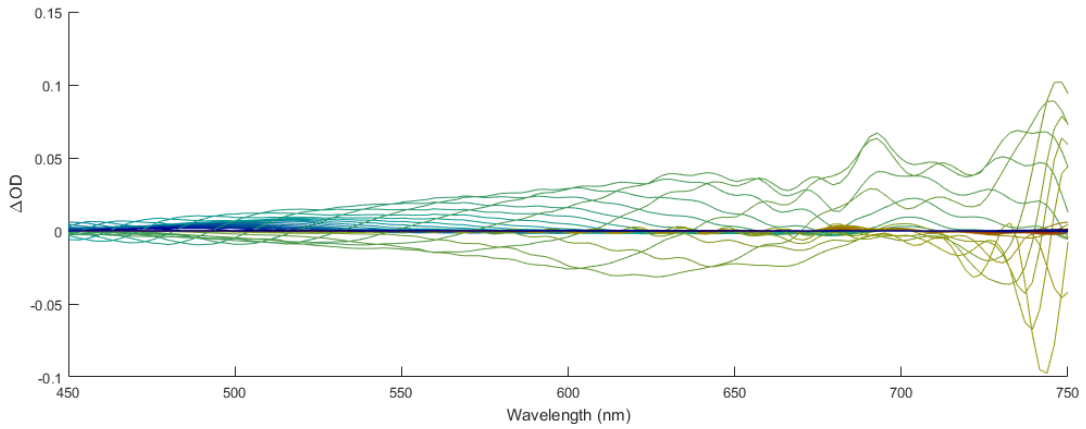

Figure B24: Full frequency pump probe sample spectrum collected during measurement of 2PA cross section for compound **2a**.

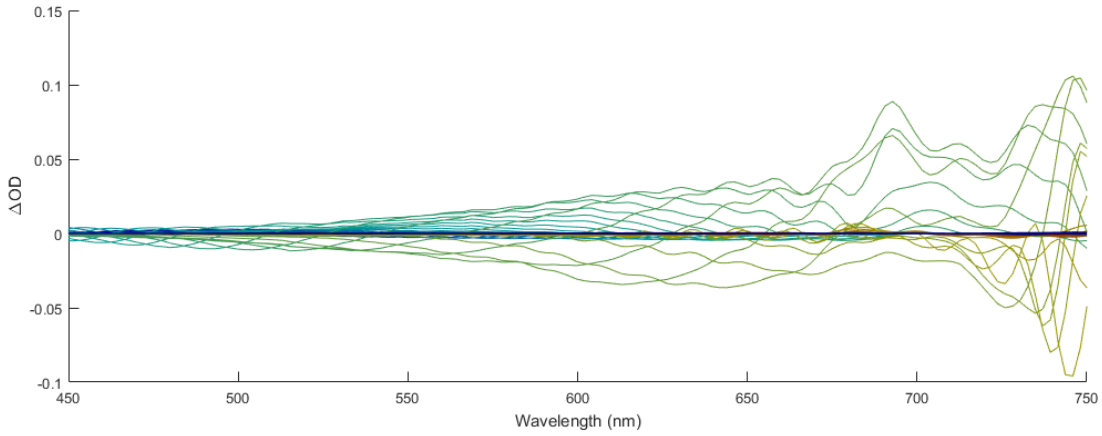

Figure B25: Full frequency pump probe solvent spectrum (d6-DMSO) collected during measurement of 2PA cross section for compound **2a**.

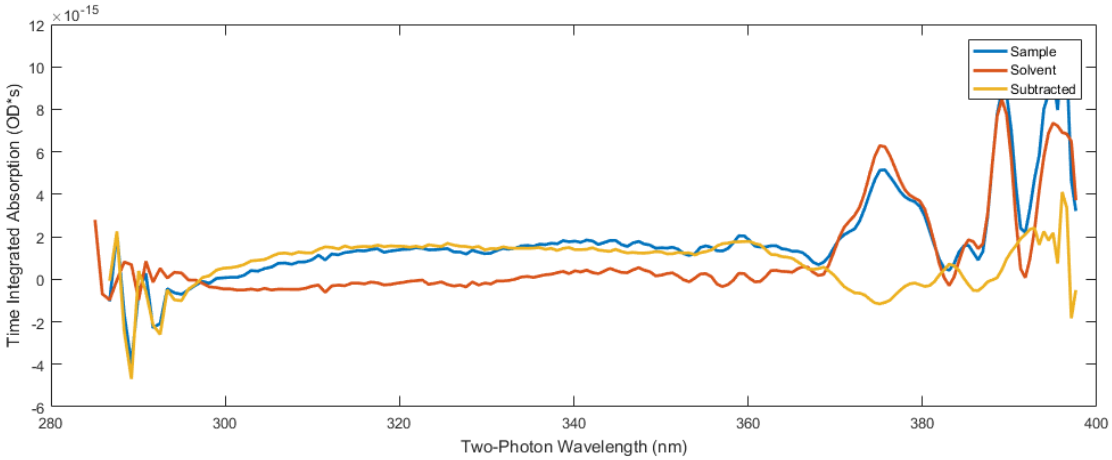

Figure B26: Time integrated spectra of the sample and solvent for **2a**.

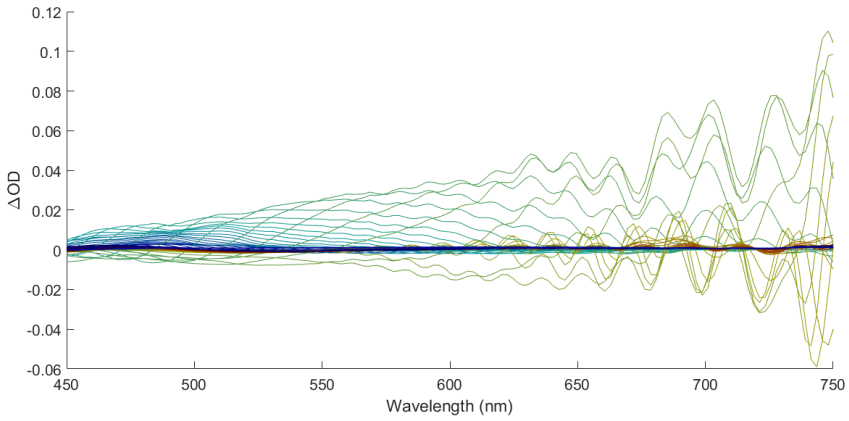

Figure B27: Full frequency pump probe sample spectrum collected during measurement of 2PA cross section for compound **2b**.

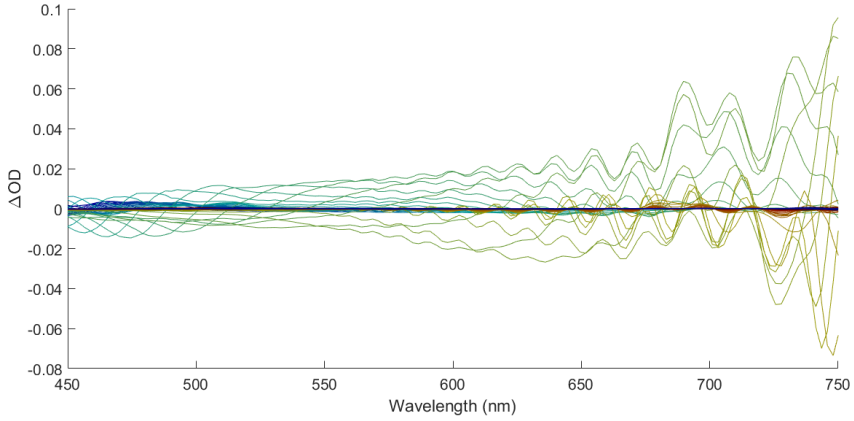

Figure B28: Full frequency pump probe solvent spectrum (d6-DMSO) collected during measurement of 2PA cross section for compound **2b**.

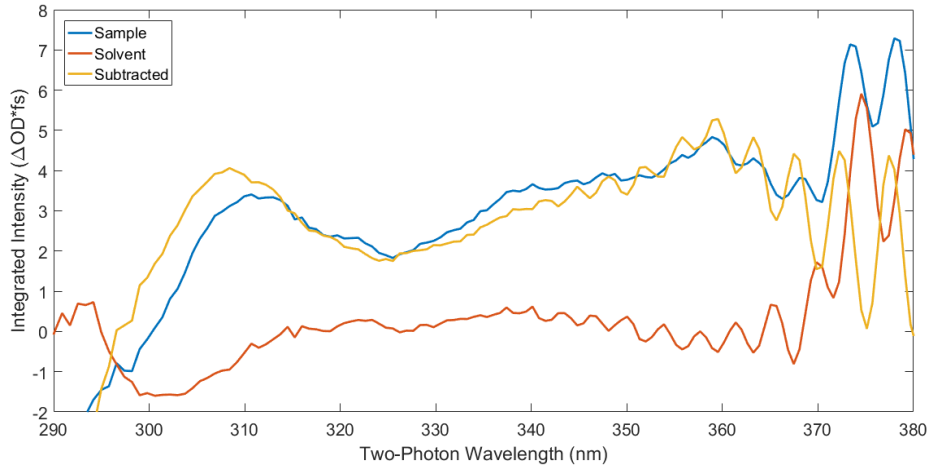

Figure B29: Time integrated spectra of the sample and solvent for **2b**.

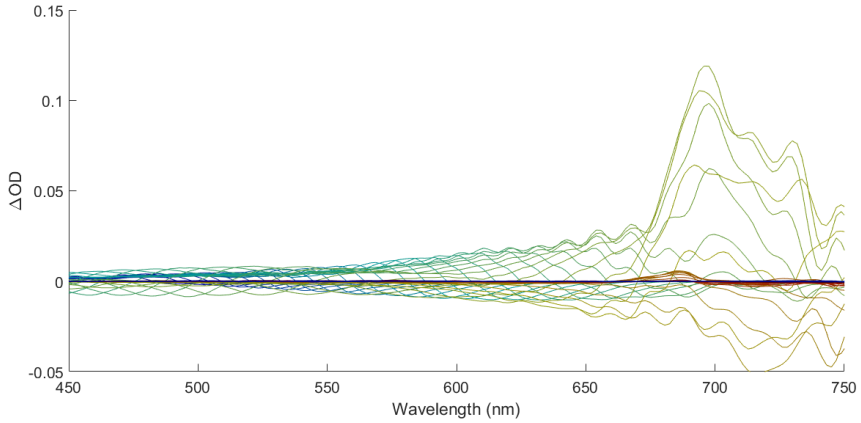

Figure B30: Full frequency pump probe sample spectrum collected during measurement of 2PA cross section for compound **3a**.

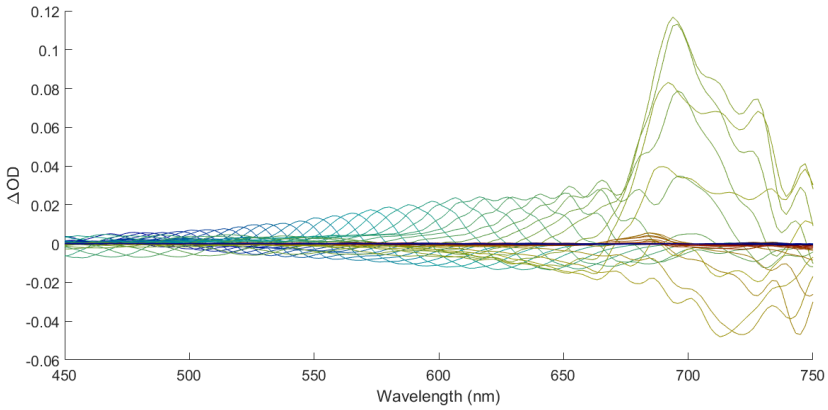

Figure B31: Full frequency pump probe solvent spectrum (d6-DMSO) collected during measurement of 2PA cross section for compound **3a**.

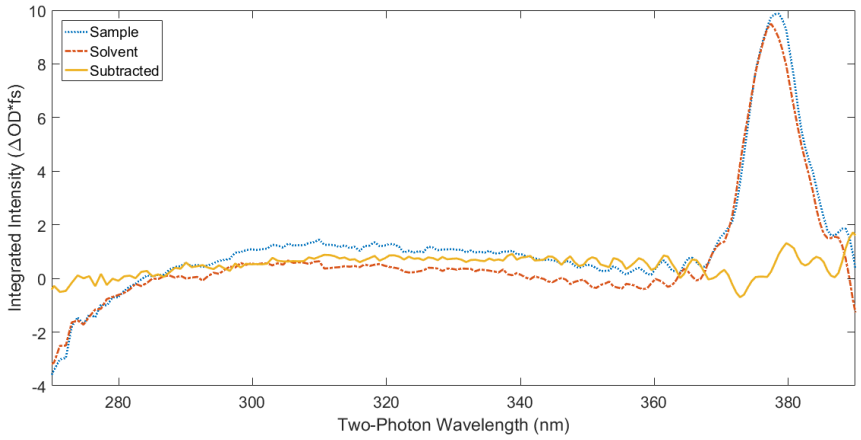

Figure B32: Time integrated spectra of the sample and solvent for **3a**.

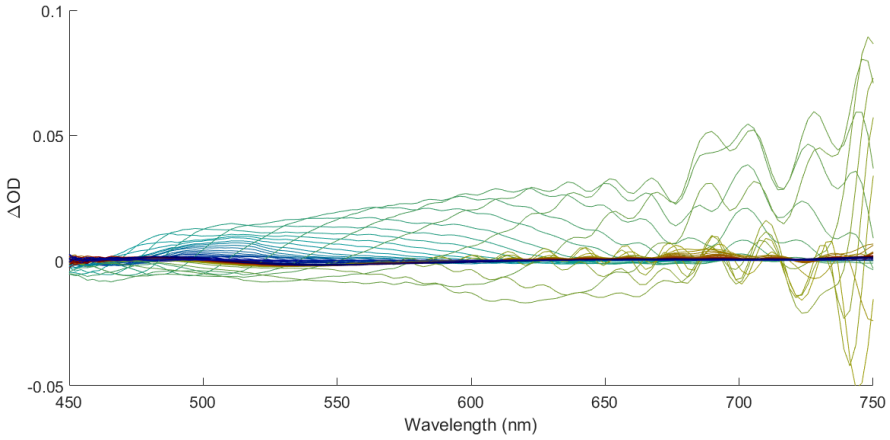

Figure B33: Full frequency pump probe sample spectrum collected during measurement of 2PA cross section for compound **3b**.

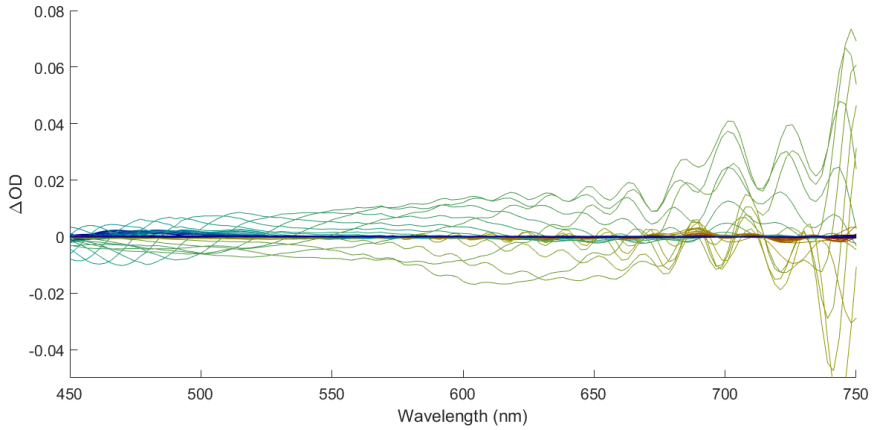

Figure B34: Full frequency pump probe solvent spectrum (d6-DMSO) collected during measurement of 2PA cross section for compound **3b**.

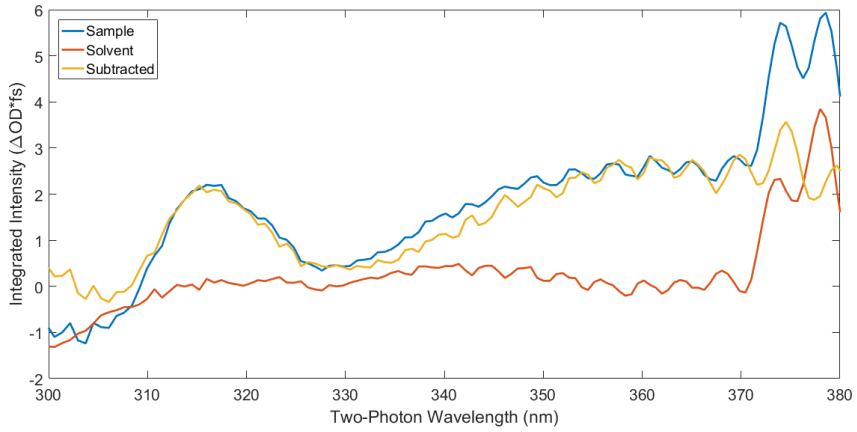

Figure B35: Time integrated spectra of the sample and solvent for **3b**.

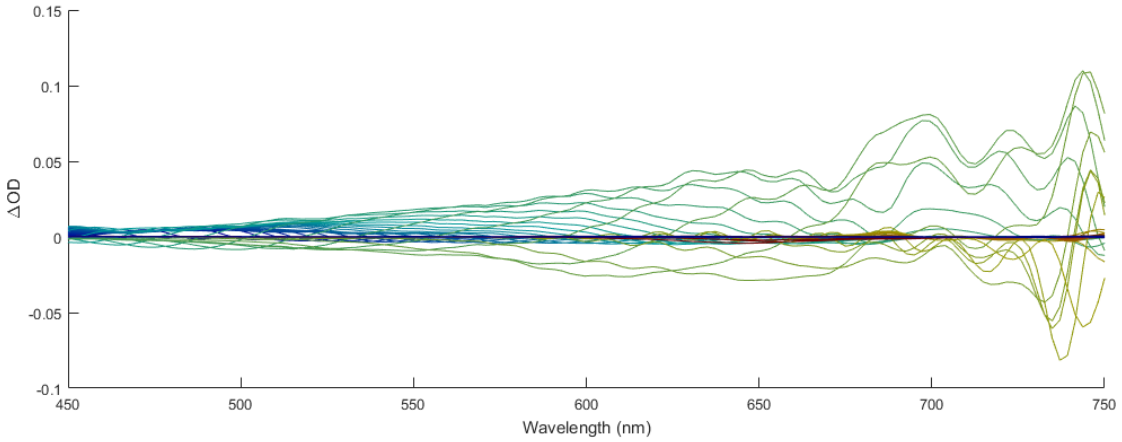

Figure B36: Full frequency pump probe sample spectrum collected during measurement of 2PA cross section for compound **4a**.

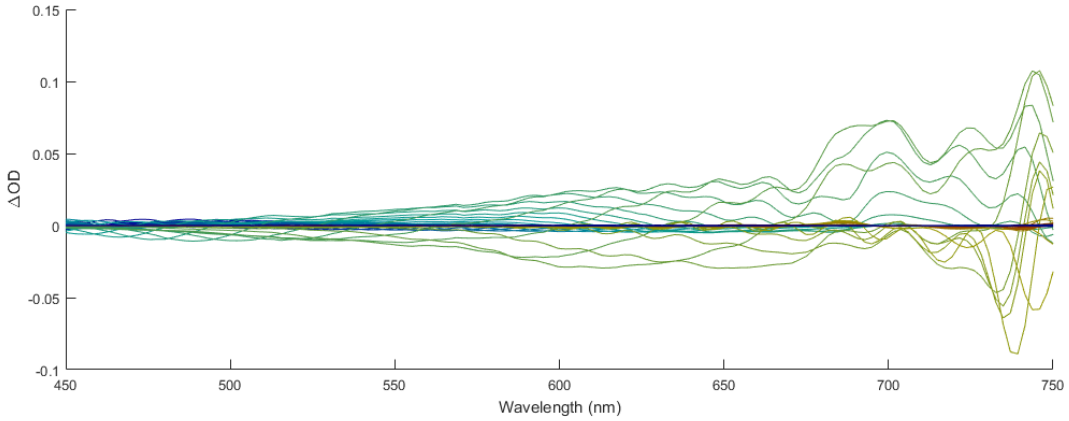

Figure B37: Full frequency pump probe solvent spectrum (d6-DMSO) collected during measurement of 2PA cross section for compound **4a**.

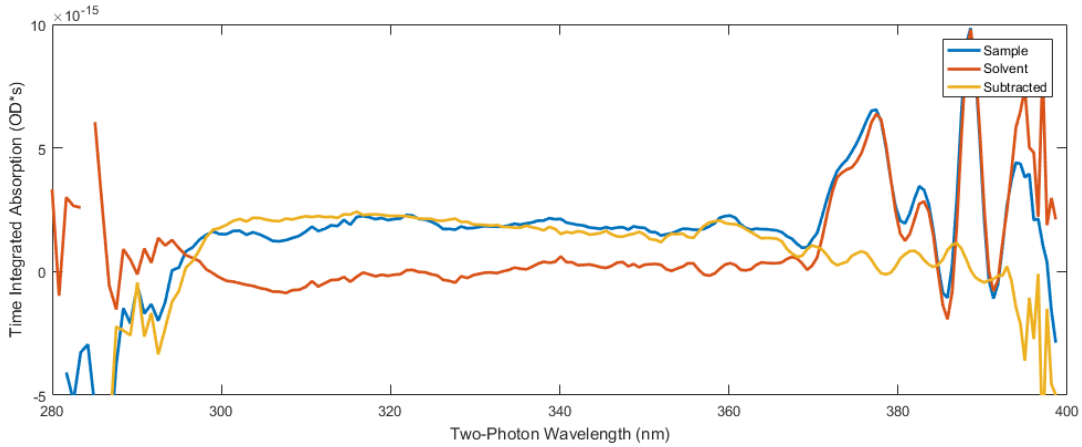

Figure B38: Time integrated spectra of the sample and solvent for **4a**.

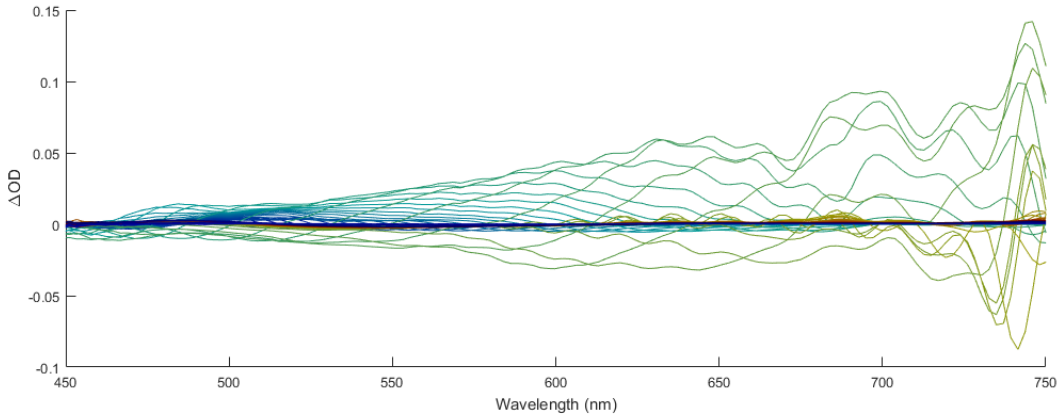

Figure B39: Full frequency pump probe sample spectrum collected during measurement of 2PA cross section for compound **4b**.

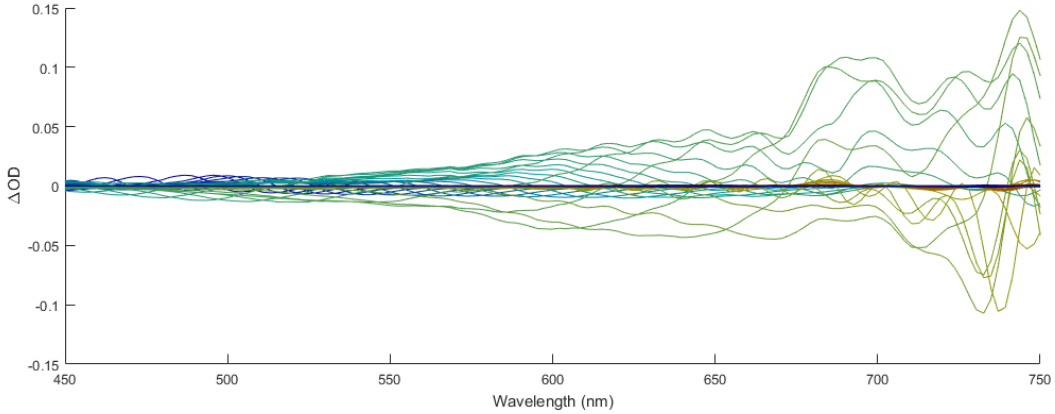

Figure B40: Full frequency pump probe solvent spectrum (d6-DMSO) collected during measurement of 2PA cross section for compound **4b**.

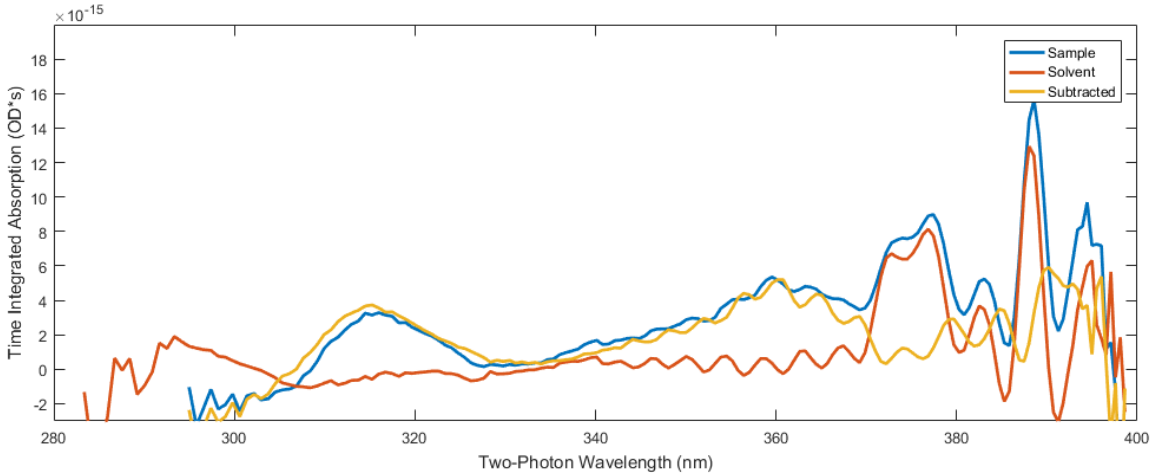

Figure B41: Time integrated spectra of the sample and solvent for **4b**.

Relevant Cartesian coordinates for each compound from Gaussian.

1a:

C	-1.67901	0.821307	-0.2908
C	-1.88688	-0.56884	-0.09327
C	-0.84443	-1.49352	0.0664
C	0.436602	-0.98751	0.054579
C	0.712993	0.381184	-0.13283
C	-0.35055	1.266861	-0.31507
H	-1.05363	-2.5462	0.200139
H	-0.15777	2.322275	-0.48396
C	2.624568	-0.82021	0.126274
C	3.970498	-1.14283	0.232121
C	4.874357	-0.0849	0.116008
C	4.438454	1.23596	-0.09721
C	3.082549	1.537874	-0.20053
C	2.157376	0.491451	-0.08728
H	4.296584	-2.16411	0.396482
H	5.173008	2.030965	-0.1821
H	2.750713	2.558588	-0.36495
O	1.585667	-1.72423	0.213893
N	-3.23044	-1.15053	-0.0561
O	-3.348	-2.35205	-0.32054
O	-4.18776	-0.43374	0.250442
C	-2.76638	1.860662	-0.49551
H	5.938226	-0.28889	0.192464
C	-3.22403	2.518869	0.818429
H	-3.98426	3.280932	0.613883
H	-2.38413	3.005463	1.326866
H	-3.65457	1.776626	1.495981
H	-2.35863	2.634303	-1.15632
H	-3.62856	1.425868	-1.00402

1b:

C	-2.44208	0.83668	-0.28505
C	-2.66612	-0.55139	-0.08941
C	-1.62894	-1.48715	0.058908
C	-0.3446	-0.99575	0.036654
C	-0.05196	0.371139	-0.14877
C	-1.1088	1.267796	-0.31897
H	-1.84784	-2.53783	0.192246

H	-0.90683	2.321723	-0.48625
C	1.847528	-0.85678	0.089561
C	3.181743	-1.20261	0.181862
C	4.11411	-0.15851	0.061479
C	3.692632	1.17493	-0.14329
C	2.338242	1.485695	-0.23146
C	1.391122	0.462626	-0.11552
H	3.511918	-2.22284	0.33902
H	4.422516	1.969631	-0.23372
H	2.030057	2.514782	-0.38907
O	0.7995	-1.74772	0.183583
N	-4.01227	-1.11878	-0.0436
O	-4.14122	-2.3264	-0.2785
O	-4.96695	-0.38731	0.239752
C	-3.51714	1.891099	-0.47782
C	-3.96799	2.539213	0.843464
H	-4.71903	3.312652	0.647617
H	-3.12265	3.00975	1.358025
H	-4.40787	1.794216	1.51192
H	-3.09986	2.667892	-1.12896
H	-4.38402	1.472109	-0.99147
O	5.415501	-0.53578	0.156799
C	6.433692	0.459453	0.0424
H	6.347002	1.210383	0.835812
H	7.378747	-0.07422	0.148687
H	6.400352	0.952111	-0.93599

2a:

C	0.914514	0.105297	0.380891
C	0.719076	1.468897	0.029415
C	-0.53828	2.020251	-0.23901
C	-1.6208	1.166252	-0.17942
C	-1.49629	-0.19429	0.152105
C	-0.22705	-0.70355	0.439047
H	-0.63912	3.066461	-0.49462
H	-0.11791	-1.74571	0.721943
C	-3.66	0.361068	-0.25377
C	-5.03605	0.265747	-0.40711
C	-5.59892	-0.99255	-0.18566
C	-4.80852	-2.10027	0.173379
C	-3.42879	-1.98231	0.321984

C	-2.84218	-0.72818	0.104969
H	-5.63615	1.12553	-0.6843
H	-5.28488	-3.06207	0.336752
H	-2.82342	-2.83996	0.599055
O	-2.92219	1.515638	-0.42896
N	1.827431	2.421957	-0.10713
O	1.590452	3.612755	0.117537
O	2.928566	2.002974	-0.46444
C	2.216416	-0.57483	0.794944
H	-6.67219	-1.11704	-0.29387
C	3.021039	0.094694	1.908556
H	3.84673	-0.56385	2.19361
H	2.382112	0.237801	2.7864
H	3.432862	1.057646	1.605911
H	1.941943	-1.5706	1.146765
O	3.037387	-0.77756	-0.3925
C	3.75459	-1.92058	-0.45533
C	4.534588	-1.99061	-1.74523
O	3.763833	-2.76844	0.41711
H	5.09212	-2.9268	-1.78698
H	3.854606	-1.9236	-2.60033
H	5.226716	-1.14475	-1.80902

2b:

C	1.62716	0.1048	0.384583
C	1.57056	1.480597	0.029307
C	0.369356	2.154096	-0.23009
C	-0.79203	1.416696	-0.15434
C	-0.80602	0.050586	0.182174
C	0.409168	-0.58299	0.457487
H	0.372707	3.203772	-0.49081
H	0.414965	-1.62996	0.743279
C	-2.90592	0.826622	-0.2055
C	-4.27881	0.880935	-0.34549
C	-4.98308	-0.31249	-0.11405
C	-4.30581	-1.50099	0.243138
C	-2.92021	-1.51724	0.375287
C	-2.19733	-0.34049	0.150501
H	-4.80367	1.788616	-0.61951
H	-4.86209	-2.4134	0.417731
H	-2.41513	-2.43801	0.650374

O	-2.05597	1.897572	-0.39312
N	2.765012	2.3161	-0.12071
O	2.640556	3.533973	0.049182
O	3.830363	1.782093	-0.4334
C	2.85358	-0.70895	0.789031
C	3.721054	-0.13755	1.910143
H	4.479771	-0.877	2.182964
H	3.099391	0.051972	2.791666
H	4.221997	0.786425	1.621245
H	2.479347	-1.67533	1.13073
O	3.649632	-0.98329	-0.40113
C	4.242952	-2.19401	-0.47745
C	5.010221	-2.3317	-1.76967
O	4.164297	-3.04808	0.385553
H	5.470369	-3.31899	-1.82016
H	4.338997	-2.18981	-2.62258
H	5.783882	-1.55936	-1.82869
O	-6.32986	-0.22307	-0.26008
C	-7.12797	-1.38803	-0.04318
H	-7.0249	-1.75497	0.984261
H	-8.15786	-1.07386	-0.21562
H	-6.86634	-2.18582	-0.74733

3a:

C	0.588251	0.586658	0.517996
C	0.191172	1.817327	-0.07704
C	-1.11845	2.081033	-0.50183
C	-2.04291	1.072454	-0.3411
C	-1.7163	-0.16981	0.232986
C	-0.40636	-0.39107	0.663337
H	-1.37064	3.034513	-0.94534
H	-0.14759	-1.33674	1.128971
C	-3.90615	-0.08581	-0.36328
C	-5.23065	-0.45165	-0.55929
C	-5.58813	-1.73552	-0.14331
C	-4.65181	-2.60762	0.442792
C	-3.3273	-2.22041	0.630552
C	-2.94594	-0.93554	0.220559
H	-5.94473	0.227553	-1.01205
H	-4.96991	-3.59831	0.752717
H	-2.60876	-2.89705	1.082982

O	-3.36394	1.135929	-0.70789
N	1.131077	2.909707	-0.32592
O	0.676687	4.047563	-0.4796
O	2.337488	2.654714	-0.39788
C	1.959472	0.229736	1.081382
S	3.224365	-0.07628	-0.26145
C	3.533316	-1.87332	0.006508
C	4.600476	-2.36849	-0.97194
H	2.607184	-2.43652	-0.14452
H	3.869202	-2.02886	1.03844
H	4.246704	-2.22338	-1.99933
H	5.512273	-1.75881	-0.8574
N	4.822063	-3.80854	-0.76966
H	5.459605	-4.14571	-1.49039
H	5.319232	-3.94547	0.110758
H	-6.61364	-2.06691	-0.27649
C	2.479963	1.155151	2.191029
H	3.374216	0.714017	2.641971
H	1.717885	1.258009	2.973107
H	2.739123	2.148246	1.82276
H	1.834182	-0.75677	1.532675

3b:

C	-1.35033	-0.61482	0.525907
C	-1.16788	-1.89103	-0.07825
C	0.082733	-2.3669	-0.50398
C	1.162227	-1.53203	-0.33289
C	1.050975	-0.25528	0.250726
C	-0.2052	0.180044	0.679585
H	0.1716	-3.34542	-0.95542
H	-0.30228	1.152774	1.151226
C	3.197518	-0.70812	-0.34306
C	4.559228	-0.57952	-0.53505
C	5.144961	0.624375	-0.10892
C	4.366277	1.64428	0.484845
C	2.995728	1.479035	0.662202
C	2.390097	0.288139	0.246333
H	5.162028	-1.35695	-0.98968
H	4.832083	2.566782	0.807836
H	2.410939	2.27118	1.119581
O	2.457288	-1.81625	-0.69833

N	-2.27476	-2.80652	-0.33502
O	-2.01504	-3.99774	-0.53834
O	-3.42777	-2.3615	-0.36364
C	-2.64086	-0.03255	1.092374
S	-3.84711	0.469292	-0.24509
C	-3.83344	2.296596	-0.00516
C	-4.79365	2.957919	-0.99603
H	-2.8218	2.684131	-0.16021
H	-4.13825	2.525494	1.022754
H	-4.46823	2.737376	-2.01936
H	-5.7992	2.520645	-0.87791
N	-4.75814	4.417408	-0.81548
H	-5.32547	4.850715	-1.54351
H	-5.2247	4.65289	0.060866
C	-3.29783	-0.85327	2.212067
H	-4.10867	-0.27172	2.661581
H	-2.55809	-1.0688	2.992681
H	-3.71192	-1.79602	1.853274
H	-2.35248	0.922761	1.536077
O	6.483906	0.716265	-0.31279
C	7.165457	1.904832	0.092202
H	7.078082	2.064382	1.172836
H	8.212213	1.745619	-0.16869
H	6.785021	2.782874	-0.44178

4a:

C	-4.3471	-0.76276	-0.64333
C	-5.24954	-1.79726	-0.28576
C	-6.60159	-1.57636	0.001521
C	-7.0529	-0.27838	-0.11553
C	-6.21424	0.788926	-0.49154
C	-4.86474	0.534828	-0.74526
H	-7.25099	-2.39638	0.277939
H	-4.20239	1.351224	-1.0147
C	-8.34309	1.49648	-0.13778
C	-9.45457	2.320753	-0.03164
C	-9.25287	3.673184	-0.31343
C	-7.98855	4.167972	-0.68403
C	-6.8861	3.322929	-0.78413
C	-7.06558	1.961101	-0.50592
H	-10.4246	1.929474	0.254755

H	-7.87332	5.226712	-0.89481
H	-5.9127	3.709627	-1.07
O	-8.34174	0.135886	0.099358
N	-4.83435	-3.2015	-0.22658
O	-5.42368	-3.94431	0.561482
O	-3.94115	-3.58767	-0.98796
H	-10.0931	4.357542	-0.24446
C	-2.8599	-0.97624	-0.88501
H	-2.56422	-1.96684	-0.54954
C	-2.48221	-0.80764	-2.36117
H	-2.74835	0.186967	-2.73145
H	-1.40905	-0.95872	-2.5127
H	-3.01834	-1.55653	-2.95432
S	-1.92881	0.217996	0.216686
C	-0.21068	-0.45044	0.090687
H	0.368746	0.188888	-0.57594
H	-0.24653	-1.4593	-0.33034
C	0.502078	-0.46062	1.468596
H	0.32476	0.508148	1.956364
C	-0.00375	-1.56452	2.415029
N	1.92616	-0.661	1.299551
H	2.318007	-1.48094	1.748732
O	-1.31731	-1.59507	2.656727
O	0.744383	-2.36789	2.934043
H	-1.79137	-0.92644	2.09875
C	2.7447	0.372103	0.961631
O	2.364724	1.480493	0.608396
O	4.043206	-0.00411	1.04956
C	5.012958	0.995859	0.671729
H	4.933768	1.843646	1.358531
H	4.799954	1.347946	-0.34154
C	6.400188	0.352747	0.757185
C	7.502578	1.369179	0.492779
H	6.502985	-0.07468	1.764946
C	6.673184	-0.70374	-0.30504
C	7.77778	2.560196	1.15704
C	8.300601	0.953977	-0.59335
C	6.002396	-1.89646	-0.56017
C	7.787508	-0.33139	-1.08715
C	8.858769	3.341598	0.729012
H	7.171538	2.884382	1.999285
C	9.37987	1.732996	-1.01768
C	6.447673	-2.7153	-1.60588

H	5.145377	-2.18841	0.038466
C	8.23122	-1.15007	-2.1286
C	9.651111	2.930053	-0.34905
H	9.084765	4.273377	1.239975
H	10.00111	1.418429	-1.85217
C	7.551673	-2.34449	-2.38247
H	5.931379	-3.64839	-1.8145
H	9.089883	-0.86844	-2.73254
H	10.48709	3.546479	-0.66834
H	7.885214	-2.99223	-3.18874

4b:

C	-3.73611	-1.30662	-0.63158
C	-4.56595	-2.41154	-0.3107
C	-5.93309	-2.28835	-0.02523
C	-6.46982	-1.02291	-0.10687
C	-5.70548	0.111691	-0.44757
C	-4.34041	-0.04448	-0.6995
H	-6.52689	-3.15801	0.222787
H	-3.73347	0.822144	-0.94117
C	-7.8814	0.659249	-0.08575
C	-9.04564	1.391409	0.039099
C	-8.95016	2.772268	-0.20216
C	-7.7169	3.367329	-0.55401
C	-6.56359	2.596686	-0.66981
C	-6.63417	1.219321	-0.43383
H	-9.99408	0.941306	0.30797
H	-7.65886	4.432916	-0.73708
H	-5.62398	3.068435	-0.94055
O	-7.78747	-0.70316	0.112505
N	-4.05884	-3.78323	-0.28966
O	-4.61741	-4.59486	0.453342
O	-3.11974	-4.08245	-1.0365
C	-2.23654	-1.4095	-0.86996
H	-1.8729	-2.38241	-0.55013
C	-1.86784	-1.1893	-2.34164
H	-2.20339	-0.20991	-2.69577
H	-0.78632	-1.26141	-2.49209
H	-2.34817	-1.96408	-2.94913
S	-1.39318	-0.17254	0.255163
C	0.366876	-0.7189	0.12157

H	0.899368	-0.03757	-0.54266
H	0.399676	-1.72595	-0.3044
C	1.080313	-0.68617	1.498715
H	0.830924	0.262574	1.994003
C	0.65925	-1.83213	2.436422
N	2.515274	-0.77669	1.327823
H	2.968446	-1.57073	1.765594
O	-0.64838	-1.96341	2.676725
O	1.46562	-2.58068	2.950167
H	-1.17168	-1.32891	2.122947
C	3.252782	0.320002	1.004056
O	2.7891	1.401593	0.668164
O	4.576289	0.041545	1.083953
C	5.466904	1.1189	0.724533
H	5.346442	1.933093	1.445377
H	5.206636	1.493036	-0.26941
C	6.89632	0.570107	0.755715
C	7.92014	1.670392	0.512017
H	7.051036	0.109881	1.742137
C	7.215106	-0.42004	-0.35642
C	8.129852	2.848644	1.221403
C	8.717135	1.357511	-0.60861
C	6.621111	-1.64464	-0.64816
C	8.280951	0.061438	-1.14647
C	9.143864	3.720399	0.804039
H	7.524154	3.094386	2.090185
C	9.72951	2.226726	-1.02244
C	7.094293	-2.38573	-1.73865
H	5.801728	-2.02034	-0.04352
C	8.752574	-0.67973	-2.23276
C	9.935037	3.410523	-0.30836
H	9.318544	4.643272	1.350078
H	10.34953	1.991316	-1.88347
C	8.149888	-1.90664	-2.52325
H	6.637866	-3.34281	-1.97616
H	9.573899	-0.31375	-2.84341
H	10.71861	4.09632	-0.61897
H	8.505916	-2.49501	-3.36466
O	-10.1127	3.460579	-0.07093
C	-10.1113	4.870826	-0.3
H	-9.81114	5.106109	-1.3273
H	-11.1398	5.194992	-0.1381
H	-9.44986	5.38735	0.40464

Orbital energies for all occupied orbitals and the first 20 unoccupied orbitals. Energy is in Hartree atomic units. The HOMO and LUMO are bolded.

1a:

-19.21889503 -19.18443615 -19.18255953 -14.57401794 -10.26120805
-10.25646677 -10.25228050 -10.22104914 -10.21535906 -10.21390044
-10.20573289 -10.20456054 -10.19968488 -10.19799585 -10.19734337
-10.19123495 -10.18515483 -10.16728368 -1.22890268 -1.11890723
-1.05365224 -0.89268263 -0.86854144 -0.82182475 -0.80033007
-0.77038514 -0.75850119 -0.73464411 -0.69969575 -0.65393871
-0.63650688 -0.60782625 -0.60224887 -0.58842035 -0.55981858
-0.53964396 -0.52529651 -0.52120360 -0.50577682 -0.49303108
-0.47302641 -0.46894533 -0.46084388 -0.44966025 -0.44717780
-0.42731855 -0.42148404 -0.41537026 -0.39339891 -0.38280589
-0.36885952 -0.36670506 -0.35674508 -0.35334940 -0.34846807
-0.34466691 -0.31705461 -0.31350092 -0.30773392 -0.29205520
-0.26947299 -0.23895944 **-0.23784092** **-0.09463293** -0.03574736
-0.01214524 0.00261420 0.02797008 0.09223787 0.09978363
0.11037778 0.12871954 0.13420063 0.14355648 0.15763012
0.16010671 0.16413241 0.17435346 0.17760354 0.18126919
0.18460882 0.18818195 0.20121655

1b:

-19.21771236 -19.18386684 -19.18183769 -19.17993049 -14.57172464
-10.26241846 -10.25940898 -10.25847463 -10.24981710 -10.23011415
-10.21997272 -10.21486223 -10.21203076 -10.20350319 -10.20245169
-10.20104545 -10.19284132 -10.19160350 -10.18431008 -10.16690193
-1.22608822 -1.11765854 -1.07312592 -1.05060416 -0.89101306
-0.86811697 -0.82098575 -0.79924967 -0.77227605 -0.76474292
-0.73433761 -0.72024908 -0.68156279 -0.65144338 -0.64050480
-0.60834857 -0.59622935 -0.58726608 -0.55862698 -0.53974335
-0.52845502 -0.52348473 -0.51256179 -0.50539758 -0.48140466
-0.47548793 -0.47444230 -0.46685047 -0.45671354 -0.45336027
-0.43924559 -0.43153635 -0.41853165 -0.41277394 -0.40735839
-0.38967001 -0.38056795 -0.37626886 -0.36003371 -0.35603867
-0.34949593 -0.34561690 -0.33612576 -0.33531025 -0.31486563
-0.31156589 -0.29727755 -0.28158935 -0.26968562 -0.23860936
-0.21970948 **-0.09292986** -0.03157207 -0.01206584 0.00516484
0.03405289 0.09065369 0.09981355 0.11064367 0.11339544
0.12943489 0.13598449 0.13756889 0.14522519 0.16070678

0.16114277 0.16396019 0.17356826 0.17485637 0.17631252
0.18320249

2a:

-19.22275015 -19.18771266 -19.18690080 -19.18669126 -19.13868309
-14.57767087 -10.31907254 -10.26641126 -10.25946030 -10.25833288
-10.25553700 -10.22729085 -10.21885506 -10.21827448 -10.21236861
-10.20799848 -10.20092035 -10.19912943 -10.19864304 -10.19244057
-10.18328429 -10.17303189 -1.23375211 -1.12311938 -1.10187951
-1.05888249 -1.01687890 -0.89774170 -0.87050680 -0.82555931
-0.81123914 -0.77368913 -0.76616716 -0.75144064 -0.73294679
-0.70381906 -0.66392539 -0.64366768 -0.62741910 -0.60645107
-0.59950071 -0.56364925 -0.56250520 -0.54201364 -0.52697607
-0.52328025 -0.50934631 -0.50648985 -0.49060118 -0.47940501
-0.47671770 -0.47255122 -0.46495772 -0.45604893 -0.44746209
-0.44399611 -0.42914908 -0.42279259 -0.41666012 -0.40879403
-0.39896957 -0.38760451 -0.37907107 -0.37322803 -0.36748477
-0.36585331 -0.36445018 -0.35145829 -0.34315463 -0.32084044
-0.31808335 -0.31327533 -0.30311867 -0.29377809 -0.28057103
-0.27431252 -0.24307424 **-0.24113315** **-0.09744665** -0.04059216
-0.01964473 -0.00080389 0.00918097 0.02164090 0.08864208
0.09559124 0.10454679 0.11843479 0.12205622 0.13171344
0.14219622 0.14708097 0.15336926 0.16241691 0.16575006
0.17434225 0.17704134 0.17846314

2b:

-19.22138330 -19.18635668 -19.18469182 -19.18461352 -19.18356353
-19.13827986 -14.57506619 -10.31869496 -10.26434754 -10.26357027
-10.26027645 -10.25676779 -10.25464343 -10.23046338 -10.22619939
-10.21770001 -10.21673091 -10.21013112 -10.20473702 -10.20321754
-10.19410281 -10.19280067 -10.18310620 -10.17207677 -1.23054501
-1.12168898 -1.10141791 -1.07399506 -1.05540843 -1.01640610
-0.89584174 -0.86996612 -0.82448626 -0.81008160 -0.77460410
-0.77041259 -0.75360052 -0.73241147 -0.72229987 -0.68511673
-0.66084957 -0.64587514 -0.62819210 -0.60439640 -0.59444416
-0.56417958 -0.56065319 -0.54060276 -0.52840075 -0.52562546
-0.51711390 -0.50935579 -0.50046875 -0.48963351 -0.47795689
-0.47402425 -0.46835261 -0.46781645 -0.46356207 -0.45875005
-0.45402196 -0.43645218 -0.43059456 -0.41879867 -0.41417761
-0.41117127 -0.40630086 -0.39729479 -0.38430083 -0.38118711
-0.37253948 -0.36719541 -0.36454542 -0.36188258 -0.34237131

-0.33713842 -0.33698301 -0.31864246 -0.31564787 -0.30512421
-0.29894527 -0.28379661 -0.27975512 -0.27429305 -0.24402362
-0.22131069 **-0.09587426** -0.03599326 -0.01874077 0.00058394
0.00977917 0.02869674 0.08797519 0.09568405 0.10499843
0.11181716 0.11974281 0.12328834 0.13217077 0.13641554
0.14401760 0.14870706 0.15820067 0.16284156 0.16657142

3a:

-88.85242404 -19.22123367 -19.18786790 -19.18567688 -14.57688717
-14.30637194 -10.26399509 -10.25806713 -10.25682654 -10.22888813
-10.22827970 -10.21799726 -10.21711318 -10.20960568 -10.20748481
-10.20458690 -10.20083604 -10.20021419 -10.19905511 -10.19836593
-10.19221091 -10.17284067 -7.92714604 -5.89150475 -5.88797437
-5.88115749 -1.23256084 -1.12149027 -1.05721372 -0.89737547
-0.87984586 -0.87005807 -0.82669015 -0.82098162 -0.77756289
-0.77082035 -0.75756932 -0.73982753 -0.70293714 -0.67423092
-0.65216061 -0.63886077 -0.61067119 -0.60417007 -0.59507489
-0.57371774 -0.56314135 -0.54118258 -0.52844769 -0.51918921
-0.50864365 -0.49910244 -0.48689251 -0.47537528 -0.47435835
-0.46522462 -0.45552266 -0.45281036 -0.44725785 -0.43557959
-0.42990785 -0.42154087 -0.41478223 -0.40160912 -0.38661532
-0.38060636 -0.37162056 -0.36784458 -0.36687991 -0.36249030
-0.35468238 -0.35089966 -0.34095377 -0.32019919 -0.31785864
-0.31307927 -0.30635812 -0.29144916 -0.27265981 -0.24354486
-0.24131155 -0.24092195 **-0.22295031** **-0.09921951** -0.03825912
-0.01711341 0.00002150 0.02132675 0.04661325 0.06243436
0.08583246 0.09220624 0.09888815 0.11103201 0.12108995
0.13457549 0.13676346 0.14409194 0.14818446 0.15504162
0.16202067 0.16316926 0.17300534

3b:

-88.85202530 -19.21999557 -19.18516958 -19.18475320 -19.18283602
-14.57443287 -14.30629762 -10.26367509 -10.26214159 -10.26006835
-10.25429221 -10.23050043 -10.22784904 -10.22754297 -10.21748959
-10.21516086 -10.20749910 -10.20470763 -10.20444080 -10.20275302
-10.19988681 -10.19384871 -10.19267193 -10.17230799 -7.92671907
-5.89107770 -5.88754814 -5.88073693 -1.22959190 -1.12016602
-1.07412326 -1.05398454 -0.89570745 -0.87972369 -0.86963532
-0.82594939 -0.81996575 -0.77741533 -0.77378314 -0.76203765
-0.73972317 -0.72219997 -0.68427695 -0.67324082 -0.64998934
-0.64226872 -0.61171559 -0.59718890 -0.59470482 -0.57394340

-0.56130791 -0.53985255 -0.53066604 -0.52405108 -0.51482714
-0.50860641 -0.48851509 -0.48592083 -0.47716259 -0.47508496
-0.46809188 -0.46056189 -0.45865859 -0.45540668 -0.44147569
-0.43860687 -0.42781834 -0.41533171 -0.41415360 -0.41197766
-0.39823055 -0.38385408 -0.38072473 -0.37589964 -0.36662516
-0.36312518 -0.36070190 -0.35444165 -0.34097913 -0.33699924
-0.33627419 -0.31832405 -0.31533893 -0.31075122 -0.29475360
-0.28404982 -0.27272139 -0.24376061 -0.24167793 -0.22330879
-0.22066983 **-0.09758078** -0.03397127 -0.01660038 0.00163028
0.02715517 0.04825886 0.06288166 0.08593676 0.09139560
0.09915629 0.11123771 0.11165578 0.12246583 0.13538891
0.13683711 0.13862090 0.14456345 0.14920251 0.15892797
0.16260841

4a:

-88.87518039 -19.22259226 -19.19584972 -19.19129711 -19.19022510
-19.18969428 -19.15076001 -19.12931894 -14.58051590 -14.36180481
-10.34039096 -10.33513108 -10.26678783 -10.26044567 -10.25854150
-10.25549524 -10.24212291 -10.23708150 -10.23282463 -10.22617983
-10.21994128 -10.21984317 -10.21287532 -10.20804225 -10.20125868
-10.20107813 -10.19929162 -10.19873117 -10.19264382 -10.19249376
-10.19177516 -10.19099287 -10.19036426 -10.18721210 -10.18644919
-10.18582033 -10.18549532 -10.18535176 -10.18473873 -10.18424497
-10.18382115 -10.18114684 -7.95101471 -5.91508358 -5.91150131
-5.90537293 -1.23583738 -1.12304599 -1.11458622 -1.10984759
-1.06139642 -1.03255834 -1.01834687 -0.94226297 -0.90184135
-0.88982634 -0.87077505 -0.84408817 -0.83935697 -0.82625198
-0.81106933 -0.79953366 -0.77564342 -0.77267965 -0.76515473
-0.75041387 -0.74291165 -0.73661889 -0.71595390 -0.71420505
-0.70448255 -0.67067729 -0.66066746 -0.64920265 -0.63623072
-0.63148980 -0.62255880 -0.60665577 -0.59810767 -0.59426809
-0.59337028 -0.58578559 -0.57816111 -0.57700924 -0.56791903
-0.56425223 -0.54782256 -0.53145793 -0.52747535 -0.52535985
-0.51463424 -0.51024214 -0.50613296 -0.49995061 -0.49421150
-0.48637484 -0.47802428 -0.47660376 -0.47396682 -0.47321628
-0.46896140 -0.46427107 -0.45956869 -0.45217504 -0.45085727
-0.44690762 -0.44293700 -0.43926916 -0.43261374 -0.42898225
-0.42610184 -0.42459669 -0.42301476 -0.42113642 -0.41899799
-0.41453106 -0.40448352 -0.40111484 -0.39197452 -0.38748956
-0.38605791 -0.38144656 -0.37753570 -0.37399897 -0.37072077
-0.36432704 -0.36204883 -0.35795326 -0.35647776 -0.35262294

-0.35142551 -0.34804597 -0.33222565 -0.33183468 -0.32922408
-0.32902064 -0.32287767 -0.31871167 -0.31083874 -0.30384827
-0.29742873 -0.29643996 -0.28486280 -0.28427770 -0.27585317
-0.26995962 -0.25342281 -0.24959357 -0.24751571 -0.24229181
-0.24148693 **-0.21881646** **-0.09883274** -0.04369184 -0.03381188
-0.02226627 -0.01460358 -0.00690193 -0.00130426 0.00499414
0.01767970 0.02039339 0.03739152 0.04081101 0.05837164
0.08103666 0.09100445 0.09626199 0.09708391 0.10174421
0.11030133 0.11321547

4b:

-88.87469236 -19.22131638 -19.19546504 -19.18961735 -19.18884536
-19.18769477 -19.18479257 -19.15047558 -19.12920712 -14.57829712
-14.36171397 -10.34028261 -10.33486081 -10.26491380 -10.26380374
-10.26049566 -10.25794271 -10.25523981 -10.24209418 -10.23623448
-10.23175995 -10.23051235 -10.22582824 -10.21940660 -10.21795939
-10.21072665 -10.20494298 -10.20325850 -10.20125540 -10.19419319
-10.19287274 -10.19266731 -10.19181121 -10.19102626 -10.19037722
-10.18726485 -10.18649281 -10.18585233 -10.18555232 -10.18538399
-10.18476843 -10.18427772 -10.18384886 -10.18082287 -7.95052049
-5.91458559 -5.91101069 -5.90488365 -1.23313045 -1.12167161
-1.11424185 -1.10969882 -1.07420524 -1.05846083 -1.03222016
-1.01826520 -0.94213539 -0.90020295 -0.88986124 -0.87028299
-0.84411525 -0.83864996 -0.82530674 -0.81092528 -0.79911359
-0.77616318 -0.77370248 -0.76935586 -0.75206506 -0.74295194
-0.73648734 -0.72318525 -0.71559023 -0.71418654 -0.68598584
-0.66816139 -0.65981441 -0.64930825 -0.63964834 -0.63150056
-0.62231653 -0.60333431 -0.59519139 -0.59355753 -0.59296312
-0.58576290 -0.57812168 -0.57703536 -0.56799096 -0.56232792
-0.54859597 -0.53410145 -0.52793306 -0.52555357 -0.51633782
-0.51435958 -0.50898342 -0.50411580 -0.49974808 -0.49127015
-0.48589161 -0.47809326 -0.47657534 -0.47528332 -0.47315218
-0.46853920 -0.46485660 -0.46196131 -0.45790251 -0.45289873
-0.45026819 -0.44833013 -0.44218120 -0.43930305 -0.43412997
-0.42866112 -0.42696198 -0.42416805 -0.42195078 -0.41921997
-0.41798980 -0.41432607 -0.40671945 -0.40276773 -0.40042740
-0.39192364 -0.38593710 -0.38380463 -0.38113968 -0.38034174
-0.37652440 -0.36672894 -0.36256504 -0.36133600 -0.35766702
-0.35647378 -0.35260776 -0.34825905 -0.33823299 -0.33721501
-0.33224690 -0.33060931 -0.32941596 -0.32843351 -0.32087391
-0.31476155 -0.30432098 -0.30371335 -0.29661470 -0.28479811

-0.28469815	-0.28428094	-0.27576372	-0.26984982	-0.25345493
-0.24913784	-0.24755109	-0.24312078	-0.22165012	**-0.21884309**
-0.09728856	-0.03973924	-0.03384922	-0.02137798	-0.01462036
-0.00648772	-0.00024199	0.00495976	0.01922512	0.02591302
0.03742494	0.04118784	0.05911153	0.08127248	0.08993774
0.09626611	0.09745526	0.10172654	0.11016993	0.11133900

Bibliography

(1) Lämmle, C. A.; Varady, A.; Müller, T. G.; Sturtzel, C. Photocaged Hoechst Enables Subnuclear Visualization and Cell Selective Staining of DNA in Vivo. *ChemBioChem* **2021**, *22*, 548–556.

(2) Bhargav, E.; Madhuri, N.; Ramesh, K.; Ravi, V. Targeted Drug Delivery- a Review. *World J. Pharm. Pharm. Sci.* **2013**, *3* (1), 150–169.

(3) Bae, Y. H.; Park, K. Targeted Drug Delivery to Tumors: Myths, Reality and Possibility. *J Control Release* **2011**, *153* (3), 198–205.

(4) Luan, J.; Zhai, G. Targeted Drug Delivery for Cardiovascular and Cerebrovascular Diseases. *Curr. Drug Targets* **2016**, *17* (4), 467–474.

(5) Gullotti, E.; Yeo, Y. Extracellularly Activated Nanocarriers: A New Paradigm of Tumor Targeted Drug Delivery. *Mol Pharm.* **2010**, *6* (4), 1041–1051.

(6) Monteiro, N.; Martins, A.; Reis, R. L.; Neves, N. M. Liposomes in Tissue Engineering and Regenerative Medicine. *J. R. Soc. Interface* **2014**, *11* (101), 20140459–20140459.

(7) Sercombe, L.; Veerati, T.; Moheimani, F.; Wu, S. Y.; Sood, A. K.; Hua, S. Advances and Challenges of Liposome Assisted Drug Delivery. *Front. Pharmacol.*

2015, *6* (DEC), 1–13.

(8) Zou, J.; Feng, H.; Sood, R.; Kinnunen, P. K. J.; Pyykko, I. Biocompatibility of Liposome Nanocarriers in the Rat Inner Ear After Intratympanic Administration. *Nanoscale Res. Lett.* **2017**, *12*, 1–14.

(9) Mallick, S.; Choi, J. S. Liposomes: Versatile and Biocompatible Nanovesicles for Efficient Biomolecules Delivery. *J. Nanosci. Nanotechnol.* **2014**, *14* (1), 755–765.

(10) Caddeo, C.; Pucci, L.; Gabriele, M.; Carbone, C.; Fernàndez-Busquets, X.; Valenti, D.; Pons, R.; Vassallo, A.; Fadda, A. M.; Manconi, M. Stability, Biocompatibility and Antioxidant Activity of PEG-Modified Liposomes Containing Resveratrol. *Int. J. Pharm.* **2018**, *538* (1–2), 40–47.

(11) Puri, A. Phototriggerable Liposomes: Current Research and Future Perspectives. *Pharmaceutics* **2014**, *6*, 1–25.

(12) Yadav, D.; Sandeep, K.; Pandey, D.; Dutta, R. K. Liposomes for Drug Delivery. *J. Biotechnol. Biomater.* **2017**, *07* (04).

(13) Ekladious, I.; Colson, Y. L.; Grinstaff, M. W. Polymer–Drug Conjugate Therapeutics: Advances, Insights and Prospects. *Nat. Rev. Drug Discov.* **2019**, *18* (4), 273–294.

(14) Duncan, R.; Vicent, M. J.; Greco, F.; Nicholson, R. I. Polymer-Drug Conjugates: Towards a Novel Approach for the Treatment of Endrocine-Related Cancer. *Endocr. Relat. Cancer* **2005**, *12* (SUPPL. 1).

(15) Kahraman, E.; Güngör, S.; Özsoy, Y. Potential Enhancement and Targeting

Strategies of Polymeric and Lipid-Based Nanocarriers in Dermal Drug Delivery. *Ther. Deliv.* **2017**, *8* (11), 967–985.

(16) Klán, P.; Šolomek, T.; Bochet, C. G.; Blanc, A.; Givens, R.; Rubina, M.; Popik, V.; Kostikov, A.; Wirz, J. Photoremovable Protecting Groups in Chemistry and Biology: Reaction Mechanisms and Efficacy. *Chem. Rev.* **2013**, *113* (1), 119–191.

(17) Silva, J. M.; Silva, E.; Reis, R. L. Light-Triggered Release of Photocaged Therapeutics - Where Are We Now? *J. Control. Release* **2019**, *298* (October 2018), 154–176.

(18) Chow, Y. L.; Cox, A.; Kirby, G. W.; Barton, D. H. R. PHOTOSENSITIVE PROTECTION OF FUNNCTIONAL GROUPS. *Tetrahedron Lett.* **1962**, *697*, 1055–1057.

(19) Patchornik, A.; Amit, B.; Woodward, R. B. Photosensitive Protecting Groups. *J. Am. Chem. Soc.* **1970**, *92* (21), 6333–6335.

(20) Barltrop, J.; Schofield, P. PHOTOSENSITIVE PROTECTING GROUP. *Tetrahedron Lett.* **1962**, No. 16, 697–699.

(21) Sheehan, J. C.; Wilson, R. M. Photolysis of Desyl Compounds. A New Photolytic Cyclization. *J. Am. Chem. Soc.* **1964**, *86* (23), 5277–5281.

(22) Sheehan, J. C.; Wilson, R. M.; Oxford, A. W. The Photolysis of Methoxy-Substituted Benzoin Esters. A Photosensitive Protecting Group for Carboxylic Acids. *J. Am. Chem. Soc.* **1971**, *93* (26), 7222–7228.

(23) Engels, J.; Schlaeger, E. J. Synthesis, Structure, and Reactivity of Adenosine

Cyclic 3′,5′-Phosphate-Benzyl Triesters. *J. Med. Chem.* **1977**, *20* (7), 907–911.

(24) Kaplan, J. H.; Forbush, B.; Hoffman, J. F. Rapid Photolytic Release of Adenosine 5′-Triphosphate from a Protected Analogue: Utilization by the Na:K Pump of Human Red Blood Cell Ghosts. *Biochemistry* **1978**, *17* (10), 1929–1935.

(25) Hwang, K.; Wu, P.; Kim, T.; Lei, L.; Tian, S.; Wang, Y.; Lu, Y. Photocaged DNAzymes as a General Method for Sensing Metal Ions in Living Cells. *Angew. Chemie - Int. Ed.* **2014**, *53* (50), 13798–13802.

(26) Shen, Y.; Li, Z.; Wang, G.; Ma, N. Photocaged Nanoparticle Sensor for Sensitive MicroRNA Imaging in Living Cancer Cells with Temporal Control. *ACS Sensors* **2018**, *3*, 494–503.

(27) Zhao, Y. R.; Zheng, Q.; Dakin, K.; Xu, K.; Martinez, M. L.; Li, W. H. New Caged Coumarin Fluorophores with Extraordinary Uncaging Cross Sections Suitable for Biological Imaging Applications. *J. Am. Chem. Soc.* **2004**, *126* (14), 4653–4663.

(28) Hauke, S.; Von Appen, A.; Quidwai, T.; Ries, J.; Wombacher, R. Specific Protein Labeling with Caged Fluorophores for Dual-Color Imaging and Super-Resolution Microscopy in Living Cells. *Chem. Sci.* **2016**, *8* (1), 559–566.

(29) Horbert, R.; Pinchuk, B.; Davies, P.; Alessi, D.; Peifer, C. Photoactivatable Prodrugs of Antimelanoma Agent Vemurafenib. *ACS Chem. Biol.* **2015**, *10* (9), 2099–2107.

(30) Korzycka, K. A.; Bennett, P. M.; Cueto-Diaz, E. J.; Wicks, G.; Drobizhev, M.; Blanchard-Desce, M.; Rebane, A.; Anderson, H. L. Two-Photon Sensitive

Protecting Groups Operating via Intramolecular Electron Transfer: Uncaging of GABA and Tryptophan. *Chem. Sci.* **2015**, *6* (4), 2419–2426.

(31) Ren, M.; Li, Z.; Nie, J.; Wang, L.; Lin, W. A Photocaged Fluorescent Probe for Imaging Hypochlorous Acid in Lysosomes †. *Chem. Commun.* **2018**, *54*, 9238–9241.

(32) Yuan, L.; Lin, W.; Cao, Z.; Long, L.; Song, J. Photocontrollable Analyte-Responsive Fluorescent Probes : A Photocaged Copper-Responsive Fluorescence Turn-On Probe. *Chem. Eur.* **2011**, *17*, 689–696.

(33) Skwarczynski, M.; Noguchi, M.; Hirota, S. Development of First Photoresponsive Prodrug of Paclitaxel. *Bioorg. Med. Chem. Lett.* **2006**, *16*, 4492–4496.

(34) Velema, W. A.; Van Der Berg, J. P.; Szymanski, W.; Driessen, A. J. M.; Feringa, B. L. Orthogonal Control of Antibacterial Activity with Light. *ACS Chem. Biol.* **2014**, *9* (9), 1969–1974.

(35) Hu, X.; Tian, J.; Liu, T.; Zhang, G.; Liu, S. Photo-Triggered Release of Caged Camptothecin Prodrugs from Dually Responsive Shell Cross-Linked Micelles. *Macromolecules* **2013**, *46* (15), 6243–6256.

(36) Kumari, P.; Kulkarni, A.; Sharma, A. K.; Chakrapani, H. Visible-Light Controlled Release of a Fluoroquinolone Antibiotic for Antimicrobial Photopharmacology. *ACS Omega* **2018**, *3* (2), 2155–2160.

(37) Endo, M.; Nakayama, K.; Kaida, Y.; Majima, T. Design and Synthesis of Photochemically Controllable Caspase-3. *Angew. Chemie - Int. Ed.* **2004**, *43* (42),

5643–5645.

(38) Marriott, G. Caged Protein Conjugates and Light-Directed Generation of Protein Activity: Preparation, Photoactivation, and Spectroscopic Characterization of Caged G-Actin Conjugates. *Biochemistry* **1994**, *33* (31), 9092–9097.

(39) Costa, S. P. G. Phototriggered Release of Tetrapeptide AAPV from Coumarinyl and Pyrenyl Cages. *Amino Acids* **2017**, *49*, 1077–1088.

(40) Kawakami, T.; Cheng, H.; Hashiro, S.; Nomura, Y.; Tsukiji, S.; Furuta, T.; Nagamune, T. A Caged Phosphopeptide-Based Approach for Photochemical Activation of Kinases in Living Cells. *ChemBioChem* **2008**, *9* (10), 1583–1586.

(41) Petersen, S.; Alonso, J. M.; Specht, A.; Duodu, P.; Goeldner, M.; Campo, A. Phototriggering of Cell Adhesion by Caged Cyclic RGD Peptides. *Zuschriften* **2008**, No. 120, 3236–3239.

(42) Measey, T. J.; Gai, F. Light-Triggered Disassembly of Amyloid Fibrils. *Langmuir* **2012**, *28* (34), 12588–12592.

(43) Ohmuro-Matsuyama, Y.; Tatsu, Y. Photocontrolled Cell Adhesion on a Surface Functionalized with a Caged Arginine-Glycine-Aspartate Peptide. *Angew. Chemie* **2008**, *120* (39), 7637–7639.

(44) Yiakouvaki, A.; Savović, J.; Al-Qenaei, A.; Dowden, J.; Pourzand, C. Caged-Iron Chelators a Novel Approach towards Protecting Skin Cells against UVA-Induced Necrotic Cell Death. *J. Invest. Dermatol.* **2006**, *126* (10), 2287–2295.

(45) Adams, R.; Lev-ram, V.; Tsienl, R. Y. A New Caged Ca2+ , Azid-1 , Is Far More

Photosensitive than Nitrobenzyl-Based Chelators. *Chem. Biol.* **1997**, *4* (11), 867.

(46) Brown, E. B.; Shear, J. B.; Adams, S. R.; Tsien, R. Y.; Webb, W. W. Photolysis of Caged Calcium in Femtoliter Volumes Using Two-Photon Excitation. *Biophys. J.* **1999**, *76* (1 I), 489–499.

(47) Delprincipe, F.; Egger, M.; Niggli, E. Two-Photon and UV-Laser Flash Photolysis of the Ca 2 + Cage , Dimethoxynitrophenyl-EGTA-4. *Cell Calcium* **1999**, *25* (1), 85–91.

(48) Agarwal, H. K.; Janicek, R.; Chi, S. H.; Perry, J. W.; Niggli, E.; Ellis-Davies, G. C. R. Calcium Uncaging with Visible Light. *J. Am. Chem. Soc.* **2016**, *138* (11), 3687–3693.

(49) Franks, A. T.; Wang, Q.; Franz, K. J. A Multifunctional, Light-Activated Prochelator Inhibits UVA-Induced Oxidative Stress. *Bioorganic Med. Chem. Lett.* **2015**, *25* (21), 4843–4847.

(50) Ellis-davies, G. C. R.; Kaplan, J. H. Nitrophenyl-EGTA , a Photolabile Chelator That Selectively Binds Ca 2+ with High Affinity and Releases It Rapidly upon Photolysis. In *Proceedings of the National Academy of Sciences*; 1994; Vol. 91, pp 187–191.

(51) Vaníkova, Z.; Hocek, M. Polymerase Synthesis of Photocaged DNA Resistant against Cleavage by Restriction Endonucleases. *Angew. Commun.* **2014**, *53*, 6734–6737.

(52) Zhang, D.; Zhou, C. Y.; Busby, K. N.; Alexander, S. C.; Devaraj, N. K. Light-

Activated Control of Translation by Enzymatic Covalent MRNA Labeling. *Angew. Chemie - Int. Ed.* **2018**, *57* (11), 2822–2826.

(53) Chaulk, S. G.; MacMillan, A. M. Synthesis of Oligo-RNAs with Photocaged Adenosine 2′-Hydroxyls. *Nat. Protoc.* **2007**, *2* (5), 1052–1058.

(54) Lusic, H.; Young, D. D.; Lively, M. O.; Deiters, A. Photochemical DNA Activation. *Org. Lett.* **2007**, *9* (10), 1903–1906.

(55) Seio, K.; Ohno, Y.; Ohno, K.; Takeshita, L.; Kanamori, T.; Masaki, Y.; Sekine, M. Bioorganic & Medicinal Chemistry Letters Photo-Controlled Binding of MutS to Photo-Caged DNA Duplexes Incorporating 4- O - (2-Nitrobenzyl) or 4- O - [2- (2-Nitrophenyl) Propyl] Thymidine. *Bioorg. Med. Chem. Lett.* **2016**, *26* (19), 4861–4863.

(56) Seyfried, P.; Heinz, M.; Pint, Ø.; Klçtzner, D.; Becker, Y.; Bolte, M.; Jonker, H. R. A.; Stelzl, L. S.; Hummer, G.; Schwalbe, H.; et al. Optimal Destabilization of DNA Double Strands by Single- Nucleobase Caging. *Chem. Eur. J* **2018**, *24*, 17568–17576.

(57) Friedman, S. H. Light-Activated RNA Interference. *Angew. Chemie* **2005**, *117*, 1352–1356.

(58) Ceo, L. M.; Koh, J. T. Photocaged DNA Provides New Levels of Transcription Control. *ChemBioChem* **2012**, *13* (4), 511–513.

(59) Höbartner, C.; Silverman, S. K. Modulation of RNATertiary Folding by Incorporation of Caged Nucleotides. *Angew. Chemie* **2005**, *117*, 7471–7475.

(60) Ogden, D.; Trentham, D. R. Photolabile Donors of Nitric Oxide: Ruthenium Nitrosyl Chlorides as Caged Nitric Oxide. *Methods Enzymol.* **1996**, *268* (1990), 266–281.

(61) Namiki, S.; Arai, T.; Fujimori, K. High-Performance Caged Nitric Oxide : A New Molecular Design , Synthesis , and Photochemical Reaction. *J. Am. Chem. Soc.* **1997**, *7863* (12), 3840–3841.

(62) Maragos, C. M.; Wink, D. A.; Dunams, T. M.; Saavedra, J. E.; Keefer, L. K.; Morley, D.; Bove, A. A.; Hoffman, A.; Isaac, L.; Hrabie, J. A. Complexes of ●NO with Nucleophiles as Agents for the Controlled Biological Release of Nitric Oxide. Vasorelaxant Effects. *J. Med. Chem.* **1991**, *34* (11), 3242–3247.

(63) Grewer, C. A New Photolabile Precursor of Glycine with Improved Properties : A Tool for Chemical Kinetic Investigations of the Glycine Receptor. *Biochemistry* **2000**, *39*, 2063–2070.

(64) Specht, A.; Thomann, J. S.; Alarcon, K.; Wittayanan, W.; Ogden, D.; Furuta, T.; Kurakawa, Y.; Goeldner, M. New Photoremovable Protecting Groups for Carboxylic Acids with High Photolytic Efficiencies at Near-UV Irradiation. Application to the Photocontrolled Release of L-Glutamate. *ChemBioChem* **2006**, *7* (11), 1690–1695.

(65) Kantevari, S.; Matsuzaki, M.; Kanemoto, Y.; Kasai, H.; Ellis-Davies, G. C. R. Two-Color, Two-Photon Uncaging of Glutamate and GABA. *Nat. Methods* **2010**, *7* (2), 123–125.

(66) Shembekar, V. R.; Chen, Y.; Carpenter, B. K.; Hess, G. P. Coumarin-Caged Glycine That Can Be Photolyzed within 3 Ms by Visible Light. *Biochemistry* **2007**, *46* (18), 5479–5484.

(67) Wieboldt, R.; Gee, K. R.; Niu, L.; Ramesh, D.; Carpenter, B. K.; Hess, G. P. Photolabile Precursors of Glutamate: Synthesis, Photochemical Properties, and Activation of Glutamate Receptors on a Microsecond Time Scale. *Proc. Natl. Acad. Sci. U. S. A.* **1994**, *91* (19), 8752–8756.

(68) Kandler, K.; Katz, L. C.; Kauer, J. A. Focal Photolysis of Caged Glutamate Produces Long-Term Depression of Hippocampal Glutamate Receptors. *Nat. Neurosci.* **1998**, *1* (2), 119–123.

(69) Zhao, H.; Sterner, E. S.; Coughlin, E. B.; Theato, P. O-Nitrobenzyl Alcohol Derivatives: Opportunities in Polymer and Materials Science. *Macromolecules* **2012**, *45* (4), 1723–1736.

(70) Kim, M. S.; Diamond, S. L. Photocleavage of o -Nitrobenzyl Ether Derivatives for Rapid Biomedical Release Applications. *Bioorg. Med. Chem. Lett.* **2006**, *16*, 4007–4010.

(71) Aujard, I.; Benbrahim, C.; Gouget, M.; Ruel, O.; Baudin, J. B.; Neveu, P.; Jullien, L. O-Nitrobenzyl Photolabile Protecting Groups with Red-Shifted Absorption: Syntheses and Uncaging Cross-Sections for One- And Two-Photon Excitation. *Chem. - A Eur. J.* **2006**, *12* (26), 6865–6879.

(72) Abou Nakad, E.; Bolze, F.; Specht, A. O-Nitrobenzyl Photoremovable Groups

with Fluorescence Uncaging Reporting Properties. *Org. Biomol. Chem.* **2018**, *16* (33), 6115–6122.

(73) Loudwig, S.; Goeldner, M. N -Methyl- N - (o -Nitrophenyl) Carbamates as Photolabile Alcohol Protecting Groups. *Tetrahedron Lett.* **2001**, *42*, 7957–7959.

(74) Amit, B.; Patchornik, A. The Photorearrangement of N-Substituted Ortho-Nitroanilides and Nitroveratramides. A Potential Photosensitive Protecting Group. *Tetrahedron Lett.* **1973**, *24*, 2205–2208.

(75) Lin, Q.; Yang, L.; Wang, Z.; Hua, Y.; Zhang, D.; Bao, B.; Bao, C.; Gong, X.; Zhu, L. Coumarin Photocaging Groups Modified with an Electron-Rich Styryl Moiety at the 3-Position: Long-Wavelength Excitation, Rapid Photolysis, and Photobleaching. *Angew. Chemie - Int. Ed.* **2018**, *57* (14), 3722–3726.

(76) Kormos, A.; Kis-petik, K. Green-Light Activatable, Water-Soluble Red-Shifted Coumarin Photocageś. *Org. Lett.* **2019**, *21*, 9410–9414.

(77) Givens, R. S.; Matuszewski, B.; Ch, N. H. Photochemistry of Phosphate Esters : An Efficient Method for the Generation of Electrophiles1 The University of Kansas Timed Release of Chemicals from Polypyrrole Films Baruch Zinger and Larry L . Miller * S-H-7. *J. Am. Chem. Soc.* **1984**, *106*, 6860–6861.

(78) Goswami, P. P.; Syed, A.; Beck, C. L.; Albright, T. R.; Mahoney, K. M.; Unash, R.; Smith, E. A.; Winter, A. H. BODIPY-Derived Photoremovable Protecting Groups Unmasked with Green Light. *J. Am. Chem. Soc.* **2015**, *137* (11), 3783–3786.

(79) Peterson, J. A.; Wijesooriya, C.; Gehrmann, E. J.; Mahoney, K. M.; Goswami, P. P.; Albright, T. R.; Syed, A.; Dutton, A. S.; Smith, E. A.; Winter, A. H. Family of BODIPY Photocages Cleaved by Single Photons of Visible/Near-Infrared Light. *J. Am. Chem. Soc.* **2018**, *140* (23), 7343–7346.

(80) Lv, W.; Li, Y.; Li, F.; Lan, X.; Zhang, Y.; Du, L.; Zhao, Q.; Phillips, D. L.; Wang, W. Upconversion-like Photolysis of BODIPY-Based Prodrugs via a One- Photon Process. *J. Am. Chem. Soc.* **2019**, *141* (44), 17482–17486.

(81) Tang, S.; Cannon, J.; Yang, K.; Krummel, M. F.; Baker, J. R.; Choi, S. K. Spacer-Mediated Control of Coumarin Uncaging for Photocaged Thymidine. *J. Org. Chem.* **2020**, *85* (5), 2945–2955.

(82) Offenbartl-Stiegert, D.; Clarke, T. M.; Bronstein, H.; Nguyen, H. P.; Howorka, S. Solvent-Dependent Photophysics of a Red-Shifted, Biocompatible Coumarin Photocage. *Org. Biomol. Chem.* **2019**, *17* (25), 6178–6183.

(83) Hammer, C. A.; Falahati, K.; Jakob, A.; Klimek, R.; Burghardt, I.; Heckel, A.; Wachtveitl, J. Sensitized Two-Photon Activation of Coumarin Photocages. *J. Phys. Chem. Lett.* **2018**, *9* (6), 1448–1453.

(84) Slanina, T.; Shrestha, P.; Palao, E.; Kand, D.; Peterson, J. A.; Dutton, A. S.; Rubinstein, N.; Weinstain, R.; Winter, A. H.; Klán, P. In Search of the Perfect Photocage: Structure-Reactivity Relationships in Meso-Methyl BODIPY Photoremovable Protecting Groups. *J. Am. Chem. Soc.* **2017**, *139* (42), 15168–15175.

(85) Lester, H. A.; Nerbonne, J. M. Physiological and Pharmacological Manipulations with Light Flashes. *Ann. Rev. Biophys. Bioeng* **1982**, *11* (84), 151–175.

(86) Slanina, T.; Shrestha, P.; Palao, E.; Kand, D.; Peterson, J. A.; Dutton, A. S.; Rubinstein, N.; Weinstain, R.; Winter, A. H.; Klán, P. In Search of the Perfect Photocage: Structure-Reactivity Relationships in Meso-Methyl BODIPY Photoremovable Protecting Groups. *J. Am. Chem. Soc.* **2017**, *139* (42), 15168–15175.

(87) Stowell, M. H. B.; Rock, R. S.; Rees, D. C.; Chan, S. I. Efficient Synthesis of Photolabile Alkoxy Benzoin Protecting Groups. *Tetrahedron Lett.* **1996**, *37* (3), 307–310.

(88) Shrestha, P.; Dissanayake, K. C.; Gehrmann, E. J.; Wijesooriya, C. S.; Mukhopadhyay, A.; Smith, E. A.; Winter, A. H. Efficient Far-Red/Near-IR Absorbing BODIPY Photocages by Blocking Unproductive Conical Intersections. *J. Am. Chem. Soc.* **2020**, *142* (36), 15505–15512.

(89) Kand, D.; Liu, P.; Navarro, M. X.; Fischer, L. J.; Rousso-Noori, L.; Friedmann-Morvinski, D.; Winter, A. H.; Miller, E. W.; Weinstain, R. Water-Soluble BODIPY Photocages with Tunable Cellular Localization. *J. Am. Chem. Soc.* **2020**, *142* (11), 4970–4974.

(90) Barun, V. V; Ivanov, A. P.; Volotovskaya, A. V; Ulashchik, V. S. ABSORPTION SPECTRA AND LIGHT PENETRATION DEPTH OF NORMAL AND PATHOLOGICALLY ALTERED HUMAN SKIN. *J. Appl. Spectrosc.* **2007**, *74* (3), 387–394.

(91) Wu, B. M.; Linsley, C. S. Recent Advances in Light-Responsive on- Demand Drug-Delivery Systems. *Ther. Deliv.* **2017**, *8*, 89–107.

(92) Smith, A. M.; Mancini, M. C.; Nie, S. Bioimaging: Second Window for in Vivo Imaging. *Nat. Nanotechnol.* **2009**, *4* (11), 710–711.

(93) Hefetz, Y.; Dunn, D. A.; Deutsch, T. F.; Buckley, L.; Kochevar, I. E.; Hillenkamp, F. Laser Photochemistry of DNA: Two-Photon Absorption and Optical Breakdown Using High-Intensity, 532-Nm Radiation. *J. Am. Chem. Soc.* **1990**, *112* (23), 8528–8532.

(94) D'Orazio, J.; Jarrett, S.; Amaro-Ortiz, A.; Scott, T. UV Radiation and the Skin. *Int. J. Mol. Sci.* **2013**, *14* (6), 12222–12248.

(95) Goppert-Mayer, M. Über Elementarakte Mit Zwei Quantensprüngen, University of Göttingen, 1931, Vol. 9.

(96) Kaiser, W.; Garrett, C. G. B. Two-Photon Excitation in CaF2:Eu2+. *Phys. Rev. Lett.* **1961**, *7* (6), 229–232.

(97) Andrews, D. Multiphoton Absorption in Molecules. In *Molecular Photophysics and Spectroscopy*; Morgan and Claypool Publishers, 2014; pp 14.1-14.7.

(98) Rakhymzhan, A.; Chichinin, A. Calculation of the Absorption Cross Sections of Some Molecules from GEISA Database at the Wavelengths of Isotopically Different CO 2 Lasers . *ISRN Anal. Chem.* **2013**, *2013*, 1–11.

(99) Dhritiman Bhattacharyya, Y. Z.; Elles, C. G.; Bradforth, S. E. Electronic Structure of Liquid Methanol and Ethanol From Polarization-Dependent Two-Photon

Absorption Spectroscopy. *J. Phys. Chem.* **2019**.

(100) Makarov, N. S.; Drobizhev, M.; Rebane, A. Two-Photon Absorption Standards in the 550-1600 Nm Excitation Wavelength Range. *Opt. Express* **2008**, *16* (6), 4029.

(101) Strickler, J. H.; Webb, W. W. Three-Dimensional Optical Data Storage in Refractive Media by Two-Photon Point Excitation. *Opt. Lett.* **1991**, *16* (22), 1780.

(102) Sadegh, S.; Yang, M.-H.; Ferri, C. G. L.; Thunemann, M.; Saisan, P. A.; Devor, A.; Fainman, Y. Measurement of the Relative Non-Degenerate Two-Photon Absorption Cross-Section for Fluorescence Microscopy. *Opt. Express* **2019**, *27* (6), 8335.

(103) Shi, L.; Rodríguez-Contreras, A.; Alfano, R. R. Gaussian Beam in Two-Photon Fluorescence Imaging of Rat Brain Microvessel. *J. Biomed. Opt.* **2014**, *19* (12), 126006.

(104) Piston, D. Two-Photon Excitation Microscopy for Three-Dimensional Imaging of Living Intact Tissues. In *Fluorescence Microscopy: From Principles to*; Kubitscheck, U., Ed.; Wiley-VCH Verlag GmbH & Co. KGaA, 2017; pp 203–242.

(105) So, P. T. Two-Photon Fluorescence Light Microscopy. *eLS* **2001**, 1–5.

(106) Oliveira, L. C.; Zilio, S. C. Single-Beam Time-Resolved Z-Scan Measurements of Slow Absorbers. *Appl. Phys. Lett.* **1994**, *65* (17), 2121–2123.

(107) Silva, D. L.; De Boni, L.; Correa, D. S.; Costa, S. C. S.; Hidalgo, A. A.; Zilio, S. C.; Canuto, S.; Mendonca, C. R. Two-Photon Absorption in Oxazole Derivatives: An Experimental and Quantum Chemical Study. *Opt. Mater. (Amst).* **2012**, *34* (7),

1013–1018.

(108) Olivier, T.; Billard, F.; Akhouayri, H. Nanosecond Z-Scan Measurements of the Nonlinear Refractive Index of Fused Silica. *Opt. Express* **2004**, *12* (7), 1377.

(109) Gu, B.; Fan, Y. X.; Chen, J.; Wang, H. T.; He, J.; Ji, W. Z-Scan Theory of Two-Photon Absorption Saturation and Experimental Evidence. *J. Appl. Phys.* **2007**, *102* (8), 083101.

(110) Gagey, N.; Neveu, P.; Benbrahim, C.; Goetz, B.; Aujard, I.; Baudin, J. B.; Jullien, L. Two-Photon Uncaging with Fluorescence Reporting: Evaluation of the o-Hydroxycinnamic Platform. *J. Am. Chem. Soc.* **2007**, *129* (32), 9986–9998.

(111) Xu, C.; Webb, W. W. Measurement of Two-Photon Excitation Cross Sections of Molecular Fluorophores with Data from 690 to 1050 Nm. *J. Opt. Soc. Am. B* **1996**, *13* (3), 481.

(112) de Reguardati, S.; Pahapill, J.; Mikhailov, A.; Stepanenko, Y.; Rebane, A. High-Accuracy Reference Standards for Two-Photon Absorption in the 680–1050 Nm Wavelength Range. *Opt. Express* **2016**, *24* (8), 9053.

(113) Rebane, A.; Drobizhev, M.; Makarov, N. S.; Wicks, G.; Wnuk, P.; Stepanenko, Y.; Haley, J. E.; Krein, D. M.; Fore, J. L.; Burke, A. R.; et al. Symmetry Breaking in Platinum Acetylide Chromophores Studied by Femtosecond Two-Photon Absorption Spectroscopy. *J. Phys. Chem. A* **2014**, *118* (21), 3749–3759.

(114) Negres, R. a; Hales, J. M.; Kobyakov, A.; Hagan, D. J.; Van Stryland, E. W. Experiment and Analysis of Two-Photon Absorption Spectroscopy Using a White-

Light Continuum Probe. *IEEE J. Quantum Electron.* **2002**, *38* (9), 1205–1216.

(115) Houk, A. L.; Zheldakov, I. L.; Tommey, T. A.; Elles, C. G. Two-Photon Excitation of Trans-Stilbene: Spectroscopy and Dynamics of Electronically Excited States above S1. *J. Phys. Chem. B* **2015**, *119* (29), 9335–9344.

(116) Houk, A. L.; Givens, R. S.; Elles, C. G. Two-Photon Activation of p - Hydroxyphenacyl Phototriggers : Toward Spatially Controlled Release of Diethyl Phosphate and ATP. 1–12.

(117) Bhattacharyya, D.; Zhang, Y.; Elles, C.; Bradforth. Electronic Structure of Liquid Methanol and Ethanol From Polarization-Dependent Two-Photon Absorption Spectroscopy. *J. Phys. Chem.* **2019**, *123* (27), 5789–5804.

(118) Elles, C. G.; Rivera, C. A.; Zhang, Y.; Pieniazek, P. A.; Bradforth, S. E. Electronic Structure of Liquid Water from Polarization-Dependent Two-Photon Absorption Spectroscopy. *J. Chem. Phys.* **2009**, *130* (8).

(119) Yamaguchi, S.; Tahara, T. Two-Photon Absorption Spectrum of All- Trans Retinal. *Chem. Phys. Lett.* **2003**, *376*, 237–243.

(120) Yamaguchi, S.; Tahara, T. Observation of an Optically Forbidden State of C60 by Nondegenerate Two-Photon Absorption Spectroscopy. *Chem. Phys. Lett.* **2004**, *390* (1–3), 136–139.

(121) Chunosova, S. S.; Svetlichnyi, V. A.; Meshalkin, Y. P. Measurement of the Two-Photon Absorption Cross Sections of Dicyanomethylene-Pyrans by the z-Scan Method. *Kvantovaya Elektron.* **2005**, *35* (5), 415–418.

(122) Klausen, M.; Dubois, V.; Clermont, G.; Tonnelé, C.; Castet, F.; Blanchard-Desce, M. Dual-Wavelength Efficient Two-Photon Photorelease of Glycine by π-Extended Dipolar Coumarins. *Chem. Sci.* **2019**, *10* (15), 4209–4219.

(123) Rogers, J. E.; Slagle, J. E.; Krein, D. M.; Burke, A. R.; Hall, B. C.; Fratini, A.; McLean, D. G.; Fleitz, P. A.; Cooper, T. M.; Drobizhev, M.; et al. Platinum Acetylide Two-Photon Chromophores. *Inorg. Chem.* **2007**, *46* (16), 6483–6494.

(124) Morales, A. R.; Frazer, A.; Woodward, A. W.; Ahn-White, H. Y.; Fonari, A.; Tongwa, P.; Timofeeva, T.; Belfield, K. D. Design, Synthesis, and Structural and Spectroscopic Studies of Push-Pull Two-Photon Absorbing Chromophores with Acceptor Groups of Varying Strength. *J. Org. Chem.* **2013**, *78* (3), 1014–1025.

(125) Abe, M.; Chitose, Y.; Jakkampudi, S.; Thuy, P. T. T.; Lin, Q.; Van, B. T.; Yamada, A.; Oyama, R.; Sasaki, M.; Katan, C. Design and Synthesis of Two-Photon Responsive Chromophores for Near-Infrared Light-Induced Uncaging Reactions. *Synth.* **2017**, *49* (15), 3337–3346.

(126) Pawlicki, M.; Collins, H. A.; Denning, R. G.; Anderson, H. L. Two-Photon Absorption and the Design of Two-Photon Dyes. *Angew. Chemie - Int. Ed.* **2009**, *48* (18), 3244–3266.

(127) Momotake, A.; Lindegger, N.; Niggli, E.; Barsotti, R. J.; Ellis-Davies, G. C. R. The Nitrodibenzofuran Chromophore: A New Caging Group for Ultra-Efficient Photolysis in Living Cells. *Nat. Methods* **2006**, *3* (1), 35–40.

(128) Mahmoodi, M. M.; Abate-Pella, D.; Pundsack, T. J.; Palsuledesai, C. C.; Goff, P.

C.; Blank, D. A.; Distefano, M. D. Nitrodibenzofuran: A One-and Two-Photon Sensitive Protecting Group That Is Superior to Brominated Hydroxycoumarin for Thiol Caging in Peptides. *J. Am. Chem. Soc.* **2016**, *138* (18), 5848–5859.

(129) Dreuw, A.; Polkehn, M. A.; Binder, R.; Heckel, A.; Knippenberg, S. Computational Design of Improved Two-Photon Active Caging Compounds Based on Nitrodibenzofuran. *J. Comput. Chem.* **2012**, *33* (22), 1797–1805.

(130) Becker, Y.; Unger, E.; Fichte, M. A. H.; Gacek, D. A.; Dreuw, A.; Wachtveitl, J.; Walla, P.; Heckel, A. A Red-Shifted Two-Photon-Only Caging Group for Three-Dimensional Photorelease. *Chem. Sci.* **2018**, *9*, 2797–2802.

(131) Becker, Y.; Roth, S.; Scheurer, M.; Jakob, A.; Gacek, D. A.; Walla, P. J.; Dreuw, A.; Wachtveitl, J.; Heckel, A. Selective Modification for Red-Shifted Excitability: A Small Change in Structure, a Huge Change in Photochemistry. *Chem. - A Eur. J.* **2021**, *27* (6), 2212–2218.

(132) Suellen, C.; Freitas, R. G.; Loos, P. F.; Jacquemin, D. Cross-Comparisons between Experiment, TD-DFT, CC, and ADC for Transition Energies. *J. Chem. Theory Comput.* **2019**, *15* (8), 4581–4590.

(133) Beerepoot, M. T. P.; Alam, M.; Bednarska, J.; Bartkowiak, W.; Ruud, K.; Zales, R. Benchmarking the Performance of Exchange-Correlation Functionals for Predicting Two-Photon Absorption Strengths. *J. Chem. Theory Comput.* **2018**, *14*, 3677–3685.

(134) Beerepoot, M. T. P.; Friese, D. H.; List, N. H.; Kongsted, J.; Ruud, K.

Benchmarking Two-Photon Absorption Cross Sections: Performance of CC2 and CAM-B3LYP. *Phys. Chem. Chem. Phys.* **2015**, *17* (29), 19306–19314.

(135) Nanda, K. D.; Krylov, A. I. Two-Photon Absorption Cross Sections within Equation-of-Motion Coupled-Cluster Formalism Using Resolution-of-the-Identity and Cholesky Decomposition Representations: Theory, Implementation, and Benchmarks. *J. Chem. Phys.* **2015**, *142* (6).

(136) Leszczynski, J. *Handbook of Computational Chemistry*; 2012.

(137) Sałek, P.; Vahtras, O.; Guo, J.; Luo, Y.; Helgaker, T.; Ågren, H. Calculations of Two-Photon Absorption Cross Sections by Means of Density-Functional Theory. *Chem. Phys. Lett.* **2003**, *374* (5–6), 446–452.

(138) Silva, D. L.; Krawczyk, P.; Bartkowiak, W.; Mendoņa, C. R. Theoretical Study of One- and Two-Photon Absorption Spectra of Azoaromatic Compounds. *J. Chem. Phys.* **2009**, *131* (24).

(139) Nayyar, I. H.; Masunov, A. E.; Tretiak, S. Comparison of TD-DFT Methods for the Calculation of Two-Photon Absorption Spectra of Oligophenylvinylenes. *J. Phys. Chem. C* **2013**, *117* (35), 18170–18189.

(140) Friese, D. H.; Beerepoot, M. T. P.; Ringholm, M.; Ruud, K. Open-Ended Recursive Approach for the Calculation of Multiphoton Absorption Matrix Elements. *J. Chem. Theory Comput.* **2015**, *11* (3), 1129–1144.

(141) Salem, M. A.; Brown, A. Two-Photon Absorption in Fluorescent Protein Chromophores : TDDFT and CC2 Results. *J. Chem. Theory Comput.* **2014**, *10*,

3260–3269.

(142) Friese, D. H.; Hättig, C.; Ruud, K. Calculation of Two-Photon Absorption Strengths with the Approximate Coupled Cluster Singles and Doubles Model CC2 Using the Resolution-of-Identity Approximation. *Phys. Chem. Chem. Phys.* **2012**, *14* (3), 1175–1184.

(143) Gattuso, H.; Dumont, E.; Marazzi, M.; Monari, A. Two-Photon-Absorption DNA Sensitization: Via Solvated Electron Production: Unraveling Photochemical Pathways by Molecular Modeling and Simulation. *Phys. Chem. Chem. Phys.* **2016**, *18* (27), 18598–18606.

(144) Vivas, M. G.; Silva, D. L.; Boni, L. De; Zalesny, R.; Bartkowiak, W.; Mendonca, C. R. Two-Photon Absorption Spectra of Carotenoids Compounds. *J. Appl. Phys.* **2011**, *109* (10).

(145) Pálfi, D.; Chiovini, B.; Szalay, G.; Kaszás, A.; Turi, G. F.; Katona, G.; Ábrányi-Balogh, P.; Szori, M.; Potor, A.; Frigyesi, O.; et al. High Efficiency Two-Photon Uncaging Coupled by the Correction of Spontaneous Hydrolysis. *Org. Biomol. Chem.* **2018**, *16* (11), 1958–1970.

(146) Frisch, M. J.; Trucks, G. W.; Schlegel, H. B.; Scuseria, G. E.; Robb, M. A.; Cheeseman, J. R.; Scalmani, G.; Barone, V.; Petersson, G. A.; Nakatsuji, H.; Li, X.; Caricato, M.; Marenich, A. V.; Bloino, J.; Janesko, B. G.; Gomperts, R.; Mennucci, B.; Hratch, D. J. Gaussian 16. Gaussian Inc.: Wallingford Conneticut 2016.

(147) Becke, A. D. Density-Functional Thermochemistry. III. The Role of Exact Exchange. *J. Chem. Phys.* **1993**, *98* (7), 5648–5652.

(148) Hertwig, R. H.; Koch, W. On the Parametrization of the Local Correlation Functional. What Is Becke-3--LYP? *Chem. Phys. Lett.* **1997**, *268* (97), 345.

(149) Stephens, P. J.; Devlin, F. J.; Chabalowski, C. F.; Frisch, M. J. Ab Initio Calculation of Vibrational Absorption and Circular Dichroism Spectra Using Density Functional Force Fields. *J. Phys. Chem.* **1994**, *98* (45), 11623–11627.

(150) Petersson, G. A.; Al-Laham, M. A. A Complete Basis Set Model Chemistry. II. Open-Shell Systems and the Total Energies of the First-Row Atoms. *J. Chem. Phys.* **1991**, *94* (9), 6081–6090.

(151) Petersson, G. A.; Bennett, A.; Tensfeldt, T. G.; Allaham, M. A.; Shirley, W. A.; Mantzaris, J. A Complete Basis Set Model Chemistry .1. The Total Energies of Closed-Shell Atoms and Hydrides of the 1st-Row Elements. *J. Chem. Phys.* **1988**, *89* (4), 2193–2218.

(152) Foresman, J. B.; Keith, T. A.; Wiberg, K. B.; Snoonian, J.; Frisch, M. J. Solvent Effects. 5. Influence of Cavity Shape, Truncation of Electrostatics, and Electron Correlation on Ab Initio Reaction Field Calculations. *J. Phys. Chem.* **1996**, *100* (40), 16098–16104.

(153) Aidas, K.; Angeli, C.; Bak, K. L.; Bakken, V.; Bast, R.; Boman, L.; Christiansen, O.; Cimiraglia, R.; Coriani, S.; Dahle, P.; et al. The Dalton Quantum Chemistry Program System. *Wiley Interdiscip. Rev. Comput. Mol. Sci.* **2014**, *4* (3), 269–284.

(154) Vosko, S. H.; Wilk, L.; Nusair, M. Accurate Spin-Dependent Electron Liquid Correlation Energies for Local Spin Density Calculations: A Critical Analysis. *Can. J. Phys.* **1980**, *58* (8), 1200–1211.

(155) Sałek, P.; Vahtras, O.; Helgaker, T.; Ågren, H. Density-Functional Theory of Linear and Nonlinear Time-Dependent Molecular Properties. *J. Chem. Phys.* **2002**, *117* (21), 9630–9645.

(156) Chattopadhyaya, M.; Alam, M. M. A Theoretical Study of One-and Two-Photon Activity of D-Luciferin. *Computation* **2016**, *4* (4), 1–10.

(157) Caricato, M.; Trucks, G. W.; Frisch, M. J.; Wiberg, K. B. Oscillator Strength: How Does TDDFT Compare to EOM-CCSD? *J. Chem. Theory Comput.* **2011**, *7* (2), 456–466.

(158) Harada, N.; Chen, S. L.; Nakanishi, K. Quantitative Definition of Exciton Chirality and the Distant Effect in the Exciton Chirality Method. *J. Am. Chem. Soc.* **1975**, *345* (19), 5345–5352.

(159) Berova, N.; Ellestad, G. A.; Harada, N.; York, N. Characterization by Circular Dichroism Spectroscopy; 2010; pp 91–146.

(160) Vahtras, Olav; Salek, Pawel; Helgaker, Trygve; Agren, H. Density-Functional Theory of Linear and Nonlinear Time-Dependent Molecular Properties. *J. Chem. Phys.* **2002**, *117* (21), 9630.

(161) Sałek, P.; Vahtras, O.; Guo, J.; Luo, Y.; Helgaker, T.; Agren, H. Calculations of Two-Photon Absorption Cross Sections by Means of Density-Functional Theory.

Chem. Phys. Lett. **2003**, *374*, 446–452.

(162) Ohta, K.; Antonov, L.; Yamada, S.; Kamada, K. Theoretical Study of the Two-Photon Absorption Properties of Several Asymmetrically Substituted Stilbenoid Molecules. *J. Chem. Phys.* **2007**, *127* (8).

(163) Monson, P. R. .; McClain, W. M. Polarization Dependence of the Two- Photon Absorption of Tumbling Molecules with Application to Liquid 1-Chloronaphthalene and Benzene. *J. Chem.* **1970**, *53* (1), 29.

(164) Mcclain, W. M. Excited State Symmetry Assignment through Polarized Two-Photon Absorption Studies of Fluids. *J. Chem. Phys.* **1971**, *55* (6), 2789–2796.

(165) De Wergifosse, M.; Elles, C. G.; Krylov, A. I. Two-Photon Absorption Spectroscopy of Stilbene and Phenanthrene: Excited-State Analysis and Comparison with Ethylene and Toluene. *J. Chem. Phys.* **2017**, *146* (17).

(166) Peticolas, W. MUL TIPHOTON SPECTROSCOPY. *Annu. Rev. Phys. Chem.* **1967**, *18*, 233–260.

(167) Yang, G.; Qin, C.; Su, Z.; Dong, S. Calculations of Two-Photon Absorption Cross-Sections of Stibene and Bis (Styryl) Benzene Derivatives by Means of TDDFT-SOS Method. *J. Mol. Struct.* **2005**, *726*, 61–65.

(168) Olsen, J.; Jørgensen, P. Linear and Nonlinear Response Functions for an Exact State and for an MCSCF State. *J. Chem. Phys.* **1984**, *82* (7), 3235–3264.

(169) Houk, A. L.; Givens, R. S.; Elles, C. G. Two-Photon Activation of p-Hydroxyphenacyl Phototriggers: Toward Spatially Controlled Release of Diethyl

Phosphate and ATP. *J. Phys. Chem. B* **2016**, *120* (12), 3178–3186.

(170) Charaf-eddin, A.; Planchat, A.; Mennucci, B.; Adamo, C.; Jacquemin, D. Choosing a Functional for Computing Absorption and Fluorescence Band Shapes with TD-DFT. *J. Chem. Theory Comput.* **2013**, *9*, 2749–2760.

(171) Dreuw, A.; Head-gordon, M. Single-Reference Ab Initio Methods for the Calculation of Excited States of Large Molecules. *Chem. Rev.* **2005**, *105*, 4009–4037.

(172) Jacquemin, D.; Wathelet, V.; Perpe, E. A.; Adamo, C. Extensive TD-DFT Benchmark : Singlet-Excited States of Organic Molecules. *J. Chem. Theory Comput.* **2009**, *5*, 2420–2435.

(173) Peach, M. J. G.; Benfield, P.; Helgaker, T.; Tozer, D. J. Excitation Energies in Density Functional Theory: An Evaluation and a Diagnostic Test. *J. Chem. Phys.* **2008**, *128* (4).

(174) Lerch, M. M.; Hansen, M. J.; van Dam, G. M.; Szymanski, W.; Feringa, B. L. Emerging Targets in Photopharmacology. *Angew. Chemie - Int. Ed.* **2016**, *55* (37), 10978–10999.

(175) Piant, S.; Bolze, F.; Specht, A. Two-Photon Uncaging, from Neuroscience to Materials. *Opt. Mater. Express* **2016**, *6* (5), 1679.

(176) Vorobev, A. Y.; Moskalensky, A. E. Long-Wavelength Photoremovable Protecting Groups: On the Way to in Vivo Application. *Comput. Struct. Biotechnol. J.* **2020**, *18*, 27–34.

(177) Weissleder, R. A Clearer Vision for in Vivo Imaging. *Nat. Biotechnol.* **2001**, *19* (4), 316–317.

(178) Piloto, A. M.; Costa, S. P. G.; Goncalves, M. S. T. Wavelength-Selective Cleavage of o -Nitrobenzyl and Polyheteroaromatic Benzyl Protecting Groups. *Tetrahedron* **2014**, *70*, 650–657.

(179) Sikder, A.; Banerjee, M.; Singha, T.; Mondal, S.; Datta, P. K.; Anoop, A.; Singh, N. D. P. A Natural Alkaloid, β-Carboline, as a One- And Two-Photon Responsive Fluorescent Photoremovable Protecting Group: Sequential Release of the Same or Different Carboxylic Acids. *Org. Lett.* **2020**, *22* (17), 6998–7002.

(180) Sun, H.; Yee, S. S.; Gobeze, H. B.; He, R.; Martinez, D.; Risinger, A. L.; Schanze, K. S. One- and Two-Photon Activated Release of Oxaliplatin from a Pt(IV)-Functionalized Poly(Phenylene Ethynylene). *ACS Appl. Mater. Interfaces* **2022**, *14* (14), 15996–16005.

(181) Pascal, S.; Bellier, Q.; David, S.; Bouit, P. A.; Chi, S. H.; Makarov, N. S.; Le Guennic, B.; Chibani, S.; Berginc, G.; Feneyrou, P.; et al. Unraveling the Two-Photon and Excited-State Absorptions of Aza-BODIPY Dyes for Optical Power Limiting in the SWIR Band. *J. Phys. Chem. C* **2019**.

(182) Wang, P. Photolabile Protecting Groups: Structure and Reactivity. *Asian J. Org. Chem.* **2013**, *2* (6), 452–464.

(183) Wong, P. T.; Tang, S.; Cannon, J.; Mukherjee, J.; Isham, D.; Gam, K.; Payne, M.; Yanik, S. A.; Baker, J. R.; Choi, S. K. A Thioacetal Photocage Designed for Dual

Release: Application in the Quantitation of Therapeutic Release by Synchronous Reporter Decaging. *ChemBioChem* **2017**, *18* (1), 126–135.

(184) Furuta, T.; Wang, S. S.-H.; Dantzker, J. L.; Dore, T. M.; Bybee, W. J.; Callaway, E. M.; Denk, W.; Tsien, R. Y. Brominated 7-Hydroxycoumarin-4-Ylmethyls: Photolabile Protecting Groups with Biologically Useful Cross-Sections for Two Photon Photolysis. *Proc. Natl. Acad. Sci.* **1999**, *96* (4), 1193–1200.

(185) Bader, T. K.; Xu, F.; Hodny, M. H.; Blank, D. A.; Distefano, M. D. Methoxy-Substituted Nitrodibenzofuran-Based Protecting Group with an Improved Two-Photon Action Cross-Section for Thiol Protection in Solid Phase Peptide Synthesis. *J. Org. Chem.* **2020**, *85* (3), 1614–1625.

(186) Canola, S.; Mardegana, L.; Bergamini, G.; Villa, M.; Acocella, A.; Zangoli, M.; Ravotto, L.; Vinogradov, S. A.; Maria, F. Di; Ceroni, P.; et al. One- and Two-Photon Absorption Properties of Quadrupolar Thiophene-Based Dyes with Acceptors of Varying Strength. *Photochem Photobiol Sci.* **2019**, *18* (9), 2180–2190.

(187) Houk, A. L.; Zheldakov, I. L.; Tommey, T. A.; Elles, C. G. Two-Photon Excitation of Trans -Stilbene : Spectroscopy and Dynamics of Electronically Excited States above S 1. *J. Phys. Chem. B* **2014**.

(188) Underwood, D. F.; Blank, D. A. Ultrafast Solvation Dynamics: A View from the Solvent's Perspective Using a Novel Resonant-Pump, Nonresonant-Probe Technique. *J. Phys. Chem. A* **2003**, *107* (7), 956–961.

(189) Houk, A. L.; Givens, R. S.; Elles, C. G. SI: Two-Photon Activation of p-Hydroxyphenacyl Phototriggers: Toward Spatially Controlled Release of Diethyl Phosphate and ATP. *J. Phys. Chem. B* **2016**, *120* (12), 3178–3186.

(190) Kovalenko, S. A.; Dobryakov, A. L.; Ruthmann, J.; Ernsting, N. P. Femtosecond Spectroscopy of Condensed Phases with Chirped Supercontinuum Probing. *Phys. Rev. A - At. Mol. Opt. Phys.* **1999**, *59* (3), 2369–2384.

(191) Burns, K. H.; Srivastava, P.; Elles, C. G. Absolute Cross Sections of Liquids from Broadband Stimulated Raman Scattering with Femtosecond and Picosecond Pulses. *Anal. Chem.* **2020**, *92* (15), 10686–10692.

(192) Martin, R. L. Natural Transition Orbitals. *J. Chem. Phys.* **2003**, *118* (11), 4775–4777.

(193) Hammers, M. D.; Hodny, M. H.; Bader, T. K.; Mahmoodi, M. M.; Fang, S.; Fenton, A. D.; Nurie, K.; Trial, H. O.; Xu, F.; Healy, A. T.; et al. Two-Photon Uncaging of Bioactive Thiols in Live Cells at Wavelengths above 800nm. *Org. Biomol. Chem.* **2020**.

(194) Wiggins, P.; Williams, J. A. G.; Tozer, D. J. Excited State Surfaces in Density Functional Theory: A New Twist on an Old Problem. *J. Chem. Phys.* **2009**, *131* (9).

(195) Seshan, P. K. The Absorption Spectra of Some Aromatic Compounds. In *Proceedings of the Indian Academy of Sciences, A, Vol III*; 1935; pp 148–171.

(196) Zhang, D.; Garcı, I.; Costela, A.; Pe, M. E. Development of Excellent Long-

Wavelength BODIPY Laser Dyes with a Strategy That Combines Extending p - Conjugation and Tuning ICT Effect W. **2011**, 13026–13033.

(197) Meier, H.; Stalmach, U.; Kolshorn, H. Effective Conjugation Length and UV/Vis Spectra of Oligomers. *Acta Polym.* **1997**, *48* (9), 379–384.

(198) Gug, S.; Bolze, F.; Specht, A.; Bourgogne, C.; Goeldner, M.; Nicoud, J. F. Molecular Engineering of Photoremovable Protecting Groups for Two-Photon Uncaging. *Angew. Chemie - Int. Ed.* **2008**, *47* (49), 9525–9529.

(199) Komori, N.; Jakkampudi, S.; Motoishi, R.; Abe, M.; Kamada, K.; Furukawa, K.; Katan, C.; Sawada, W.; Takahashi, N.; Kasai, H.; et al. Design and Synthesis of a New Chromophore, 2-(4-Nitrophenyl)Benzofuran, for Two-Photon Uncaging Using near-IR Light. *Chem. Commun.* **2016**, *52* (2), 331–334.

(200) Zara, Z.; Iqbal, J.; Ayub, K.; Irfan, M.; Mahmood, A.; Khera, R. A.; Eliasson, B. A Comparative Study of DFT Calculated and Experimental UV/Visible Spectra for Thirty Carboline and Carbazole Based Compounds. *J. Mol. Struct.* **2017**, *1149*, 282–298.

(201) Jacquemin, D.; Perpète, E. A.; Ciofini, I.; Adamo, C. On the TD-DFT UV/Vis Spectra Accuracy: The Azoalkanes. *Theor. Chem. Acc.* **2008**, *120* (4–6), 405–410.

(202) Sarkar, R.; Boggio-Pasqua, M.; Loos, P. F.; Jacquemin, D. Benchmarking TD-DFT and Wave Function Methods for Oscillator Strengths and Excited-State Dipole Moments. *J. Chem. Theory Comput.* **2021**, *17* (2), 1117–1132.

(203) Abou Nakad, E.; Chaud, J.; Morville, C.; Bolze, F.; Specht, A. Monitoring of

Uncaging Processes by Designing Photolytical Reactions. *Photochem. Photobiol. Sci.* **2020**, *19* (9), 1122–1133.

(204) Skwarczynski, M.; Noguchi, M.; Hirota, S.; Sohma, Y.; Kimura, T.; Hayashi, Y.; Kiso, Y. Development of First Photoresponsive Prodrug of Paclitaxel. *Bioorganic Med. Chem. Lett.* **2006**, *16* (17), 4492–4496.

(205) Weissleder, R. A Clearer Vision for in Vivo Imaging: Progress Continues in the Development of Smaller, More Penetrable Probes for Biological Imaging. *Nat. Biotechnol.* **2001**, *19* (4), 316–317.

(206) Rebane, M. D. S. T. N. S. M. T. E. H. A. Absolute Two-Photon Absorption Spectra and Two-Photon Brightness of Orange and Red Fluorescent Proteins. *J Phys Chem B* **2009**, *113* (4), 855–859.

(207) Molecular, A. P. I.; Honig, B.; Jortner, J.; Szöke, A. Theoretical Studies of Two-Photon. **2004**, *2714* (June 1966).

(208) Lorenc, M.; Ziolek, M.; Naskrecki, R.; Karolczak, J.; Kubicki, J.; Maciejewski, A. Artifacts in Femtosecond Transient Absorption Spectroscopy. *Appl. Phys. B Lasers Opt.* **2002**, *74* (1), 19–27.

(209) Bechtel, J. H.; Smith, W. L. Two-Photon Absorption in Semiconductors with Picosecond Laser Pulses. *Phys. Rev. B* **1976**, *13* (8), 3515–3522.

(210) Pálfi, D.; Chiovini, B.; Szalay, G.; Kaszás, A.; Turi, G. F.; Katona, G.; Ábrányi-Balogh, P.; Szori, M.; Potor, A.; Frigyesi, O.; et al. High Efficiency Two-Photon Uncaging Coupled by the Correction of Spontaneous Hydrolysis. *Org. Biomol.*

Chem. **2018**, *16* (11), 1958–1970.

(211) Maruo, S.; Kawata, S. Two-Photon-Absorbed near-Infrared Photopolymerization for Three-Dimensional Microfabrication. *J. Microelectromechanical Syst.* **1998**, *7* (4), 411–415.

(212) Maruo, S.; Nakamura, O.; Kawata, S. Three-Dimensional Microfabrication with Two-Photon-Absorbed Photopolymerization. *Opt. Lett.* **1997**, *22* (2), 132–134.

(213) Becker, Y.; Unger, E.; Fichte, M. A. H.; Gacek, D. A.; Dreuw, A.; Wachtveitl, J.; Walla, P. J.; Heckel, A. A Red-Shifted Two-Photon-Only Caging Group for Three-Dimensional Photorelease. *Chem. Sci.* **2018**, *9* (10), 2797–2802.

(214) Zhang, D.; Martín, V.; García-Moreno, I.; Costela, A.; Pérez-Ojeda, M. E.; Xiao, Y. Development of Excellent Long-Wavelength BODIPY Laser Dyes with a Strategy That Combines Extending π-Conjugation and Tuning ICT Effect. *Phys. Chem. Chem. Phys.* **2011**, *13* (28), 13026–13033.

(215) Peterson, J. A.; Wijesooriya, C.; Gehrmann, E. J.; Mahoney, K. M.; Goswami, P. P.; Albright, T. R.; Syed, A.; Dutton, A. S.; Smith, E. A.; Winter, A. H. Family of BODIPY Photocages Cleaved by Single Photons of Visible/Near-Infrared Light. *J. Am. Chem. Soc.* **2018**, *140* (23), 7343–7346.

(216) Chitose, Y.; Abe, M.; Furukawa, K.; Lin, J. Y.; Lin, T. C.; Katan, C. Design and Synthesis of a Caged Carboxylic Acid with a Donor-π-Donor Coumarin Structure: One-Photon and Two-Photon Uncaging Reactions Using Visible and Near-Infrared Lights. *Org. Lett.* **2017**, *19* (10), 2622–2625.

(217) Chaudhuri, A.; Venkatesh, Y.; Das, J.; Gangopadhyay, M.; Maiti, T. K.; Singh, N. D. P. One- And Two-Photon-Activated Cysteine Persulfide Donors for Biological Targeting. *J. Org. Chem.* **2019**, *84* (18), 11441–11449.

(218) Wang, P. Photolabile Protecting Groups: Structure and Reactivity. *Asian J. Org. Chem.* **2013**, *2* (6), 452–464.

(219) Momotake, A.; Lindegger, N.; Niggli, E.; Barsotti, R. J.; Ellis-Davies, G. C. R. The Nitrodibenzofuran Chromophore: A New Caging Group for Ultra-Efficient Photolysis in Living Cells. *Nat. Methods* **2006**, *3* (1), 35–40.

(220) Booth, D.; Noyes, R. M. The Effect of Viscosity on the Quantum Yield for Iodine Dissociation. *J. Am. Chem. Soc.* **1960**, *82*, 1868–1872.

(221) Lian, T.; Bromberg, S. E.; Asplund, M. C.; Yang, H.; Harris, C. B. Femtosecond Infrared Studies of the Dissociation and Dynamics of Transition Metal Carbonyls in Solution. *J. Phys. Chem.* **1996**, *100* (29), 11994–12001.

(222) Oelkers, A. B.; Scatena, L. F.; Tyler, D. R. Femtosecond Pump-Probe Transient Absorption Study of the Photolysis of [Cp′Mo(CO) 3] 2 (Cp′ = η 5-C 5H 4CH 3): Role of Translational and Rotational Diffusion in the Radical Cage Effect. *J. Phys. Chem. A* **2007**, *111* (25), 5353–5360.

(223) Oelkers, A. B.; Tyler, D. R. Radical Cage Effects: A Method for Measuring Recombination Efficiencies of Secondary Geminate Radical Cage Pairs Using Pump-Probe Transient Absorption Methods. *Photochem. Photobiol. Sci.* **2008**, *7* (11), 1386–1390.

(224) Schwartz, B. J.; King, J. C.; Zhang, J. Z.; Harris, C. B. Direct Femtosecond Measurements of Single Collision Dominated Geminate Recombination Times of Small Molecules in Liquids. *Chem. Phys. Lett.* **1993**, *203* (5–6), 503–508.

(225) Harris, C. B. Dynamics of Chemical Reactions in Liquids on Ultrafast Time Scales. *Ann. Rev. Phys. Chem* **1987**, *39*, 116.

(226) Oelkers, A. B.; Schutte, E. J.; Tyler, D. R. Solvent Cage Effects: The Influence of Radical Mass and Volume on the Recombination Dynamics of Radical Cage Pairs Generated by Photolysis of [CpCH2CH2N(CH3)C(O)(CH2)NCH3Mo(CO)3]2 (n = 3, 8, 13, 18) (Cp = H5-C5H4) Complexes. *Photochem. Photobiol. Sci.* **2008**, *7* (2), 228–234.

(227) Male, J. L.; Lindfors, B. E.; Covert, K. J.; Tyler, D. R. The Effect of Radical Size and Mass on the Cage Recombination Efficiency of Photochemically Generated Radical Cage Pairs. *J. Am. Chem. Soc.* **1998**, *120* (50), 13176–13186.

(228) Drobizhev, M.; Stepanenko, Y.; Dzenis, Y.; Karotki, A.; Rebane, A.; Taylor, P. N.; Anderson, H. L. Understanding Strong Two-Photon Absorption in Pi-Conjugated Porphyrin Dimers via Double-Resonance Enhancement in a Three-Level Model. *J. Am. Chem. Soc.* **2004**, *2* (1), 15352–15353.

(229) Karotki, A.; Drobizhev, M.; Dzenis, Y.; Taylor, P. N.; Anderson, H. L.; Rebane, A. Dramatic Enhancement of Intrinsic Two-Photon Absorption in a Conjugated Porphyrin Dimer. *Phys. Chem. Chem. Phys.* **2004**, *6*, 7–10.

(230) Zheng, S.; Beverina, L.; Barlow, S.; Zojer, E.; Fu, J.; Padilha, L. A.; Fink, C.;

Kwon, O.; Yi, Y.; Shuai, Z.; et al. High Two-Photon Cross-Sections in Bis (Diarylaminostyryl) Chromophores with Electron-Rich Heterocycle and Bis (Heterocycle) Vinylene Bridges. **2007**, 1372–1374.

(231) Albota, M.; Beljonne, D.; Brédas, J. L.; Ehrlich, J. E.; Fu, J. Y.; Heikal, A. A.; Hess, S. E.; Kogej, T.; Levin, M. D.; Marder, S. R.; et al. Design of Organic Molecules with Large Two-Photon Absorption Cross Sections. *Science (80-.).* **1998**, *281* (5383), 1653–1656.

(232) Reinhardt, B. A.; Brott, L. L.; Clarson, S. J.; Dillard, A. G.; Bhatt, J. C.; Kannan, R.; Yuan, L.; He, G. S.; Prasad, P. N. Highly Active Two-Photon Dyes: Design, Synthesis, and Characterization toward Application. *Chem. Mater.* **1998**, *10* (7), 1863–1874.